การจับยึดอนุภาคระดับไมโครและนาโนในสนามแม่เหล็กเกรเดียนต์สูง

นายกนก หวลกำเนิด

วิทยานิพนธ์นี้ เป็นส่วนหนึ่งของการศึกษาตามหลักสูตรปริญญาวิทยาศาสตรดุษฎีบัณฑิต
สาขาวิชาฟิสิกส์ ภาควิชาฟิสิกส์
คณะวิทยาศาสตร์ จุฬาลงกรณ์มหาวิทยาลัย
ปีการศึกษา 2554

CAPTURE OF MICRO- AND NANO-PARTICLES IN HIGH GRADIENT MAGNETIC FIELD

Mr. Kanok Hournkumnuard

A Dissertation Submitted in Partial Fulfillment of the Requirements

for the Degree of Doctor of Philosophy Program in Physics

Department of Physics

Faculty of Science

Chulalongkorn University

Academic Year 2011

Thesis Title	CAPTURE OF MICRO- AND NANO-PARTICLES IN HIGH GRADIENT MAGNETIC FIELD
By	Mr. Kanok Hournkumnuard
Field of Study	Physics
Thesis Advisor	Associate Professor Mayuree Natenapit, Ph.D.

Accepted by the Faculty of Science, Chulalongkorn University in Partial Fulfillment of the Requirements for the Doctoral Degree

.....Dean of the Faculty of Science
(Professor Supot Hannongbua, Dr. rer. nat.)

THESIS COMMITTEE

.....Chairman
(Assistant Professor Sojiphong Chatraphorn, Ph.D.)

.....Thesis Advisor
(Associate Professor Mayuree Natenapit, Ph.D.)

.....Examiner
(Chatchai Srinitiwarawong, Ph.D.)

.....Examiner
(Orapin Wannadelok, Ph.D.)

.....External Examiner
(Supitch Khemmani, Ph.D.)

กนก หวลกำเนิด : การจับยึดอนุภาคระดับไมโครและนาโนในสนามแม่เหล็กเกรเดียนต์สูง. (CAPTURE OF MICRO- AND NANO-PARTICLES IN HIGH GRADIENT MAGNETIC FIELD) อ.ที่ปรึกษาวิทยานิพนธ์: รศ.ดร. มยุรี เนตรนภิส, 127 หน้า.

งานวิจัยนี้ ได้ศึกษาการจับอนุภาคขนาดไมโครเมตรโดยกลุ่มลวดตัวจับแบบสุ่มในตัวกรองแม่เหล็กแบบตามแนวแกนโดยใช้รูปแบบสนามแม่เหล็กเกรเดียนต์สูงและสนามการไหลของของไหลรอบกลุ่มลวดตัวจับที่ได้คำนวณไว้แล้วโดยใช้วิธีตัวกลางยังผลและแบบจำลองเซลล์ของฮาเพลตามลำดับ เราได้ศึกษาประสิทธิภาพของตัวกรองโดยมีความเข้มของสนามแม่เหล็กที่ป้อนให้ตัวกรอง สัดส่วนโดยปริมาตรของกลุ่มลวดตัวจับภายในตัวกรองและความเร็วของของไหลที่ทางเข้าตัวกรองเป็นพารามิเตอร์ งานวิจัยนี้ยังศึกษาการจับแบบการแพร่ของอนุภาคขนาดนาโนเมตรโดยใช้ลวดตัวจับขนาดไมโครเมตรที่ถูกใส่ไว้ในหลอดเลือดเป็นครั้งแรกและเปรียบเทียบผลกับกรณีที่พิจารณาเฉพาะการจับแบบการชนเท่านั้น สนามแม่เหล็กและสนามการไหลรอบลวดตัวจับแต่ละตัวถูกหาโดยวิธีการเชิงวิเคราะห์และวิธีการเชิงตัวเลขตามลำดับ เราได้ศึกษารูปแบบการกระจายค่าความเข้มข้นของอนุภาคขนาดนาโนเมตรบนระนาบที่ตั้งฉากกับแกนลวดตัวจับโดยแก้สมการความต่อเนื่องด้วยวิธีการเชิงตัวเลขและใช้เงื่อนไขค่าเริ่มต้นและค่าขอบที่กำหนด พารามิเตอร์ที่แปรค่าได้แก่ ความเข้มสนามแม่เหล็ก รัศมีอนุภาค และความเร็วเฉลี่ยของเลือด

ผลการศึกษาพบว่าประสิทธิภาพการจับอนุภาคขนาดไมโครเมตรโดยตัวกรองแม่เหล็กแบบตามแนวแกนที่หาโดยใช้วิธีตัวกลางยังผลสนับสนุนผลการทดลองที่ได้มีผู้รายงานไว้ก่อนแล้ว จากการศึกษายังได้ให้เกณฑ์พื้นฐานเรื่องข้อจำกัดของการประมาณตัวจับเดี่ยวอีกด้วย สำหรับผลการศึกษาการจับอนุภาคขนาดนาโนเมตรพบว่าความเข้มข้นของอนุภาคบนผิวลวดตัวจับสามารถถูกทำให้มีค่าเพิ่มขึ้นจนสูงกว่าค่าความเข้มข้นอนุภาคที่ถูกฉีดเข้าหลอดเลือดอย่างมาก ผลการศึกษาแสดงนัยถึงความเป็นไปได้และความมีประสิทธิผลของการใช้ลวดตัวจับขนาดไมโครเมตรสำหรับแยกเม็ดเลือดปริมาณมากและการกำหนดเป้าหมายของอนุภาคขนาดนาโนเมตรไปยังตำแหน่งเฉพาะที่ภายในหลอดเลือด

ภาควิชา ฟิสิกส์ ลายมือชื่อนิสิต .....

สาขาวิชา ฟิสิกส์ ลายมือชื่อ อ.ที่ปรึกษาวิทยานิพนธ์ .....

ปีการศึกษา 2554

5073801823 : MAJOR PHYSICS

KEYWORDS : HGMS OF BLOOD CELLS /EFFECTIVE MEDIUM TREATMENT / MAGNETIC AXIAL FILTER / MAGNETIC DRUG TARGETING/DIFFUSIVE CAPTURE

KANOK HOURNKUMNUARD: CAPTURE OF MICRO- AND NANO-PARTICLES IN HIGH GRADIENT MAGNETIC FIELD. ADVISOR: ASSOC. PROF. MAYUREE NATENAPIT, Ph.D., 127 pp.

We investigate the capture of micro-particles by random wires in axial magnetic filters by using the expressions of high gradient magnetic field and fluid flow field around the wires previously determined, respectively, by using the effective medium treatment (EMT) and Happel's cell model. We determine filter efficiency with the strength of applied magnetic field, the wire volume packing fraction in the filter and the fluid entrance velocity as parameters. We newly investigate diffusive capture of nano-particles by micro-wires implanted in blood vessel and compare the results with those obtained by considering only interception capture. Magnetic and fluid flow fields around each wire are determined analytically and numerically, respectively. We study the pattern of particle concentration distribution on a plane perpendicular to wire's axis by solving the continuity equation numerically and using assigned initial and boundary conditions. The varied parameters are magnetic field strength, particle radius, and blood average velocity.

From our results, the efficiency of micro-particle capture by axial filter determined by using the EMT model supports the previously reported experimental data. From this study, the basic criterion of the limitation of the single wire approximation is also provided. For results of nano-particle capture, particle concentration on the wire surface can be increased much higher than the injected value. The results imply the feasibility and the efficacy of using micro-wires for large scale blood separation and targeting nano-particles at specific sites within blood vessel.

Department : Physics Student's Signature .....

Field of Study : Physics Advisor's Signature .....

Academic Year : 2011

Acknowledgements

This thesis is finished with the great attention, helpful suggestions and supports from my thesis advisor, Associate Professor Dr. Mayuree Natenapit and I wish to express my sincere gratitude to her. The completeness of this thesis is achieved with valuable comments and suggestions from every thesis examiner, Assistance Professor Dr. Sojiphong Chatraphorn, Dr. Chatchai Srinitiwarawong, Dr. Orapin Wannadelok, Dr. Supitch Khemmani and my sincere gratitude is also expressed for every examiner.

My great gratitude is also expressed to Mr. Chanin Potisook, Mr. Natthaphon Choomphon-anomakhun and every staff of the Department of Physics at Chulalongkorn University and Silpakorn University for their helps and encouragements.

I express my great gratitude to the Faculty of Science, Chulalongkorn University for the financial support from the A1B1 research fund project. The financial support from the 90th Anniversary of Chulalongkorn University Fund (Ratchadaphisek-somphot Endowment Fund) is also gratefully acknowledged.

Lastly, I would like to give a special thank to my parents for my birth, their loves and encouragements.

Contents

page

Chapter page

Chapter page

List of Tables

Table **page**

List of Figures

Figure page

Figure page

Figure page

Figure page

List of Abbreviations

EMT	effective medium treatment
HGMS	high gradient magnetic separation
RBCs	red blood cells
WBCs	white blood cells
MDT	magnetic drug targeting
IA-MDT	implant assisted-magnetic drug targeting
MDCPs	magnetic drug carrier particles
$\vec{H}_0$	uniform magnetic field
H	local strength of the magnetic field
$\vec{F}_m$	magnetic force
c_p	magnetic susceptibility of magnetic particle
c_f	magnetic susceptibility of the fluid
m_0	magnetic permeability of free space
b_p	radius of a magnetic particle
V_p	volume of a magnetic particle
m_p	mass of a magnetic particle
$\vec{a}_p$	acceleration of magnetic particle
$\vec{F}_v$	force drag force
h	fluid viscosity
$\vec{v}_p$	velocity of magnetic particle
$\vec{v}_f$	velocity of fluid
c	particle volume concentration
$\vec{\nabla}$	gradient operator
$\vec{J}$	total particle volume flux
$\vec{J}_D$	particle volume flux due to diffusion
$\vec{J}_C$	particle volume flux due to fluid convection
$\vec{J}_F$	particle volume flux due to convection by particle drift velocity relative to fluid

D	particle diffusion coefficient
u	particle mobility
k_B	Boltzmann's constant
T	absolute temperature
$\mathbf{u}$ V_0	inlet velocity of fluid at the entrance of magnetic filter
r , q	radial distance and angle in polar coordinates
x , y , z	distances in Cartesian coordinates
a	radius of cylindrical magnetic collector or wire
r_a	normalized radial distance
x_a , y_a , z_a	normalized distances in Cartesian coordinates
F	volume packing fraction of cylindrical magnetic collectors in magnetic filter
b	radius of composite representative cell in the effective medium treatment
m_c	magnetic permeability of the cylindrical magnetic collector or wire
m_f	magnetic permeability of the fluid
m^*	magnetic permeability of the effective medium
H_{eff}	local magnetic field strength in the effective medium
v_{za}	normalized particle velocity in z direction
V_{0a}	magnitude of normalized inlet velocity of fluid at the entrance of magnetic filter
V_{ma}	magnitude of normalized magntic velocity of particle
Ku	Kuwabara's factor
A_C	capture cross section
l	filter length
l_a	filter length in unit of the radius of cylindrical magnetic collector
L_a	normalized filter length
L_a^*	critical normalized filter length
N	number of cylindrical magnetic collectors in a magnetic filter
A_{filter}	cross sectional area of the magnetic filter
z_{ae}	the length along the filter that particle travel until it is captured on the wire

r_{ai} , q_i	normalized radial and angular coordinates on the boundary of capture cross Section
r_b	density of blood
h_b	viscosity of blood
Re	Reynold 's number
$\vec{m}$	magnetic moment of a nano-drug carrier particle
$\vec{B}_0$	uniform magnetic flux density vector
B	local strength of magnetic flux density vector
$\vec{M}$	magnetization
c	magnetic susceptibility of nano-drug carrier particle
$\vec{M}_s$	saturation magnetization
$c_{fm,p}$	weight fraction of ferromagnetic material in a nano-drug carrier particle
$w_{fm,p}$	volume fraction of ferromagnetic material in a nano-drug carrier particle
$c_{fm,p,0}$	zero field magnetic susceptibility of ferromagnetic material in nano-drug carrier particle
$M_{fm,p,s}$	saturation magnetization of ferromagnetic material in nano-drug carrier Particle
$r_{fm,p}$	density of ferromagnetic material in nano-drug carrier particle
$r_{pol,p}$	density of polymer material in nano-drug carrier particle
r_p	average density of a nano-drug carrier particle
$L(b)$	Langevin function
b	Langevin argument
$c_{W,0}$	zero field magnetic susceptibility of ferromagnetic material in cylindrical collector or wire
$M_{W,s}$	saturation magnetization of ferromagnetic material in cylindrical collector or wire
P	Local pressure in blood vessel
t	normalized time

i, j, n	indices of radial and angular position in simulation domain and index of normalized time step, respectively
$\mathbf{£}$	numerical value of particle volume concentration
C_{in}	the value of particle volume concentration injected into blood vessel
C_{sat}	the saturation value of particle volume concentration in simulation domain
R_{ca}	the capture length of capture by interception
l_c	the relative capture length of capture by interception
D_a	diameter of the simulation domain in unit of a cylindrical collector or wire
P_{sat}	the ratio between volume of nano-drug carrier particles captured within saturation region and total volume of nano-drug carrier particles in the simulation domain

CHAPTER I

INTRODUCTION

1.1 Particle Capture in High Gradient Magnetic Field

The technique of using high gradient magnetic field for capturing, separating, or filtering magnetic particles from suspensions has been applied in many fields of works and researches, for examples, mineral processing [1], treatment of industrial waste water [2], separation of biological entities for diagnostic and therapeutic objectives [3-5], magnetic drug targeting (MDT) [6-8], implant assisted-magnetic drug targeting (IA-MDT) [9-11]. It is seen that these techniques provide significant contributions to various works from large scale down to small scale ones so particle capture in high gradient magnetic field becomes an important part of future technology. The capture behaviors of particles depend on various factors such as particle size, the scales of the associated works, the magnetic properties of the particles (paramagnetic, diamagnetic, ferromagnetic materials), the configuration of fluid flow in the considered system, etc. Consequently, it is useful to study and understand the capture behaviors and the mechanisms of particle transport for each situation so that we can predict and improve the efficiency of particle capture.

The principle of particle capture in high gradient magnetic field can be described as follows. Consider an assemblage of micro- or nano-size magnetic particles suspended in a fluid medium. If the suspension is placed in a region of magnetic field, there exists magnetic force ($\vec{F}_m$) acting on each suspended particle which can be expressed as [12, 13]

$$\vec{F}_m = m_0 \left(c_p - c_f \right) V_p H \vec{\nabla} H , \qquad (1.1)$$

where $m_0 = 4p \times 10^{-7}$ H/m is magnetic permeability of free space, c_p and c_f are magnetic susceptibilities of particle and fluid, respectively, V_p is particle volume, H and ∇H are local strength and gradient of magnetic field at particle position, respectively.

From Eq. (1.1), it is observed that the magnetic force depends on both local strength and gradient of magnetic field at particle position. Consequently, strong magnetic force can be obtained from high gradient of magnetic field although the local magnetic strength at particle position is not high. To produce high gradient magnetic field within the suspension, magnetic collectors of cylindrical or spherical shape are firstly placed in the suspension. Then uniform magnetic field is applied across the collectors and suspension. The collectors disturb the background uniform magnetic field and there exists high gradient magnetic field in regions near the surface of the collectors. Any suspended particles entering these regions are subjected to strong magnetic force and are captured on the collectors. As stated in pages 37 to 38 of Ref. [14], the force density (force per unit volume) on the suspended particle is inversely proportional to the size of the collectors so the smaller the radius of cylindrical or spherical collectors, the stronger magnetic force acting on the suspended particle. If the size of the collectors is in the order of micrometer, the magnitude of applied uniform magnetic field is in the order of 10^5- 10^6 A/m and the collectors made of ferromagnetic material such as stainless steel then the magnitude of force density on a suspended particle is in the order of 10^{10}- 10^{11} N/m^3. Consequently, even weakly magnetic particles, of which very low magnetic susceptibility, can be effectively captured by using the high gradient magnetic field produced by the collectors.

1.2 Thesis Background

The technique of particle capture using high gradient magnetic field has been studied and applied by many researchers. Initially, the studies were performed for the case of micro-particles by applying Newton's law of motion on each particle. Then

particle's equation of motion was solved, by using analytical or numerical methods. The motions of many particles were analyzed to know whether they are captured by interception. Consequently, the features of particle capture and capture lengths or capture cross section can be obtained to determined capture efficiency. To produce high gradient magnetic field, magnetic collectors, which are wires or spherical collectors, are placed within the background uniform magnetic field. Then there exist regions of high gradient magnetic field around the collectors. Any particle entering these regions is subjected by magnetic traction force and is brought to retained on the collector surface. Particle capture in high gradient magnetic field can be categorized into three configurations [15] as transverse, longitudinal, and axial modes as shown in Fig. 1.1.

For transverse and longitudinal modes shown in Fig. 1.1(a) and1.1 (b), the directions of fluid flow towards the cylindrical collector are perpendicular and parallel to the direction of the applied magnetic field, respectively. For the axial mode shown in Fig. 1.1(c), the direction of fluid flow towards the cylindrical collector is parallel to collector 's axis. The transverse and longitudinal modes are suitable for the capture of large amounts of particles within a relatively short time interval [2] since collector 's surface is placed against trajectories of incoming particles. Consequently, the incoming particles within the capture length are attracted towards collector 's surface rapidly and are captured by collision or interception. The axial mode is suitable for the capture of easily damaged particles such as red and white blood cells.

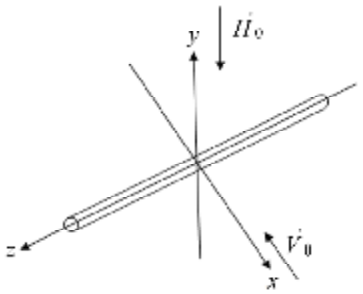

(a) transverse mode

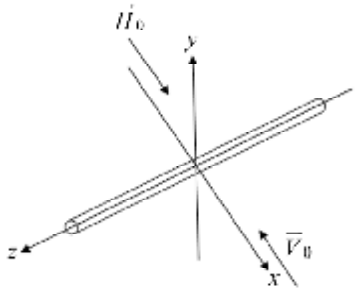

(b) longitudinal mode

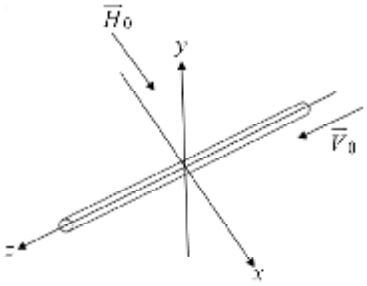

(c) axial mode

Figure 1.1: Three configurations of particle capture in high gradient magnetic field [15].

The capture of micro-particles in high gradient magnetic field using various modes has been studied and developed for many years until now. The work of J. H. P. Watson [16] studied longitudinal mode capture of micro-particle in high gradient magnetic field by magnetic wires. Particle's equations of motion in potential flow field of fluid were formulated and solved numerically and capture efficiency was predicted. The work of M.

Natenapit and W. Sanglek [17] studied the capture of micro-particles, in both transverse and longitudinal modes, by random matrices of cylindrical wires in high gradient magnetic field. The magnetic field around any wire was determined by the effective medium treatment (EMT) [18]. Particle's equations of motion in potential flow field of fluid were formulated and solved numerically and capture radius was predicted by using trajectory-analysis method. The work of R. Gerber [19] studied the capture of micro-particles in axial magnetic filter. The magnetic field around the cylindrical collector was determined by using the single-wire approximation. Particle's trajectories in laminar flow field of fluid were solved analytically then the capture cross-section of a wire, which specifies capture efficiency, was determined. Later, although the axial flow field of viscous fluids relative to an array of wires was incorporated into the study [20], the magnetic field was still calculated using the single-wire approximation. The study of particle capture was developed further when both the magnetic and fluid flow fields around wires were calculated using the periodic-wires model [21]. In the work of Kuntabutr [15], the magnetic field around any wire in the axial magnetic filter calculated by using the effective medium treatment (EMT) [18] was used while the fluid flow field around any wire was calculated by using the periodic-wire model [20].

In this research, the capture of micro-particles by an assemblage of parallel wires randomly distributed in the filter was investigated based on the EMT model. The magnetic field around the representative wire determined by Natenapit [18] using the EMT model and the axial flow field of the viscous fluid, derived by Happel [22], relative to a bundle of randomly distributed parallel cylinders were used. Particle trajectories were traced numerically to determine the capture cross-section. This study is the generalization of the single-wire model to a range of higher packing fraction. Capture cross-sections are reported and compared with those obtained by using the magnetic field calculated from the single-wire approximation [19]. The discussion about basic criterion of limitation of the single-wire model is initiated in this article.

The advantages of the axial mode of high gradient magnetic separation lie in the separating specific biological entities such as red blood cells (RBCs) and white

blood cells (WBCs) from whole blood. For diagnostic objectives in clinical or laboratory applications, small amounts of blood samples are used and the specific cells are captured in a small apparatus consisting of only a single magnetic wire of micron size [23-24]. For therapeutic objectives such as blood component transfusion, the volume of blood and number of RBCs and WBCs to be separated are far greater than the diagnostic case and, therefore the design of an effective macro-scale filter of high efficiency is important. This would be very useful such as for plasma separation ready for use in compensating for the lost fluids and blood proteins in burn victims [25]. Albumin which is one of the main serum proteins in plasma is used for replenishing and maintaining blood volume after traumatic injury during surgery [25]. Plasma separations from whole blood have been studied by various authors using microchannels [26-27].

In this research, we also apply the EMT model to study the capture of RBCs and WBCs from whole blood, by using their native magnetic properties, in an axial magnetic filter. The filter efficiency is predicted. The feasibility of macro-scale blood cells separation that provides high gradient magnetic field and high efficiency is investigated.

For particles which are much smaller than the micron size, Brownian motion causes significant effect on the kinematics of the particles. Consequently, diffusion should be taken into account and diffusive capture was considered. In 1983, R. Gerber, M. Takayasu and F.J. Fridlaender formulated the HGMS theory describing the capture mechanism of ultra-fine particles [28-29] by incorporating diffusion in describing the capture mechanism of nano-particles. One-dimensional model of nano-particles capture by a single ferromagnetic wire was investigated. Results of the study revealed the features of nano-particles buildup on the wire. In 1990, L. P. Davies and R. Gerber developed a two-dimensional model for the capture of nano-particles on a single ferromagnetic wire [30]. This model generalized the one-dimensional model formulated in 1983. The capture of nano-particles was simulated in various cases. Simulation results showed the feature of nano-particle buildup in various regions around the wire at a given time. K. Hournkumnuard and M. Natenapit [31] extended the work of L. P. Davies and R.

Gerber [30] to the multi-wire case by investigating diffusive capture of weakly nano-particles by an assemblage of random wires.

In recent years, the technique of using high gradient magnetic field to capture nano-particles in flowing fluid has been applied on the studies of magnetic drug targeting (MDT) and implant assisted-magnetic drug targeting (IA-MDT) [6-11]. The idea of MDT is the guidance of therapeutic particles [32], which are injected into blood circulation system, to specific regions within the body by using an external magnetic field generated by permanent magnet poles or electromagnets. The objectives of MDT are to improve the efficiency of various therapies, such as cancers and tumors therapies [33], by concentrating the therapeutic agents within the target sites. Consequently, the therapeutic agent concentration and the time that therapeutic agents are retained within the target sites were high enough to accomplish the therapy. Moreover, the injected concentration of the therapeutic agents can be reduced so that the parts of therapeutic agents that are not confined within the target sites can not cause potential toxicities on other organs of patient's body. However, the limitation of MDT technique is that the strength of magnetic force necessary to capture therapeutic agents within the target sites may not high enough. The reasons are the magnetic force acting on the particles depends highly on volume of magnetic material in the particle hence nano-particles are subjected by very small magnetic force and the magnetic field strength decreased sharply with increasing depth within the body. Consequently, the technique MDT was successfully applied for the target sites near to the skin and it is almost impossible to use MDT for target sites deep into the body. To increase the possibility of targeting therapeutic agents in target sites deep into the body, the technique of implant assisted-magnetic drug targeting (IA-MDT) was firstly proposed [6]. For IA-MDT, various implants such as ferromagnetic stents [34-36], wire [37] or seeds [9, 38] were placed within or near to the target sites. When an external magnetic field is applied across the target sites, there exist regions of high gradient magnetic field around the implants. So, the high gradient magnetic field is produced within the body and the magnetic force for trapping therapeutic agents is increased. The work of Ritter et al. [6] proposed a

hypothetical IA-MDT system that used a ferromagnetic wire of micro-size implanted within blood vessel for capturing magnetic drug carrier particles (MDCPs). The principle of particle capture by high gradient magnetic field was applied to investigate the feasibility and efficacy of targeting MDCPs to specific site within blood vessel. The capture behaviors were considered on a plane that sliced through the wire's cross section and vessel's central axis. The magnetic and blood laminar flow fields around the wire were determined numerically. Capture behaviors were investigated by solving particle's equations of motion numerically and the capture efficiency was predicted for various parameters. It was shown that targeting of MDCPs using internally produced high gradient magnetic field was feasible and was hoped to be a promising technique that provided high targeting efficiency. Avilés and co-workers studied magnetic targeting of ferromagnetic nano-particles by ferromagnetic seeds implanted within capillary beds in both theoretical [9] and *in-vitro* experimental aspects [38]. Their results supported the feasible and efficacy of implant assisted-magnetic drug targeting (IA-MDT) proposed by Ritter et al. [6]. The work of Cregg et al. [39] extended the work of Avilés et al. [9] by considering superparamagnetic property of nano-particles of which diameter small than about 100 nm and determined particle's magnetic moment by using the Langevin function.

In this research, we further investigate the works of Ritter et al. [6] and Cregg et al. [39] by studying diffusive capture of ferromagnetic nano-particles by a micro-sized ferromagnetic wire implanted within blood vessel. Significant effect from diffusion process is taken into account. Diffusive capture behaviors are investigated on a plane that slices through wire's cross section. Particle dynamic is described statistically by the continuity equation. By solving the continuity equation as an initial and boundary value problem, the distribution of particle concentration on the considered plane can be determined. The feasibility of increasing nano-particle concentration in blood vessel by using the wire implanted in blood vessel is then investigated.

1.3 Thesis Objectives

In conclusion, the objectives of this thesis are:

1) To determine the capture efficiency of micro-particles in axial magnetic filters and to investigate the criterion of validity of the single-wire approximation.

2) To determine the targeting efficacy of nano-particles by a micro-size ferromagnetic wire in blood vessel.

1.4 Thesis Outline

A brief outlines of this thesis are as follows: Chapter I provides introduction to particle capture in high gradient magnetic field, background and objectives of this research. Chapter II describes basic theories of particle capture in high gradient magnetic field for both micro-and nano-particles. Also with the method for investigating capture behaviors and predicting capture efficiency. In Chapter III, the capture of weakly magnetic micro-particles, in high gradient magnetic filed, by an assemblage of randomly distributed cylindrical collectors in axial magnetic filters is investigated in details. The methods of particle dynamics simulation and filter efficiency prediction are also described. In Chapter IV, the capture of ferromagnetic nano-particles, in high gradient magnetic field, by a micro-size ferromagnetic wire implanted within blood vessel is investigated. Simulation methodologies are described. The results of the simulations and discussions were presented in Chapter V. Finally, Chapter VI provides the conclusions of this research.

CHAPTER II

Theory of Particle Capture in High Gradient Magnetic Field

In this chapter, the capture behaviors of various scales particles in high gradient magnetic field are described. In the first section, we describe the capture of weakly magnetic particle of micro-size which can be applied for the study of high gradient magnetic separation of biological entities, such as red and white blood cells [5, 23-24], using magnetic filters. The capture behaviors are investigated by analyzing particles' trajectories obtained from numerical solutions of particle's equations of motion. The capture efficiency is determined in terms of capture length or capture cross section. In the second section, we describe the capture of ferromagnetic nano-particles where the effect from diffusion is taken into account. Particle's behaviors are described statistically by using the continuity equation. The capture of ferromagnetic nano-particles can be applied for the study of both conventional magnetic drug targeting (MDT) [40-42] and implant assisted-magnetic drug targeting (IA-MDT) [9-11, 35-39].

2.1 The Capture of Weakly Magnetic Micro-Particles in High Gradient Magnetic Field

To capture weakly magnetic micro-particles from a fluid by using high gradient magnetic field, magnetic filters containing an assemblage of magnetic collectors are used. While in operation, the external uniform magnetic field $\vec{H}_0$ is applied across the magnetic collectors. Then the fluid containing the suspended particles is fed into the filter. The applied magnetic field magnetizes both the collectors and particles. By using an assumption that both particle and fluid are linear isotropic

homogeneous magnetic media of susceptibilities c_p and c_f, respectively, there exists the magnetic force acting on each particle which can be expressed as

$$\vec{F}_m = \frac{1}{2} m_0 \left(c_p - c_f \right) V_p \vec{\nabla} \left(H^2 \right), \tag{2.1}$$

where m_0 = $4\pi \times 10^{-7}$ H / m is the permeability of free space, V_p is volume of a particle and H is the magnetic field strength at particle 's position.

In this research, only dominant magnetic force ($\vec{F}_m$) and fluid drag force ($\vec{F}_v$) acting on the particles are considered while other forces, such as gravitational and electric forces, and processes, such as diffusion and collision, are not taken into account. The fluid drag force acting on a particle traveling in the fluid is assumed to satisfied Stokes' law and can be expressed as

$$\vec{F}_v = -6 p h b_p \left(\vec{v}_p - \vec{v}_f \right), \tag{2.2}$$

where h is fluid dynamic viscosity, b_p is particle radius, $\vec{v}_p$ and $\vec{v}_f$ are particle and fluid velocities, respectively. The motion of a particle in fluid satisfies Newton 's equation of motion,

$$\sum \vec{F} = m_p \vec{a}_p, \tag{2.3}$$

where $\sum \vec{F} = \vec{F}_m + \vec{F}_v$ is the total force acting on a particle, m_p is mass of a particle and $\vec{a}_p$ is particle acceleration.

For a given particle 's initial position and velocity, the equation of motion (2.3) can be solved, by using analytical or numerical methods, to obtain particle trajectory. Then particle's trajectories starting from various initial positions are analyzed and the probability for a particle entering the filter to be captured within the filter, which implies filter efficiency, can be determined. In this research, we study in detail the capture of weakly magnetic micro-particles in an axial magnetic filter containing an

assemblage of random magnetic wires. The details of the study will be described in Chapter III.

2.2 The Capture of Ferromagnetic Nano-Particles in High Gradient Magnetic Field

When particle size becomes much smaller than 1 micron, the effect of diffusion on particle motion becomes significant and should be taken into account also with the effect of magnetic force and fluid flow. Diffusion is the random process that causes fluctuation of particle's trajectories. Consequently, studying capture behaviors by considering and analyzing particle's trajectories may be inconvenient. Alternatively, capture behaviors of nano-particles in high gradient magnetic field can be described statistically in terms of particle volume concentration that satisfied the continuity equation.

2.2.1 The Continuity Equation

In 1983, Gerber et al. [28-29] formulated a theory of capture process of particles that were very smaller than 1 micron. Particle dynamics were described in terms of particle volume concentration denoted by c. The particle volume concentration at a given point in the fluid is defined as the fraction of particles volume contained in an infinitesimal volume element of the system (mixture of particle and fluid) at that point and can be expressed as

$$c \equiv \lim_{\nabla V_s \to 0} \frac{\Delta V_p}{\Delta V_s}, \tag{2.4}$$

where subscripts p and s refer to the particle and the system, respectively.

At any time, particle volume concentration in any volume elements of the system satisfies the continuity equation

$$\frac{\partial c}{\partial t} + \nabla \cdot \vec{J} = 0, \tag{2.5}$$

where $\vec{J}$ is the total particle volume flux that pass through the considered infinitesimal volume element. We define the particle volume flux as the net volume of particles that flow through an area perpendicular to the flow direction per unit area per unit time.

In this research, the total particle volume flux, $\vec{J}$, consistes of three contributions as

$$\vec{J} = \vec{J}_D + \vec{J}_C + \vec{J}_F, \tag{2.6}$$

where $\vec{J}_D$ is the diffusion flux due to diffusion, $\vec{J}_C$ is the convection flux due to fluid flow and $\vec{J}_F$ is the flux driven by the actions of external forces on the particles.

Diffusion flux satisfied Fick's law [28],

$$\vec{J}_D = -D\vec{\nabla}c, \tag{2.7}$$

where D is the diffusion coefficient of particles in the fluid. The convection flux caused by fluid flow can be expressed as

$$\vec{J}_C = c\vec{v}_f. \tag{2.8}$$

The particle volume flux driven by the actions of external forces on particles can be expressed as [28]

$$\vec{J}_F = cu\vec{F}, \tag{2.9}$$

where u is the mobility of particles in the fluid and $\vec{F}$ is the driving force that causes the relative velocity between particles and fluid. In this research, it is assumed that the

driving force is mainly contributed by the magnetic force hence $\vec{F} = \vec{F}_m$ and other forces and processes are not taking into account.

By substituting expressions of $\vec{J}_D$, $\vec{J}_C$ and $\vec{J}_F$ in Eqs. (2.7) to (2.9) in Eq. (2.5) we obtain the continuity equation as

$$\frac{\partial c}{\partial t} = \vec{\nabla} \cdot \left(D \vec{\nabla} c \right) - \vec{\nabla} \cdot \left(c \vec{v}_f \right) - \vec{\nabla} \cdot \left(cu \vec{F}_m \right). \tag{2.10}$$

The diffusion coefficient of particle in the fluid is assumed to satisfied Einstein' s relation [30],

$$D = uk_B T, \tag{2.11}$$

where k_B and T are the Boltzmann' s constant and the absolute temperature, respectively. The value of D is assumed to be isotropic hence the continuity equation (2.10) can be rewritten as

$$\frac{\partial c}{\partial t} = D \vec{\nabla}^2 c - \vec{\nabla} \cdot \left(c \vec{v}_f \right) - \vec{\nabla} \cdot \left(cu \vec{F}_m \right). \tag{2.12}$$

Equation (2.12) is the continuity equation which is used for describing the capture of nano-particles in high gradient magnetic field. By solving the continuity equation as an initial and boundary value problem, dynamics of concentration distribution and behaviors of particle transport within the considered regions can be investigated. In this research, the continuity equation is used for investigating the technique of implant assisted-magnetic drug targeting (IA-MDT). The technique of IA-MDT here uses a ferromagnetic wire of micro-size as an implant in a blood vessel for capturing nano-drug carriers that are injected into blood circulating system. We study the feasibility of increasing the concentration of nano-drug carriers in the region around the wire. The details of the study are described in Chapter IV.

CHAPTER III

Capture of Weakly Magnetic Micro-Particles by an Assemblage of Random Wires in Axial Magnetic Filters

In this chapter, we study the capture of weakly magnetic micro-particles by an assemblage of random magnetic wires in axial magnetic filters. Magnetic filters operating in axial mode are applied in the separating and capturing specific biological entities from fluid such as the separation of red blood cells (RBCs) and white blood cells (WBCs) from whole blood [5, 23-24]. For diagnostic objectives in clinical or laboratory applications, small amounts of blood samples are used and the specific cells are captured by small apparatuses consisting of only a single magnetic wire of micron size [23-24]. For therapeutic objectives such as blood component transfusion, the volumes of blood and also RBCs and WBCs to be processed are much larger than the diagnostic case and, therefore the design of an effective macro-scale filter of high efficiency is important. This would be very useful such as for plasma separation ready for use in compensating for the lost fluids and blood proteins in burn victims [25] and also other therapeutic applications of blood components. To study micro-particles captures by random wires, the effective medium treatment (EMT) of axial magnetic filters is applied. The magnetic field around an assemblage of random cylindrical collectors transversely magnetized by background uniform magnetic field $\vec{H}_0$ calculated by Natenapit [18] is used to determine the magnetic field around a representative wire in an axial filter. The velocity field of viscous fluid flow axially pass a bundle of parallel cylinder derived by Hapepel [22] is used to determine fluid velocity field around the representative wire in the filter. Particle trajectories are traced numerically. Filter efficiency is determined in terms of the capture cross-section. We generalize the single-wire model to more general cases of higher packing fraction.

3.1 Character of the Problem

We consider an axial magnetic filter that consisted of an assemblage of randomly distributed parallel magnetic wires. A viscous suspension is fed axially through the filter with an entrance velocity $\vec{V}_0$. All wires in the filter are magnetized by an applied uniform magnetic field $\vec{H}_0$ that is perpendicular to wires' axes. A dimensionless cylindrical coordinates system (r_a, q, z_a), of which all linear distances were normalized by the wire radius (a), is introduced with the z_a axis parallel to the wires' axes. A particle with radius b_p is carried by the suspension. Figure 3.1 depicts the configuration of coordinates used in the study. In Fig. 3.1, $\vec{v}_{za}$ is the component of particle velocity, normalized by wire' s radius, in the direction that parallel to wire's axis.

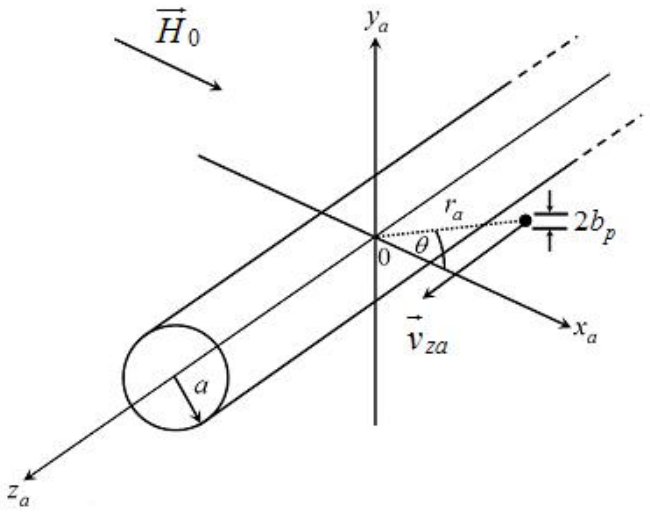

Figure 3.1: The axial mode of particle capture in high gradient magnetic field and the associated coordinates setting.

3.2 The Magnetic Field in the Filter

Determining the magnetic field in the filter is one major contribution to the study of the capture process. In an axial filter which contains many wires, the existence of other wires produces certain effects on the capture behavior of each individual wire. In this study, all parallel wires in the filter are assumed to be randomly distributed. When an arbitrary wire is considered, all residual wires locate randomly with respect to it. This situation is the same for any wire in the filter so it is reasonable to approximate that all wire in the filter exhibit the same capture behavior and the capture behavior of only one representative wire is investigated.

The effective medium treatment (EMT) originally conceived by Hashin [43] was adopted in the work of Natenapit [18] to determine the magnetic field in a two dimensional system of cylindrical magnetic wires randomly distributed in a fluid medium. According to the EMT, the system of magnetic cylindrical wires (permeability m_c) and surrounding fluid (permeability m_f) is considered to be composed of cylindrical composite cells, each of which contains exactly one wire. The ratio of the wire to cell volume is set to be equal to the packing fraction, F, of wires in the filter or $a^2/b^2 = F$ where a and b are radii of the representative wire and the cell, respectively. In the calculation procedure, only a representative cell is considered while all residual neighbouring cells are replaced by a homogeneous effective medium with the effective permeability m^* which can be determined. Figure 3.2 depicts a representative cell in the effective medium model.

The boundary value problem of a coaxial magnetic cylinder subjected to the boundary condition of a uniform magnetic field in the direction perpendicular to the wires' axes was solved to determine the magnetic field in the cell and the effective medium. A self consistency must be satisfied that the magnetic induction averaged over the representative cell (cylindrical wire and fluid tube) has to be equal to the volume average of the magnetic induction over the effective medium.

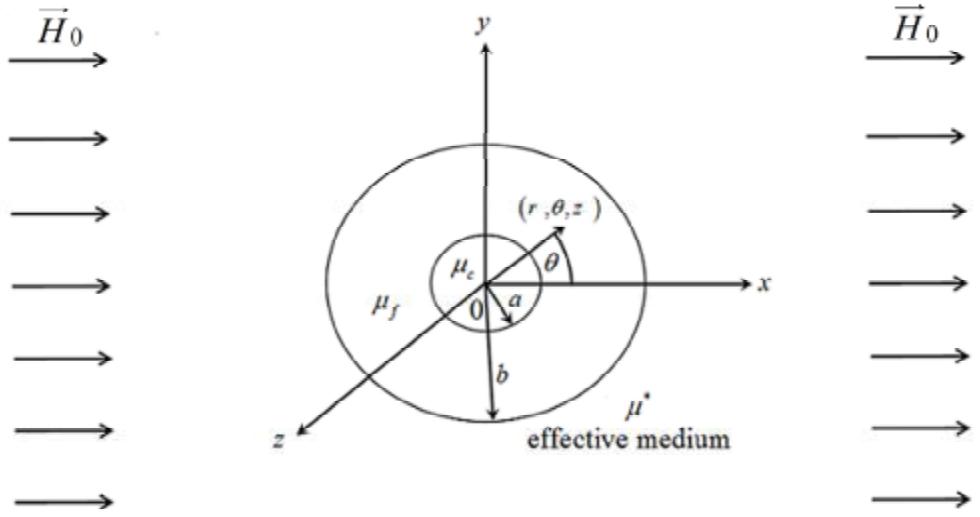

Figure 3.2: A representative cell and surrounding effective medium with associated coordinates setting.

According to Natenapit [18] and Natenapit and Sanglek [17], the magnetic field in the fluid region surrounding the representative wire in the cell was determined as

$$\vec{H} = AH_0\left[\left(1+\frac{K_c}{r_a^2}\right)\cos\theta\,\hat{r} - \left(1-\frac{K_c}{r_a^2}\right)\sin\theta\,\hat{\theta}\right],\ 1<r_a<b/a, \qquad (3.1)$$

where $r_a = r/a$, $A = 1/(1-FK_c)$, $K_c = (n-1)/(n+1)$, and $n = m_c/m_f$.

The magnetic field in the effective medium outside the representative cell was determined as

$$\vec{H}_{eff} = \vec{H}_0, \quad b/a < r_a < \infty. \qquad (3.2)$$

From equation (3.1), it is observed that the magnetic effect of the other wires on the magnetic field around the representative wire is contained in the factor A. In the limit of dilute packing fraction (F approaches zero), factor A approaches unity and the

problem is reduced to the case of single-wire approximation. Consequently, it is seen that, by using the EMT, the problem of micro-particle capture by an assemblage of random cylindrical wires can simply analyzed by considering a single representative cell.

3.3 The Fluid Axial Flow Profile in the Filter

Determination of the fluid flow profile in the filter is also an important contribution to the study of the capture process. The fluid axial flow profile around a system of parallel cylinders was determined using the effective medium approximation of Li and Park [44]. However, the result contained rather complicated special functions and the more practical and most successful laminar axial flow field for viscous fluid passing through a filter, as derived by Happel [22] using the cell model, is applied in this study and this can be expressed as

$$v_{za}(r_a) = \frac{FV_{0a}}{2Ku}\left(1 - r_a^2 + \frac{2}{F}\ln r_a\right), \tag{3.3}$$

where $v_{za} = v_z / a$ is the magnitude of a normalized fluid velocity component in the z_a direction which is parallel to wire axis, $Ku = F - 0.5\ln F - 0.25F^2 - 0.75$ is Kuwabara's constant and $V_{0a} = V_0 / a$ is the magnitude of the normalized fluid entrance velocity. If the inertia of the particle is neglected then the component of the normalized particle velocity in the z_a direction is always equal to the v_{za} of the fluid.

3.4 Equations of Motion

To investigate particle capture, equations of motion are constructed and solved numerically to obtain particle trajectories which are analyzed later. For micro-particle, it is assumed that the magnetic and fluid drag forces are the major forces while the other forces and effects such as gravitational force, inertial effect, thermal diffusion,

etc. are neglected. The magnetic force acting on a particle when it is traveling in the fluid that is flowing in the region of high gradient magnetic field can be expressed as [14]

$$\vec{F}_m = \frac{1}{2} m_0 \left(c_p - c_f \right) V_p \vec{\nabla} \left(H^2 \right), \tag{3.4}$$

where c_p and c_f are the particle and fluid magnetic susceptibilities, respectively, m_0 is the magnetic permeability of free space, V_p is the volume of a particle, and H is the magnetic field strength at the position of the particle. The fluid drag force ($\vec{F}_d$) is assumed to satisfies Stokes' law,

$$\vec{F}_d = -6 p h b_p \left(\vec{v}_p - \vec{v}_f \right), \tag{3.5}$$

where h is fluid viscosity, b_p is particle radius, $\vec{v}_p$ and $\vec{v}_f$ are particle and fluid velocities, respectively.

By substituting Eq. (3.1) in Eq. (3.4), the magnetic force can be expressed as

$$\vec{F}_m = -\frac{8 p m_0 \left(c_p - c_f \right) K_c H_0^2 b_p^3 A^2}{3a} \left[\left(\frac{\cos 2q}{r_a^3} + \frac{K_c}{r_a^5} \right) \hat{r} + \left(\frac{\sin 2q}{r_a^3} \right) \hat{q} \right]. \tag{3.6}$$

The radial and angular components of particle acceleration are [45]

$$a_r = \frac{d^2 r}{dt^2} - r \left(\frac{dq}{dt} \right)^2 \tag{3.7a}$$

and

$$a_q = r \frac{d^2 q}{dt^2} + 2 \left(\frac{dr}{dt} \right) \left(\frac{dq}{dt} \right). \tag{3.7b}$$

Particle equations of motion for each coordinate are

$$F_{mr} + F_{vr} = m_p a_r \,, \tag{3.8a}$$

$$F_{mq} + F_{vq} = m_p a_q \,, \tag{3.8b}$$

$$v_{pz} = v_{fz} \,. \tag{3.8c}$$

In equation (3.8c), the component of particle velocity in the direction parallel to wire' s axis is assigned equal to that of fluid since it is seen in equation (3.6) that magnetic force in that direction is equal to zero so particles do not have relative velocity respective to fluid in the direction parallel to wire 's axis . By using Eqs. (3.3), (3.5), (3.6), (3.7a), and (3.7b) in Eqs. (3.8a) to (3.8c), and writing particle mass as product of density and particle volume we obtain

$$\left(\frac{2r_p b_p^2}{9h}\right)\left[\frac{d^2 r_a}{dt^2} - r_a\left(\frac{dq}{dt}\right)^2\right] + \frac{dr_a}{dt} = -V_{ma}A^2\left(\frac{\cos 2q}{r_a^3} + \frac{K_c}{r_a^5}\right), \tag{3.9a}$$

$$\left(\frac{2r_p b_p^2}{9h}\right)\left[r_a\frac{d^2 q}{dt^2} + 2\left(\frac{dr_a}{dt}\right)\left(\frac{dq}{dt}\right)\right] + r_a\frac{dq}{dt} = -V_{ma}A^2\left(\frac{\sin 2q}{r_a^3}\right), \tag{3.9b}$$

$$v_{pz} = \frac{FV_0}{2Ku}\left(1 - r_a^2 + \frac{2}{F}\ln r_a\right), \tag{3.9c}$$

where $V_{ma} = V_m / a$, $V_m = 4m_0\left(c_p - c_f\right)H_0^2 b_p^2 K_c / 9ha$ is the magnetic velocity.

From Eqs. (3.9a) and (3.9b), we consider the order of magnitude of various terms. It is estimated that $b_p : 10^{-6}$ m, $r_p : 10^3$ kg/m^3, $h : 10^{-3}$ Pa·s, $c_p - c_f : 10^{-3}$, $H_0 : 10^5$ A/m, $a : 10^{-5}$ m, $K_c : 1$, and $A : 1$. We obtain that $2r_p b_p^2 / 9h : 10^{-6}$ and $V_{ma}A^2 : 10$ so Eqs. (3.9a) and (3.9b) can be simplified by neglecting the first term on the left hand side of each equation and we obtain particle 's equations of motion within the representative cell ($1 < r_a < b/a$) as

$$\frac{dr_a}{dt} = -V_{ma}A^2\left(\frac{K_c}{r_a^5} + \frac{\cos 2q}{r_a^3}\right), \tag{3.10a}$$

$$\frac{dq}{dt} = -V_{ma}A^2\left(\frac{\sin 2q}{r_a^4}\right), \tag{3.10b}$$

$$\frac{dz_a}{dt} = \frac{FV_{0a}}{2Ku}\left(1 - r_a^2 + \frac{2}{F}\ln r_a\right), \tag{3.10c}$$

The equations of motion (3.10a) to (3.10c) are solved numerically by using the standard fourth-order Runge-Kutta method and the particle trajectories are traced. A particle is captured if its trajectory intercepts the wire surface within the filter length. From Eq. (3.2), it is seen that $\vec{F}_m$ = 0 outside the representative cell. Consequently, any particles travelling outside the representative cell are not captured and are carried through the filter by fluid flow.

3.5 Capture Cross-Section and Filter Efficiency

The capture cross-section (A_c) of a representative wire is defined as a certain area on a plane perpendicular to the wire's axis at the entrance of the filter. Any particles which enter the filter within the region of capture cross-section is always captured on the wire surface at a certain distance z_a along the wire axis not more than $l_a = l/a$ where l is the filter length. According to the EMT model, the capture cross-section of a representative wire is bounded by the normalized radius, in the unit of wire radius (a), of the fluid envelope around that wire equal to $1/\sqrt{F}$ since the magnetic force is equal to zero outside the fluid envelope. The boundary of the capture cross-section area is determined by using trajectory-analysis methods. Dividing Eq. (3.10a) by Eq. (3.10b), we obtain dr_a/dq which is a function of K_c. Dividing Eq. (3.10c) by Eq. (3.10b) we obtain, with a little arrangement, $dz_a\left(V_m/V_0\right)/dq$ as a function of F and K_c. It is, therefore, suitable to use the normalized distance $z_a\left(V_m/V_0\right)$ instead of z_a

and then capture cross-section A_c depends on the parameters K_c, F and the normalized filter length $L_a = (V_m / V_0) l_a$.

Suppose that N is the number of wires in the filter, then the total capture cross-section in the filter equals NA_c. Let A_{filter} be the filter cross-section. The filter efficiency, denoted by e, can be determined as the ratio between the total capture cross-section and the filter cross-section, $e = NA_c / A_{filter}$. Since the packing fraction (F) is $Np\,a^2 / A_{filter}$, then the filter efficiency can be expressed as

$$e = FA_{ca}, \tag{3.11}$$

where $A_{ca} = A_c / p\,a^2$ is the capture cross-section normalized by the wire cross-section.

3.6 Computational Method

Particle trajectories and capture cross-sections are obtained by using computational method. Main computational procedures can be described as follows.

Step 1: Set up parameters such as K_c, F, L_a. An additional computational parameter Δt required for the stability and accuracy of the results is also assigned. After parameters are assigned, various constants such as A, radius of fluid envelop $1/\sqrt{F}$, Ku, etc. can be computed.

Step 2: Determine the boundary of fluid envelop.

Step 3: Compute capture cross-section by using numerical integration and then compute filter efficiency. Procedures for determining the boundary of capture cross-section can be described by a flowchart shown in Fig. 3.3. We can conclude all procedures in Fig. 3.3 as follows. For each angle q_i, we collect values of r_{ai}, where $1 \le r_{ai} \le 1/\sqrt{F}$, that cause the particle to be captured at certain distances $z_{ae} \le l_a$ on the wire surface. Then we select the optimum r_{ai} that gives the maximal capture distance z_{ae}. After these processes are performed for every q_i that $0 \le q_i \le p/2$ (we determine the boundary of capture cross-section only in the first quadrant because of

the symmetry of capture cross-section around the wire), we obtain locus of points (r_{ai}, q_i) which is the boundary of capture cross-section. Then we integrate numerically the area within the boundary of capture cross-section and obtain the capture cross-section area. Finally, filter efficiency can be computed by using Eq. (3.11).

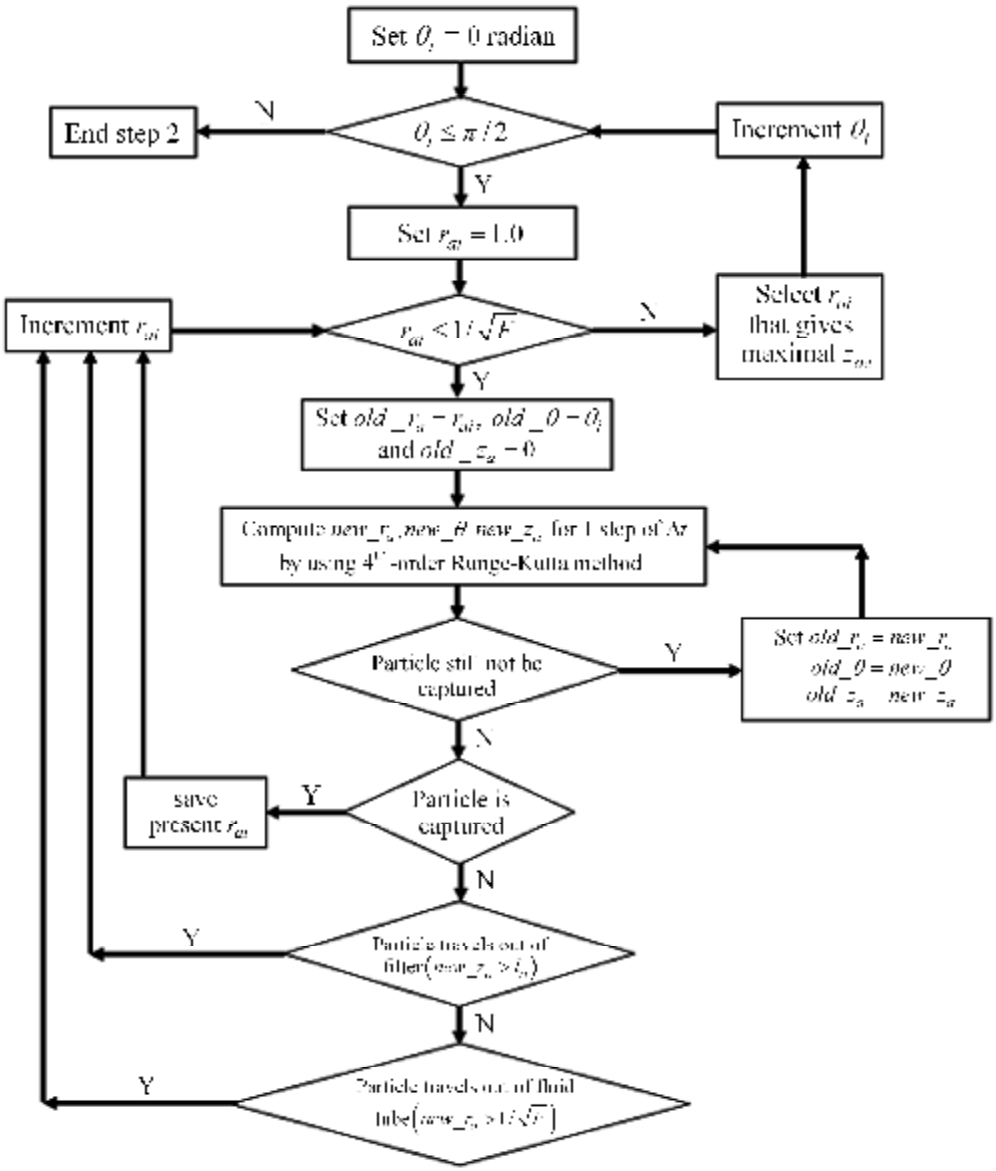

Figure 3.3: The computational procedure of determining capture cross-section.

CHAPTER IV

Capture of Ferromagnetic Nano-Particles by Ferromagnetic Wires Implanted in Blood Vessel

In this chapter, we study the capture of ferromagnetic nano-particles by ferromagnetic wires implanted in a blood vessel. The objective of the study is to investigate the feasibility of using implant assisted-magnetic drug targeting (IA-MDT) to increase the chance of targeting magnetic nano-therapeutic particles at specific site in blood vessel when the effect of nano-particle diffusion is taken into account.

The work of Ritter et al. [6] proposed a hypothetical magnetic drug targeting system that used a ferromagnetic wire of micro-size implanted within blood vessel for capturing magnetic drug carrier particles (MDCPs). The principle of particle capture by high gradient magnetic field was applied to investigate the feasibility and efficacy of targeting MDCPs to specific site within blood vessel. In their work, the capture behaviors were considered on a plane that perpendicularly slice through the wire's cross section. The magnetic and blood laminar flow fields around the wire were determined numerically. Capture behaviors were investigated by solving particle's equations of motion numerically and the capture efficiency was predicted for various parameters. It was shown that targeting of MDCPs using internally produced high gradient magnetic field was feasible and was hoped to be a promising technique that provided high targeting efficiency. Avilés and co-workers studied magnetic targeting of ferromagnetic nano-particles by ferromagnetic seeds implanted within capillary beds in both theoretical [9] and *in- vitro* experimental aspects [11]. Their results supported the feasible and efficacy of implant assisted-magnetic drug targeting (IA-MDT) proposed by Ritter et al. [6]. The work of Cregg et al. [39] extended the work of Avilés et al. [9] by considering superparamagnetic property of nano-particles and determined particle's magnetic moment by using the Langevin function. Nacev et al. [46] studied the

behaviors of ferromagnetic nano-particles in blood vessels and surrounding tissues under applied magnetic force by taking into account the effect of particle diffusion.

In this research, the work of Ritter et al. [6] is extended by studying diffusive capture of ferromagnetic nano-particles by a ferromagnetic micro-wire implanted in a blood vessel. Today, the technologies of fabricating biocompatible micro- and nano-wires used for biomedical applications has been developed continuously [47]. In this research, we study the using of ferromagnetic micro-wire implanted within a blood vessel for targeting ferromagnetic nano-therapeutic particles to specific site around the wire. Significant effect from diffusion of nano-particles is taken into account. The two-dimensional diffusive capture behaviors are investigated on a plane that perpendicularly slices through wire's cross section. Particle dynamics are described statistically by the continuity equation. By solving the continuity equation as an initial and boundary values problem, the distribution of particle concentration in regions around the wire can be determined. The feasibility of increasing the concentration of nano-therapeutic particles at the target in blood vessel by using IA-MDT is investigated.

4.1 Statements of the Problem

Consider an assemblage of ferromagnetic wires implanted within a certain length of a blood vessel. There exists a background uniform magnetic field $\vec{H}_0$ across the considered vessel's length in the direction transverse to the incoming blood flow direction. It is assumed that the wire orientation is transverse to both background uniform magnetic field $\vec{H}_0$ and the incoming blood flow. The ferromagnetic nano-particles are carried by the blood stream towards the region of $\vec{H}_0$. According to the existence of the wires in the background uniform field $\vec{H}_0$, the high gradient magnetic fields produced around the wires. Consequently, certain amounts of the incoming nano-particles are subjected to magnetic force that depends significantly on the magnetic field gradient. These particles are attracted toward each wire and are concentrated there. In this research, we assumed that the volume fraction of ferromagnetic wires in

the considered vessel's length is very low hence the single-wire approximation of the magnetic and blood flow fields around each wire is used and the process of nano-particle capture is considered only for a wire. Figure 4.1 shows the feature of the problem to be studied.

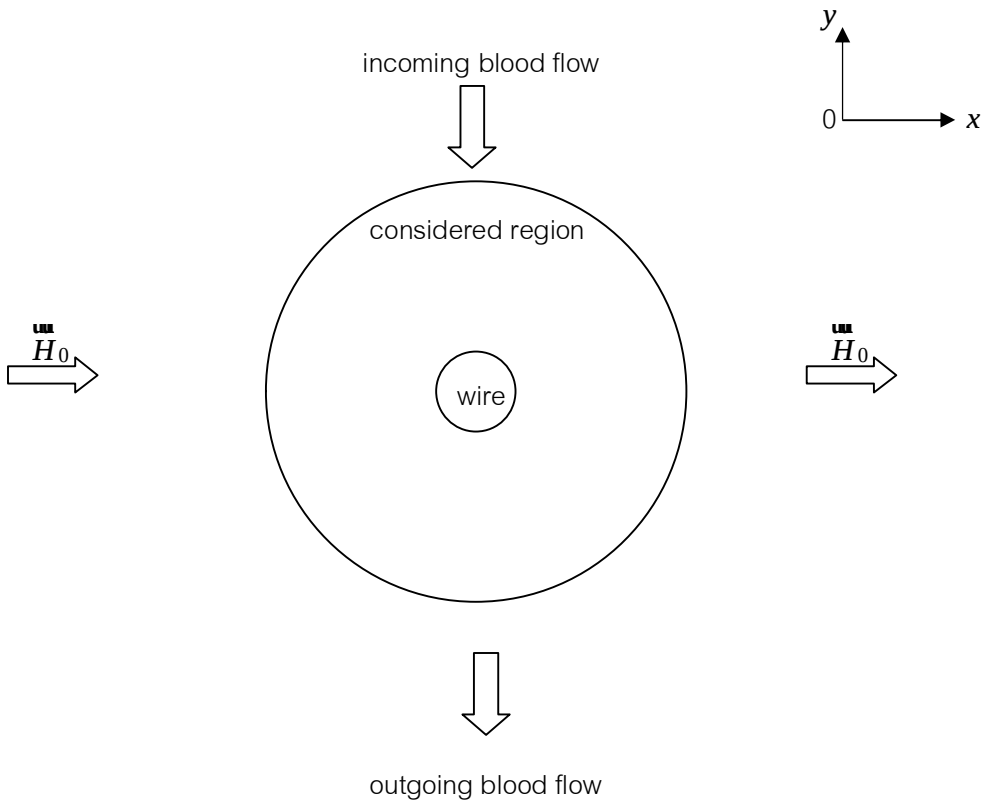

Figure 4.1: The feature of the problem.

In Fig. 4.1, it is considered that the length of the wire is much higher than its radius. Consequently, the problem has the symmetry in the direction of wire' s axis and the complexity of the problem is reduced from three to two dimensions. The considered region for studying diffusive capture of nano-particles is a circular region on a plane normal to wire' s axis that slices through wire's cross section. The considered region has the same center as the wire. In this research, dynamics of nano-particle transport in the region around each wire is governed by three dominant effects as particle diffusion,

convections by blood flow and magnetic drift velocity. Since the magnetic force produced by the magnetic field gradient around the wire surface is a short range force, the radius of the considered region is limited at 10 times of wire's radius and it is assumed that the effect of magnetic force on particles in regions which are farther than 10 times of wire's radius from wire's axis is negligible. We formulate and solve the continuity equation in the considered region. According to the values of micro-wire radius (a : 10^{-6} m.), the average velocity of blood flow in blood vessel (V_0 : 10^{-2} m/s), the value of blood density ($r_b = 1040$ kg/m^3) and the value of blood viscosity ($h_b = 2.0 \times 10^{-3}$ Pa·s), Reynold number of blood flow pass the micro-wire, $\mathrm{Re} = 2a r_b V_0 / h_b$, is much smaller than unity. Consequently, blood flow around the micro-wire is modeled as a laminar flow field of single-phase Newtonian fluid which is the same as that in the work of Avilés et al. [9] and Cregg et al. [39].

4.2 The Magnetic Force Acting on the Ferromagnetic Nano-Particles

According to Jackson [48], the magnetic force, $\vec{F}_m$, acting on a ferromagnetic particle of magnetic moment $\vec{m}$ and locates in a region of magnetic flux density $\vec{B}$ can be expressed as

$$\vec{F}_m = \vec{\nabla}\left(\vec{m} \cdot \vec{B}\right). \tag{4.1}$$

If the magnetic flux density is a steady state field or $\vec{\nabla} \times \vec{B} = 0$ then the Eq. (4.1) has its equivalent form as [48]

$$\vec{F}_m = \left(\vec{m} \cdot \vec{\nabla}\right)\vec{B}. \tag{4.2}$$

So, to determine the magnetic force acting on a ferromagnetic particle, particle magnetization $\vec{M}$ and the magnetic flux density field $\vec{B}$ at particle 's position must be determined.

In this research, we consider that the magnetizations of ferromagnetic materials in wire and nano-particles vary linearly with local magnetic field before the magnetizations of the materials are saturated. The magnetizations of the materials are constants after they are saturated. This approximation is used by many authors [6, 9, 11, 41]. It can be expressed that

$$\vec{M} = c\vec{H}, \tag{4.3a}$$

before magnetizations of the materials are saturated where c is the material 's magnetic susceptibility. When ferromagnetic materials in wire and particles are saturate magnetized, the magnetization is a constant vector and can be expressed as

$$\vec{M} = \vec{M}_s, \tag{4.3b}$$

where $\vec{M}_s$ is the saturation magnetization of the considered ferromagnetic material. From Eq. (4.3a), if we define $w_{fm,p}$ as the volume fraction of ferromagnetic material contained within a particle, the magnetic force acting on a spherical particle that is not saturated magnetized can be expressed as

$$\vec{F}_m = \frac{1}{2} V_p m_0 w_{fm,p} c_p \vec{\nabla}\left(H^2\right), \tag{4.4}$$

where $c_p = 3c_{fm,p,0} / \left(3 + c_{fm,p,0}\right)$ is magnetic susceptibility of the particle, $c_{fm,p,0}$ is the magnetic susceptibility of ferromagnetic material in the particle at zero magnetic field and H is the local magnetic field at particle' s position. In Eq. (4.4), the magnetic susceptibility of blood is neglected since it is much smaller than that of ferromagnetic material in the particle. When the ferromagnetic material within the particle is saturate magnetized, the magnetic force acting on the particle can be expressed as

$$\vec{F}_m = V_p m_0 w_{fm,p} M_{fm,p,s} \vec{\nabla}\left(H\right), \tag{4.5}$$

where $M_{fm,p,s}$ is the saturation magnetization of the ferromagnetic material in the particle. The expressions of magnetic forces in Eq.s (4.4) and (4.5) are used for particles of which ferromagnetic core contains many ferromagnetic domains. For smaller particles that its ferromagnetic cores contains only single ferromagnetic domain and thermal agitation of particle's magnetic moment vector $\left(\vec{m}\right)$ becomes significant, particles' magnetic property is then superparamagnetic type [29, 39] and the magnetic moment $\left(\vec{m}\right)$ can be described, by using the Langevin function, as [39]

$$\vec{m} = w_{fm,p} V_p M_{fm,p,s} L(b) \frac{\vec{B}}{B}, \tag{4.6}$$

where $b = w_{fm,p} V_p M_{fm,p,s} B / kT$ is the Langevin argument and

$$L(b) = \coth(b) - \frac{1}{b} \tag{4.7}$$

is the Langevin function.

According to wire's geometry, we use a normalized coordinates (r_a, q) for describing the magnetic field and particle concentration distribution around the wire. The coordinate $r_a = r / a$ is the radial distance from the wire center in unit of wire radius a, and q is measured from the positive x axis in counter clock-wise direction.

The magnetic field $\vec{H}$ outside the wire that is magnetized by an applied uniform magnetic field $\vec{H}_0$ perpendicular to wire's axis, as shown in Figure 4.2, can be determined as [15]

$$\vec{H}(r_a, q) = H_0 \left[\left(1 + \frac{K_W}{r_a^2} \right) \cos q \hat{r} - \left(1 - \frac{K_W}{r_a^2} \right) \sin q \hat{q} \right]. \tag{4.8}$$

The value K_W in Eq. (4.9) is the magnetic constant of the wire which depends on the value of $\vec{H}_0$. If the magnetization of ferromagnetic material contained in the wire is not saturated, the value of K_W is

$$K_W = \frac{c_{W,0}}{2 + c_{W,0}}, \tag{4.9a}$$

where $c_{W,0}$ is magnetic susceptibility of ferromagnetic material in the wire at zero magnetic field. In contrast, at higher magnetic field strength, the ferromagnetic material in the wire is saturate magnetized, the value of K_W is

$$K_W = \frac{M_{W,s}}{2H_0}, \tag{4.9b}$$

where $M_{W,s}$ is the saturation magnetization of ferromagnetic material in the wire.

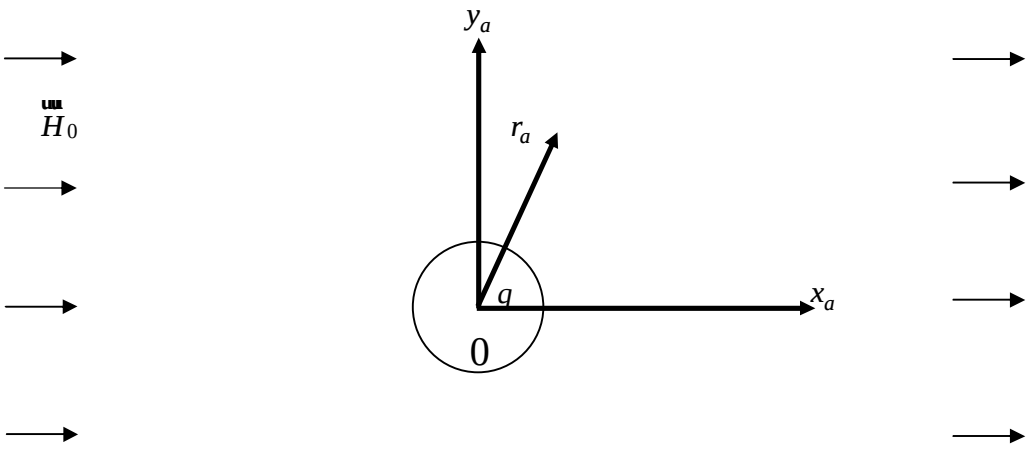

Figure 4.2: The ferromagnetic wire magnetized perpendicularly to the wire axis by a background uniform magnetic field $\vec{H}_0$.

By using the expression of the magnetic field in Eqs. (4.8), we can obtain analytical expressions of the magnetic force acting on ferromagnetic nano-particles for

various situations as follows. The magnetic forces in Eqs. (4.4) and (4.5) can be expressed respectively as

$$\vec{F}_{m,non-sat} = \left(\frac{-2\pi V_p w_{fm,p} c_p K_W H_0^2}{a} \right) \left[\left(\frac{\cos 2\theta}{r_a^3} + \frac{K_W}{r_a^5} \right) \hat{r} + \left(\frac{\sin 2\theta}{r_a^3} \right) \hat{\theta} \right] \quad (4.10)$$

and

$$\vec{F}_{m,sat} = \left(\frac{-2\pi V_p w_{fm,p} M_{fm,p,s} K_W H_0^2}{aH} \right) \left[\left(\frac{\cos 2\theta}{r_a^3} + \frac{K_W}{r_a^5} \right) \hat{r} + \left(\frac{\sin 2\theta}{r_a^3} \right) \hat{\theta} \right]. \quad (4.11)$$

In similar way, we can express the magnetic force acting on a very small ferromagnetic nano-particle that contains only one magnetic domain as

$$\vec{F}_{m,Langevin} = \left(\frac{-2\pi V_p w_{fm,p} M_{fm,p,s} K_W H_0^2}{aH} \right) f(b) \left[\left(\frac{\cos 2\theta}{r_a^3} + \frac{K_W}{r_a^5} \right) \hat{r} + \left(\frac{\sin 2\theta}{r_a^3} \right) \hat{\theta} \right], \quad (4.12)$$

where ,

$$f(b) = \coth(b) - b \csc h^2(b) \quad (4.13)$$

and $b = w_{fm,p} V_p M_{fm,p,s} B / kT$ is the Langevin argument. The expressions of magnetic force in Eqs. (4.10) to (4.12) are used for the study of ferromagnetic nano-particles capture by high gradient magnetic field in various situations.

4.3 The Velocity Field of Blood Flow in Blood Vessel

The flow of blood in the blood vessels such as microvasculatures and capillaries is treated as a laminar flow of incompressible, single-phase Newtonian [9, 39] that satisfies the continuity equation

$$\vec{\nabla}\cdot\vec{v}_b = 0\,, \tag{4.14}$$

and the Navier-Stokes equation,

$$r_b\left[\left(\vec{v}_b\cdot\vec{\nabla}\right)\vec{v}_b\right] = -\vec{\nabla}P + h_b\vec{\nabla}^2\vec{v}_b\,, \tag{4.15}$$

where r_b, P, and h_b are blood density, local pressure in blood vessel and blood viscosity, respectively.

To obtain blood flow field within the considered region that surrounds a representative wire, Eqs. (4.14) and (4.15) are solved numerically. The two-dimensional problem is assumed since the length of the representative wire is considered very smaller than vessel' diameter. Moreover, the variation of velocity of blood that flow towards the considered region is very little. Consequently, it is approximated that the blood flowing towards the considered region has uniform velocity distribution as average blood velocity in the vessel. The numerical values of blood velocity components are determined numerically and are saved in output files. The values are read and used in the simulation program for solving the continuity equation of particle volume concentration.

4.4 The Continuity Equations Describing Diffusive Capture

In this section, we derive the continuity equations used in the simulation. Consider the continuity equation, Eq. (2.12), in Chapter II,

$$\frac{\partial c}{\partial t} = D\vec{\nabla}^2 c - \vec{\nabla}\cdot\left(c\vec{v}_b\right) - \vec{\nabla}\cdot\left(cu\vec{F}_m\right), \tag{4.16}$$

where c is particle volume concentration, D is particle diffusion coefficient, $u = DkT$ is particle mobility, k is Boltzmann's constant and T is the absolute temperature. We define normalized time t, vector $\vec{G}_v$ and $\vec{G}_m$ as

$$t = \frac{Dt}{a^2}, \tag{4.17}$$

$$\vec{G}_v = \frac{a\vec{v}_b}{D}, \tag{4.18}$$

$$\vec{G}_m = \frac{a\vec{F}_m}{kT}, \tag{4.19}$$

and then by using the expression of Laplacian and divergence operators in coordinates (r_a, q) we obtain the continuity equation used for the simulation as

$$\frac{\partial c}{\partial t} = \left\{ \frac{\partial^2 c}{\partial r_a^2} + \frac{1}{r_a}\frac{\partial c}{\partial r_a} + \frac{1}{r_a^2}\frac{\partial^2 c}{\partial q^2} \right\} - \left\{ \frac{G_r c}{r_a} + \frac{\partial}{\partial r_a}(G_r c) + \frac{1}{r_a}\frac{\partial}{\partial q}(G_q c) \right\}, \tag{4.20}$$

where

$$G_r = G_{vr} + G_{mr} = \frac{6ph_b a v_{br} + F_{mr}}{kT}, \tag{4.21}$$

and

$$G_q = G_{vq} + G_{mq} = \frac{6ph_b a v_{bq} + F_{mq}}{kT}. \tag{4.22}$$

The values of v_{br} and v_{bq} are obtained from the numerical values of blood velocity components in blood vessel that are saved in the data files. The value of F_{mr} and F_{mq} are determined by using analytical expression of the magnetic force for each case.

The continuity equation (4.20) is used to determine particle concentration in ordinary regions that are not adjacent to impervious surfaces (the surface of the wire and the surface of static build-up of particle). For regions that are adjacent to impervious surfaces, the governing continuity equation has the different form and can be expressed as [30]

$$\frac{\partial c}{\partial t} = \frac{1}{r_a^2}\frac{\partial^2 c}{\partial q^2} - \frac{1}{r_a}\frac{\partial}{\partial q}(G_q c) + \frac{1}{d r_a}\left(G_r c - \frac{\partial c}{\partial r_a}\right), \qquad (4.23)$$

where $d r_a$ is the normalized radial distance from the impervious surface to the center of the considered region. The details of deriving Eq. (4.23) are shown in the Appendix A.

4.5 Simulation Methodology

4.5.1 The Explicit Finite Difference Method

Dynamics of diffusive capture in the considered region are investigated by obtaining time-dependent solutions of the continuity equations (4.20) and (4.23). In this research, we solve the continuity equations (4.20) and (4.20) by using the explicit finite difference method. The circular region shown in Fig. 4.1 is divided into many elements by dividing normalized radial distance r_a and angle q, as shown in Figure 4.3.

In Fig. 4.3, each element is specified by two indices i and j that indicate the radial and angular position (r_{am}, q_m) at the center of the element. The value of coordinates (r_{am}, q_m) at the center of an element indexed by (i, j) can be determined from

$$(r_{am})_i = 1 + (i + 0.5)(\Delta r_a), \qquad 0 \le i \le i_{\max}, \quad (4.24)$$

$$(q_m)_j = (j + 0.5)(\Delta q), \qquad 0 \le j \le j_{\max}, \quad (4.25)$$

where $i_{\max}$ is the normalized distance index at the most outer element and $j_{\max}$ is the angular index of the largest angle. The values of $i_{\max}$ and $j_{\max}$ depend on the step sizes Δr_a and Δq.

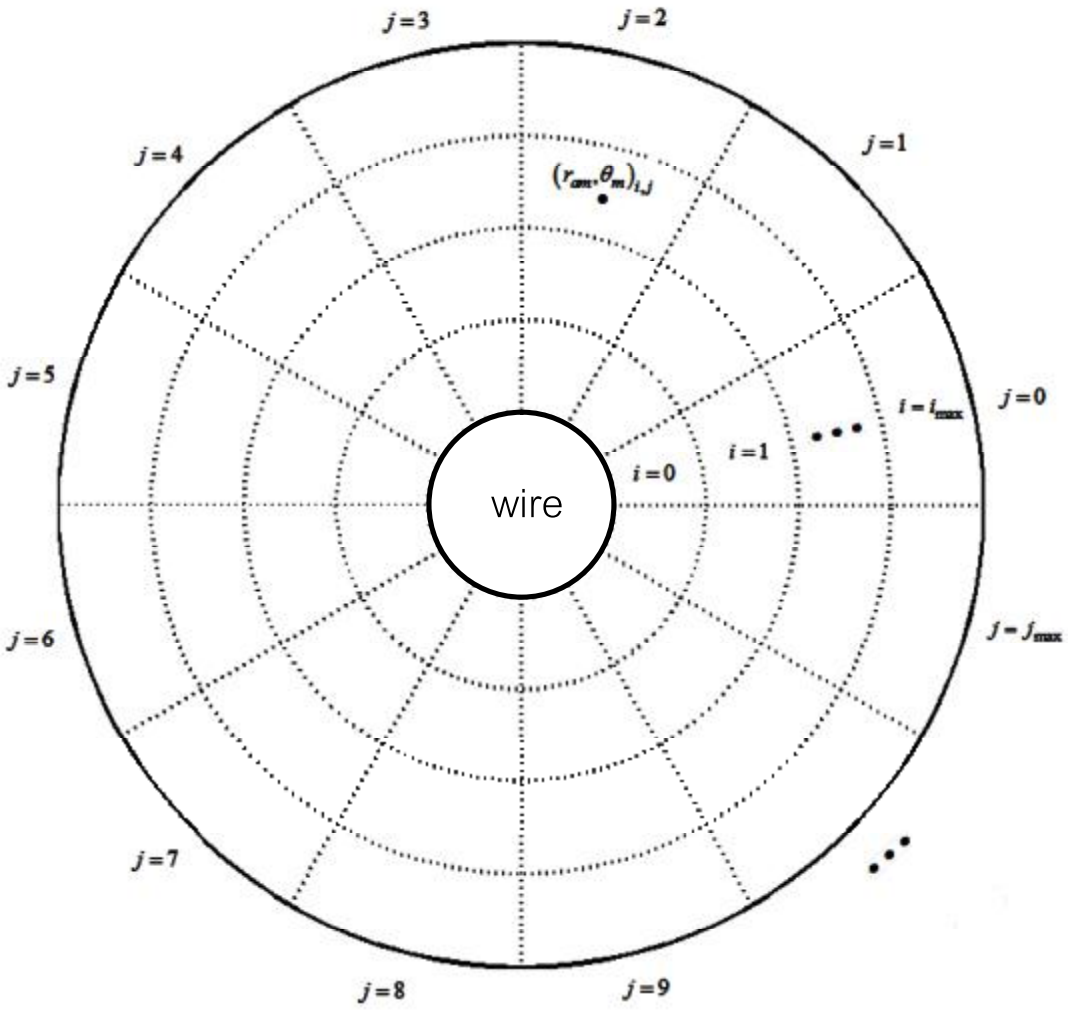

Figure 4.3: Dividing of considered region into many elements.

By using the explicit finite difference method, the continuity equations (4.20) and (4.23) are approximated with their corresponding difference equations. Consider Eq. (4.20), by expanding derivatives of variable multiplications we obtain the equation

$$\frac{\partial c}{\partial t} = \frac{\partial^2 c}{\partial r_a^2} + \frac{1}{r_a}\frac{\partial c}{\partial r_a} + \frac{1}{r_a^2}\frac{\partial^2 c}{\partial q^2} - \frac{G_r c}{r_a} - G_r \frac{\partial c}{\partial r_a} - c\frac{\partial G_r}{\partial r_a} - \frac{G_q}{r_a}\frac{\partial c}{\partial q} - \frac{c}{r_a}\frac{\partial G_q}{\partial q}. \quad (4.26)$$

Then, all partial derivatives are approximated by their corresponding explicit difference relations. The term $\partial c / \partial t$ is approximated by the first-order forward difference, the

terms $\partial^2 c/\partial r_a^2$ and $\partial^2 c/\partial q^2$ are approximated by the second-order central difference, the terms $\partial c/\partial r_a$ and $\partial c/\partial q$ are approximated by the first-order central difference(see Appendix B), For the terms G_r , G_q , $\partial G_r/\partial r_a$ and $\partial G_q/\partial q$ that compose of numerical values of blood velocity components and analytical expression of magnetic force components, we approximate the spatial derivatives of blood velocity components and use the exact value of spatial derivatives of magnetic force components evaluated at the center of each element.

After all approximations are performed, the continuity equation (4.26) is replaced by its corresponding difference equation,

$$\frac{\mathbf{£}_{i,j}^{n+1}-\mathbf{£}_{i,j}^{n}}{\Delta t}=\left(\frac{\mathbf{£}_{i+1,j}^{n}-2\mathbf{£}_{i,j}^{n}+\mathbf{£}_{i-1,j}^{n}}{(\Delta r_a)^2}\right)+\frac{1}{(r_{am})_i}\left(\frac{\mathbf{£}_{i+1,j}^{n}-\mathbf{£}_{i-1,j}^{n}}{2(\Delta r_a)}\right)+\frac{1}{(r_{am})_i^2}\left(\frac{\mathbf{£}_{i,j+1}^{n}-2\mathbf{£}_{i,j}^{n}+\mathbf{£}_{i,j-1}^{n}}{(\Delta q)^2}\right)$$

$$-\frac{(G_r)_{i,j}\,\mathbf{£}_{i,j}^{n}}{(r_{am})_i}-(G_r)_{i,j}\left(\frac{\mathbf{£}_{i+1,j}^{n}-\mathbf{£}_{i-1,j}^{n}}{2(\Delta r_a)}\right)-\left(\frac{\partial G_r}{\partial r_a}\right)_{i,j}\mathbf{£}_{i,j}^{n}$$

$$-\frac{(G_q)_{i,j}}{(r_{am})_i}\left(\frac{\mathbf{£}_{i,j+1}^{n}-\mathbf{£}_{i,j-1}^{n}}{2(\Delta q)}\right)-\frac{\mathbf{£}_{i,j}^{n}}{(r_{am})_i}\left(\frac{\partial G_q}{\partial q}\right)_{i,j}, \qquad (4.27)$$

where the superscript n is the index of normalized time step,

$$(G_r)_{i,j}=\frac{6\pi h_b a b_p (v_{br})_{i,j}+a(F_{mr})_{i,j}}{kT}, \qquad (4.28)$$

$$(G_q)_{i,j}=\frac{6\pi h_b a b_p (v_{bq})_{i,j}+a(F_{mq})_{i,j}}{kT}, \qquad (4.29)$$

$$\left(\frac{\partial G_r}{\partial r_a}\right)_{i,j}=\frac{6\pi h_b a b_p}{kT}\left(\frac{(v_{br})_{i+1,j}-(v_{br})_{i-1,j}}{2(\Delta r_a)}\right)+\frac{a}{kT}\left(\frac{\partial F_{mr}}{\partial r_a}\right)_{i,j}, \qquad (4.30)$$

and $$\left(\frac{\partial G_q}{\partial q}\right)_{i,j} = \frac{6ph_b ab_p}{kT}\left(\frac{(v_{bq})_{i,j+1} - (v_{bq})_{i,j-1}}{2(\Delta q)}\right) + \frac{a}{kT}\left(\frac{\partial F_{mq}}{\partial q}\right)_{i,j} . \qquad (4.31)$$

The symbol $\mathbf{£}_{i,j}^{n}$ in Eq. (4.27) means the numerical value of particle volume concentration at the middle position (r_{am}, q_m) of an element that has the indices (i, j) at the n^{th} step of discrete normalized time t^{n}.

By arranging Eq. (4.27), the numerical value of particle volume concentration in an element at the next normalized time step, t^{n+1}, can be computed from the equation

$$\begin{aligned}
\mathbf{£}_{i,j}^{n+1} = & \left[1 - \frac{2(\Delta t)}{(\Delta r_a)^2} - \frac{2}{(r_{am})_i^2}\left(\frac{\Delta t}{(\Delta q)^2}\right) - \left(\frac{(G_r)_{i,j}}{(r_{am})_i} + \left(\frac{\partial G_r}{\partial r_a}\right)_{i,j} + \frac{1}{(r_{am})_i}\left(\frac{\partial G_q}{\partial q}\right)_{i,j}\right)(\Delta t)\right]\mathbf{£}_{i,j}^{n} \\
& + \left[\frac{\Delta t}{(\Delta r_a)^2} + \left(\frac{1}{2(r_{am})_i} - \frac{(G_r)_{i,j}}{2}\right)\left(\frac{\Delta t}{\Delta r_a}\right)\right]\mathbf{£}_{i+1,j}^{n} \\
& + \left[\frac{\Delta t}{(\Delta r_a)^2} - \left(\frac{1}{2(r_{am})_i} - \frac{(G_r)_{i,j}}{2}\right)\left(\frac{\Delta t}{\Delta r_a}\right)\right]\mathbf{£}_{i-1,j}^{n} \\
& + \left[\frac{1}{(r_{am})_i^2}\left(\frac{\Delta t}{(\Delta q)^2}\right) - \frac{(G_q)_{i,j}}{2(r_{am})_i}\left(\frac{\Delta t}{\Delta q}\right)\right]\mathbf{£}_{i,j+1}^{n} \\
& + \left[\frac{1}{(r_{am})_i^2}\left(\frac{\Delta t}{(\Delta q)^2}\right) + \frac{(G_q)_{i,j}}{2(r_{am})_i}\left(\frac{\Delta t}{\Delta q}\right)\right]\mathbf{£}_{i,j-1}^{n} \quad . \qquad (4.32)
\end{aligned}$$

It is seen from Eq. (4.32) that the concentration in the element (i, j) at the next normalized time step can be determined from the concentration in the same element and four surrounding elements that have indices $(i+1, j)$, $(i-1, j)$, $(i, j-1)$ and $(i, j+1)$ at the present normalized time step as shown in Figure 4.4. This is the configuration of the explicit scheme.

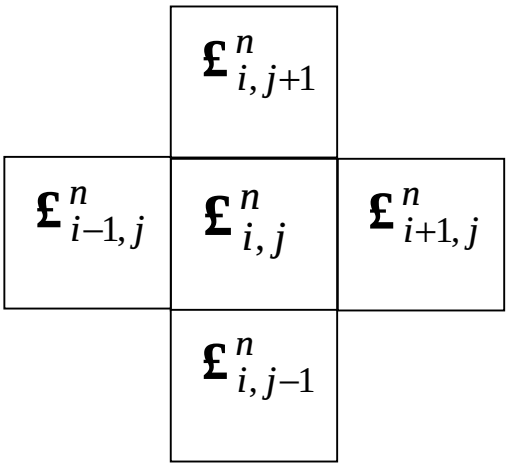

Figure 4.4: The associated elements that are used for computing the concentration in the elements which are not adjacent to any impervious surfaces.

Now consider the Eq. (4.23) for the elements that are adjacent to any impervious surfaces. By approximating various partial derivatives terms with their corresponding difference relations and arranging terms we obtain the equation used for computing the numerical concentration at the next normalized time step as

$$
\begin{aligned}
£_{s,j}^{n+1} = & \left[1-\frac{2(\Delta t)}{(r_{am})_s^2(\Delta q)^2}-\frac{(\Delta t)}{(r_{am})_s}\left(\frac{\partial G_q}{\partial q}\right)_{s,j}\right]£_{s,j}^{n} \\
& +\left[\frac{(\Delta t)}{(r_{am})_s^2(\Delta q)^2}-\frac{(G_q)_{s,j}(\Delta t)}{2(r_{am})_s(\Delta q)}\right]£_{s,j+1}^{n} \\
& +\left[\frac{(\Delta t)}{(r_{am})_s^2(\Delta q)^2}+\frac{(G_q)_{s,j}(\Delta t)}{2(r_{am})_s(\Delta q)}\right]£_{s,j-1}^{n} \\
& -\left[\frac{(\Delta t)}{(\Delta r_a)^2}+\frac{(G_r)_{s+1,j}(\Delta t)}{(\Delta r_a)}\right]£_{s+1,j}^{n}+\left[\frac{(\Delta t)}{(\Delta r_a)^2}\right]£_{s+2,j}^{n}. \qquad (4.33)
\end{aligned}
$$

In Eq. (4.33), the index s plays the same role as the index i in Fig. 4.3 and Eq. (4.32) but it is changed from index i to s in order to specify that the considered element is the

“special element” that is adjacent to an impervious surface. The scheme of computing in Eq. (4.33) can be illustrated in Figure 4.5

.

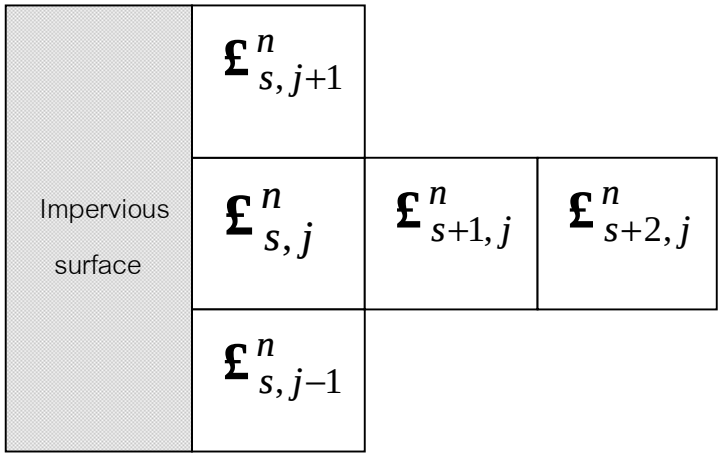

Figure 4.5: The associated elements that are used for computing the concentration in elements which are adjacent to any impervious surfaces.

From Eqs. (4.32) and (4.33), if the initial value $\mathbf{£}^{0}_{i,j}$ of particle volume concentration are given in every element at initial normalized time step $n=0$ then we can compute $\mathbf{£}^{1}_{i,j}$, $\mathbf{£}^{2}_{i,j}$, $\mathbf{£}^{3}_{i,j}$, …, $\mathbf{£}^{N}_{i,j}$ in succession with assigned boundary conditions. Consequently, time evolution of particle volume concentration distribution in the considered region can be investigated.

4.5.2 The Initial Condition

Before the simulation begins, the initial value of particle volume concentration must be assigned to every element. This value may be zero if we consider that there have no particles within the considered region at the beginning or it may be assigned as a specific function of position in the considered region. Mathematically, it can be expressed that

$$£_{i,j}^{0} = C_0\left(r_a, q\right) \text{ for all } i \text{ and } j, \tag{4.34}$$

where $C_0\left(r_a, q\right)$ can be a numerical constant of a spatial function.

4.5.3 Saturation Condition

In practical, as particle volume concentration at a given point increase, the concentration value is limited to be not more than a certain value and the saturation or static buildup is occurred. In this research, the saturation concentration is estimated by using the data from experiments [29]. The saturation concentration is used as a maximal value of the concentration within the considered region. The elements of which the concentration reaches to the saturation value are those where particles accumulate highly dense and the static build-up occurs. Then the elements are assumed to be a part of impervious surface. The concentration values in these elements are held fixed at the saturation value and they are excluded from the computational loop.

Mathematically, the saturation condition can be expressed as

$$0 \le £_{i,j}^{n} \le C_{sat} \quad \text{for all } i,\ j \text{ and } n. \tag{4.35}$$

4.5.4 Boundary Conditions

Simulation of concentration dynamics using Eqs. (4.32) and (4.33) requires assigned boundary conditions. From the statement of the problem shown in Fig. 4.1 and the domain dividing configuration shown in Fig 4.3, the boundary conditions are separated into upstream and downstream types [30]. The boundary conditions determine the value of concentration in every element of indices $\left(i_{\max}, j\right)$ on the outer boundary of the domain. In Fig. 4.1, the incoming blood flow, carrying the injected concentration C_{in} of nano-particle, enters the considered region from the upper side so the upstream boundary condition is assigned that the concentration in the outer

elements of which $0 < q_m < p$ is equal to the injected concentration C_{in}. Mathematically, this can be expressed as

$$\text{£}^{n}_{i_{\max}, j_{up}} = C_{in}, \tag{4.36}$$

for all j_{up} in the range $0 \le j_{up} \le (p/\Delta q) - 1$ and for all n.

On downstream side that the outgoing blood flow carries the escaped particles out of the considered region, the boundary condition is assigned that the concentration gradient in the direction of blood velocity across the downstream boundary is zero [30, 49] since particles are continuously refilled by blood flow so the concentration should be constant in that direction. Mathematically, this can be expressed as

$$\text{ı}\, v_b \text{g} \nabla c = 0 \tag{4.37}$$

on downstream boundary. The Eq. (4.37) is assigned for all element of indices $(i_{\max}, j_{down})$ and j_{down} is in the range $(p/\Delta q) + 1 \le j_{down} \le (2p/\Delta q) - 1$ and for all n.

From Eq. (4.37), by expanding the gradient operator in coordinates (r_a, q) then approximating the spatial derivatives with corresponding difference relations and rearranging terms, the concentration in the elements on the downstream boundary can be computed from

$$\text{£}^{n}_{i_{\max}, j_{down}} = \text{£}^{n}_{i_{\max}-1, j_{down}} - \left(\frac{(v_{bq})_{i_{\max}, j_{down}}}{(v_{br})_{i_{\max}, j_{down}}} \right) \left(\frac{\Delta r_a}{(r_{am})_{i_{\max}}} \right) \left(\frac{\text{£}^{n}_{i_{\max}, j_{down}+1} - \text{£}^{n}_{i_{\max}, j_{down}-1}}{2(\Delta q)} \right). \tag{4.38}$$

From Eq. (4.38), if the blood velocity components, v_{bq} and v_{br} are comparable and $\text{£}^{n}_{i_{\max}, j_{down}+1}$; $\text{£}^{n}_{i_{\max}, j_{down}-1}$ then the downstream boundary condition can be simplified

since $\Delta r_a / (r_{am})_{i_{\max}}$ is very small. If such conditions are satisfied, the downstream boundary condition can be simplified as

$$\mathbf{£}^{n}_{i_{\max}, j_{down}} \; ; \; \mathbf{£}^{n}_{i_{\max}-1, j_{down}} . \tag{4.39}$$

4.5.5 Simulation Procedures

The steps of simulation of particle dynamics can be described as follows.

Step 1: Setting simulation parameters and various constants.

In this step, all parameters and constants are assigned. The examples of parameters are the magnitude of background uniform magnetic flux density across the considered region B_0, the weight fraction of ferromagnetic material contained in nano-particle $c_{fm,p}$, etc.. The examples of constants are wire radius a, the average inlet blood speed V_0, spatial step sizes Δr_a and Δq, etc.. The values of all parameters and constants are reported separately in tabulate form in later section.

Step 2: Declare arrays of concentration and various variables.

In this step, we declare arrays that contain concentration value, for both present and next normalized time step, in every element in the considered region and also arrays that contain necessary data for the computation such as blood velocity components. We also declare various variables that are used in the simulation such as the local magnetic field in each element, the magnetic force components, the normalized time, etc..

Step 3: Read the numerical values of blood velocity components from the data files and save them into the corresponding elements. After this step, we know the numerical value of v_{br} and v_{bq} at the middle point of every element so we can compute G_r, G_q, $\partial G_r / \partial r_a$ and $\partial G_q / \partial q$ since we know the analytic expression of the magnetic force components.

Step 4: Assign initial concentration to every element.

Step 5: Begin the loop of concentration dynamic simulation.

In this step, we repeat the computation of particle volume concentration in every element at the next normalized time step by using Eqs. (4.32) and (4.33) until the required time is reached. The computing scheme can be described as follows.

5.1: Increase discrete time counter and specifying the position of "special elements".

When the computing starts in each time step, the discrete time counter is increased by one time step. Then it is necessary to specify the position of special element for each angular index j shown in Fig. 4.3. For each angular index j, the program checks the existence of saturation concentration from radial index $i = 0$ to $i = i_{\max}$. If no saturation concentration occurs, it means that the impervious surface is the wire's surface and we assign the radial index of special element as $s = 0$ or the special element is the element that is immediately adjacent to wire's surface as shown in Figure 4.6(a). In contrast, if there exits saturation concentration then the radial index of special element s is assigned as the radial index of the first element that adjacent to the last saturation concentration element as shown in Figure 4.6(b).

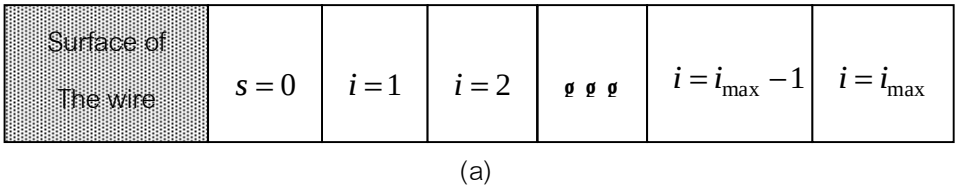

(a)

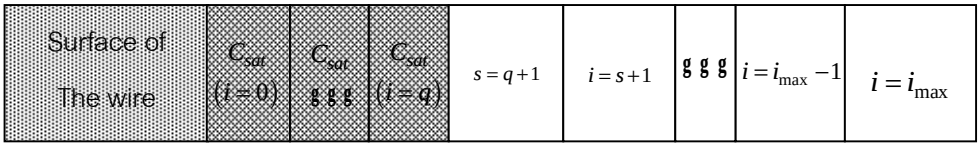

(b)

Figure 4.6: The position of special element when, (a) no saturation concentration occurs and (b) saturation concentration occurs.

5.2 Computing the concentration in elements on the upstream side.

We start the computing in every element of angular index j_{up} that satisfy the condition $0 \le j_{up} \le (p/\Delta q)-1$ by following the direction shown in Figure 4.7.

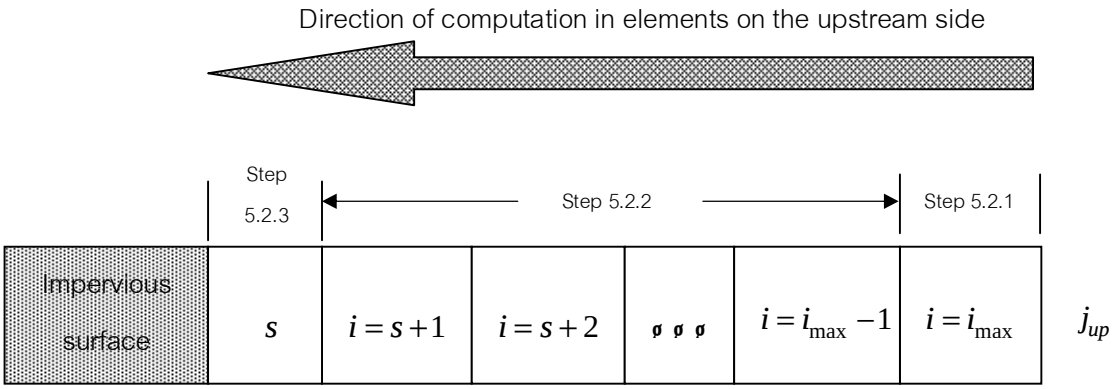

Figure 4.7: The configuration of concentration computing in elements on the upstream side.

In Fig. 4.7, step 5.2.1 is the assignment of upstream boundary condition, by using Eq. (4.36), in the element of radial index $i_{\max}$. Then the step 5.2.2 is the computing the concentration in all non-special element of radial index $i = i_{\max}-1$ down to $i = s+1$ by using Eq. (4.32). Finally, the step 5.2.3 is the computing of concentration in special element of index s by using Eq. (4.33). The steps 5.2.1 to 5.2.3 are performed for all angular index j_{up} on the upstream side.

5.3 Computing the concentration in elements on the downstream side.

After finishing the procedures of concentration computing on the upstream side then we start the computing in every element on the downstream side. The elements on the downstream side have angular index j_{down} that satisfies the condition $(p/\Delta q)+1 \le j_{down} \le (2p/\Delta q)-1$ by following the direction shown in Figure 4.8.

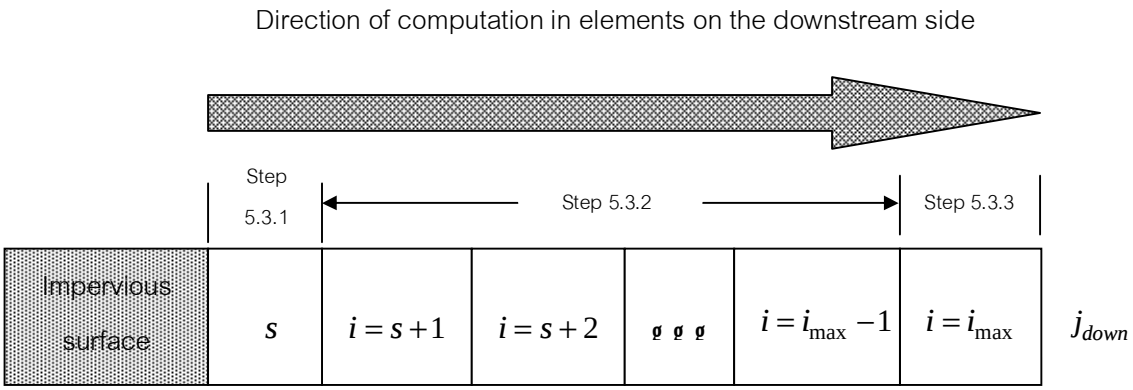

Figure 4.8: The configuration of concentration computing in elements on the downstream side.

In Fig. 4.8, step 5.3.1 is the computing the concentration in special element of index s by using Eq. (4.33). Then the step 5.3.2 is the computing the concentration in all non-special element of radial index $i = s+1$ to $i = i_{\max}-1$ by using Eq. (4.32). Finally, the step 5.3.3 is the assignment of downstream boundary condition, by using Eq. (4.38) or (4.39), on the concentration in the element of radial index $i_{\max}$. The steps 5.3.1 to 5.3.3 are performed for all angular index j_{down} on the downstream side.

5.4 Update the concentration data contained in the data arrays

After concentration computing in every element is finish, the new concentration values at the new normalized time steps are saved into the data arrays. This saved concentration values are prepared to be the present concentration values for the computing in next normalized time steps

The steps 5.1 to 5.4 are repeated until the discrete time reaches the desired value.

Step 6: Save the concentration values in all element at the last time into output data files also with the values of various parameters and constants

By following the described simulation methodology, we can obtain the pattern of concentration distribution in the considered region at a given time. These data are then analyzed to investigate the targeting of nano-particle in the considered region in various situations.

4.6 Capture of Ferromagnetic Nano-Particles by Interception

In this research, we also study the capture of ferromagnetic nano-particles by interception mechanism where effect of particle diffusion is not taken into account. Particle's dynamics are investigated by solving equations of motion of particles that are under the influence of blood convection and magnetic force.

Total velocity of a particle carried by blood flow and subjected to dominant magnetic force is

$$\mathbf{v}_p = \mathbf{v}_b + \frac{\mathbf{F}_m}{6ph_b b_p}. \tag{4.40}$$

The Eq. (4.40) can be separated into two equations of velocity and magnetic force components. By using the normalized coordinates (x_a, y_a), where $x_a = x/a$ and $y_a = y/a$, we obtain

$$\frac{dx_a}{dt} = \frac{v_{bx}}{a} + \frac{F_{mx}}{6ph_b ab_p} \tag{4.41a}$$

and

$$\frac{dy_a}{dt} = \frac{v_{by}}{a} + \frac{F_{my}}{6ph_b ab_p}, \tag{4.41b}$$

where v_{bx}, v_{by}, F_{mx} and F_{my} are components of blood velocity and magnetic force in x_a and y_a directions, respectively.

In Eqs. (4.41a) and (4.41b), the values of v_{bx} and v_{by} can be obtained from numerical values of blood velocity components saved in data files while the values of F_{mx} and F_{my} are obtained from analytical expressions of magnetic force components in Eqs. (4.10) to (4.12) and then transform the vector components in (r_a, q) coordinates to (x_a, y_a) coordinates by using the relations

$$F_{mx} = F_{mr}\cos q - F_{mq}\sin q \tag{4.42a}$$

and

$$F_{my} = F_{mr}\sin q + F_{mq}\cos q \ . \tag{4.42b}$$

To obtain particle 's trajectories, Eqs. (4.41a) and (4.41b) are solved numerically by using the fourth-order Runge-Kutta method when particle 's start position (x_{a0}, y_{a0}) is given. As seen in Eqs (4.10) to (4.12), the magnetic force decreases monotonically when the distance between wire's center and particle increases. Consequently, the effect of magnetic force on particle motion is negligible in certain regions far away from the wire and, in those regions, particles' trajectories are almost parallel to the blood flow direction. Particles' trajectories can be categorized into two types depending on whether the particle is capture or not. The borderline trajectory between trajectories of captured and non-captured particles is called the critical trajectory [14]. The normal distance between the axis of the blood flow and the start position is defined as the capture length [14] which specifies the capture efficiency. In this work, particles' trajectories are analyzed to determine capture length for various cases.

4.7 Parameters and Constants for the Simulation

From data in Ref [32], the diameter of nano-drug carriers vary from about 5 to 200 nanometer. The small drug carriers have diameter from about 5 to less than 100 nanometer. The ferromagnetic core contain only single magnetic domain. The magnetic force acting on this type of particles can be expressed by Eq. (4.12). For larger drug

carriers, the diameters range from more than 100 to 200 nanometer. The ferromagnetic cores contain many magnetic domains and the magnetic force acting on the carriers can be expressed by Eqs. (4.10) and (4.11). For the ferromagnetic material contained within the drug carriers, the magnetite (Fe_3O_4), which is a biocompatible material that is used in many biomedical applications [32, 50-51], is selected. For the ferromagnetic material in the wire implanted in blood vessel, we select stainless steel 409 which is the material used for fabricating medical stents which is used for implanted in blood vessel for therapy of blood vessel embolism [52]. The average velocities of blood flow in the vessels are assigned as $V_{avg} = 1.1\times10^{-2}$ and 2.2×10^{-2} m/s [53]. Some parameters in the works of Avilés et al. [9] and Cregg et al. [39] are used. The parameters of simulation diffusive capture of drug carrier particles are summarized in Table 1.

Table 1: The parameters of diffusive capture simulation of drug carrier particles.

Parameter	Symbol	Value	SI Unit
blood density	r_b	1.04×10^{3} [9]	kg / ms
blood viscosity	h_b	2.0×10^{-3} [9]	kg / m^3
magnitude of average blood velocity	V_{avg}	1.0×10^{-2}, 2.2×10^{-2} [53]	m / s
applied uniform magnetic flux density across the vessel	B_0	0.1 – 0.8 [39]	T
weight fraction of magnetite in drug carrier particles	c_{fmp}	0.4 [39]	-
density of magnetite	$r_{fm,p}$	5.05×10^{3} [9]	kg / m^3
density of polymer material in drug carrier particles	r_{pol}	9.5×10^{2} [9]	kg / m^3
saturation magnetization of stainless steel 409 material in the wire	$M_{W,s}$	1.397×10^{6} [9]	A / m
saturation magnetization of magnetite	$M_{fm,p,s}$	4.55×10^{5} [9]	A / m
wire radius	a	1.0×10^{-6} [39]	m
radius of drug carrier particle	b_p	10×10^{-9}, 30×10^{-9}, 50×10^{-9}, 70×10^{-9}, 100×10^{-9} [32]	m
magnetic susceptibility of SS 409 at zero magnetic field	$c_{W,0}$	1.0×10^{3} [39]	-
magnetic susceptibility of magnetite at zero magnetic field	$c_{fm,p,0}$	1.0×10^{3} [39]	-

CHAPTER V

Results and Discussions

In this chapter, we present and discuss the simulations results of micro- and nano-particles capture in high gradient magnetic field described in Chapter III and Chapter IV.

5.1 The Capture of Weakly Magnetic Micro-Particles by An Assemblage of Random Wires in Axial Magnetic Filters

The theoretical analysis and computational procedure described in Chapter III are used for simulating the capture of weakly magnetic micro-particles by an assemblage of random wires in axial magnetic filters. As stated in Chapter III, we generalize the single-wire model to the case of multi-wires model. Capture behavior of a representative wire is investigated by considering the magnetic and fluidic effects from neighboring wires that are not taking into account in the single-wire model. Three main parameters of the study are the packing fraction (F) of cylindrical wires in an axial magnetic filter, the normalized filter length defined in Chapter III, and fluid entrance velocity (V_0). Our results are compared with those obtained by the single-wire model. The limit and basic criterion of validity of the single-wire model is discussed. Finally, we apply our study to predict the efficiency of macro-scale axial filters used for capturing red and white blood cells from whole blood.

5.1.1 Capture Cross-Sections of the Single-Wire and EMT Models

For both single-wire and EMT models, capture cross-section can be determined by analyzing particle 's trajectories from the time that particle enters the filter

until it is captured within the filter or escapes the filter. For the single-wire model, capture cross-section was bounded by an isotelic curve which was defined as the locus of starting position of particles that were captured at the end of the filter. Figure 5.1 shows an example of isotelic curve and some corresponding particle ' trajectories for L_a = 400 obtained by using the single-wire model. In Fig. 5.1, the boundary of capture cross-section (line number 1) is the isotelic curve corresponding to L_a = 400.

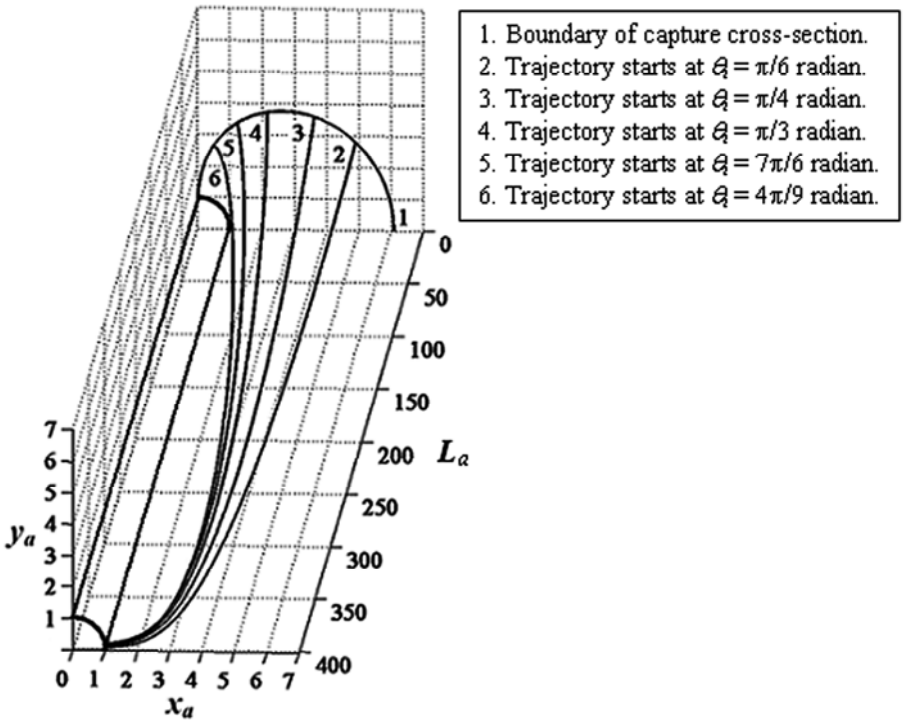

Figure 5.1: The capture cross-section of the single-wire model and corresponding particle ' trajectories for L_a = 400.

For the case of EMT model, the boundary of capture cross-section is limited by the boundary of fluid envelope. Particles that have starting positions on the boundary of capture cross-section are not necessary to be captured at the end of the filter. We determine the capture cross-section for the EMT model by considering on a plane perpendicular to wire axis at filter entrance. We use the coordinates (r_a, θ) on this plane. Then we select, for each value of angular coordinate θ, the radial coordinate $r_a \leq 1/\sqrt{F}$ that causes the particle to be captured at maximal distance within

normalized filter length L_a. Figure 5.2 shows an example of capture cross-section from the EMT model and some corresponding particle ' trajectories for the case of L_a = 400, F = 0.05, and K_c = 0.8 (K_c was define under Eq. (3.1) of Chapter III).

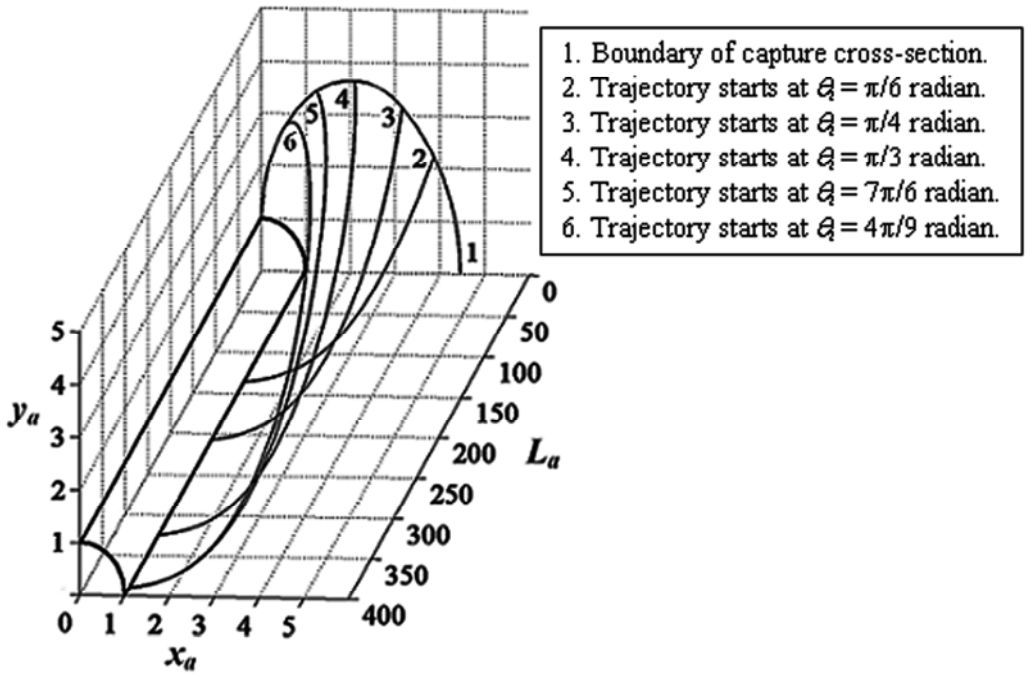

Figure 5.2: The capture cross-section of the EMT model and corresponding particle ' trajectories for L_a = 400 and F = 0.05.

5.1.2 Comparisons of Capture Cross-Sections of the Single-Wire and EMT Model

Since the EMT model is the generalization of the single-wire model to the cases of higher packing fraction, the results obtained from two models should close to each other for low packing fraction limit or $F \to 0$. Figure 5.3 (a) and (b) show the comparison of capture cross-section of two models for the dilute and higher packing fraction cases, respectively. In Fig. 5.3 (a), the parameters are F = 0.01, L_a = 400 and K_c = 0.8. The horizontal and vertical axes are distances normalized by the wire radius, $x_a = x/a$ and $y_a = y/a$. It is seen that two models provide an identical capture cross-section. Consequently, the result of the EMT model reduced to that of the single-wire model in the dilute limit and a relatively low magnetic field or a relatively high fluid flow

velocity. This comparison contributes to supporting the validity of the EMT model and also confirms the single-wire model result of Gerber [19].

In Fig. 5.3 (b), we consider the case of higher packing fraction, F = 0.05, the fluid cell boundary (dotted line) in unit of wire radius (a) is $1/\sqrt{F}$ = 4.472. The higher packing fraction means the closer distance between wires in the filter. Consequently, the magnetic effect from other wires on the capture of the representative wire becomes significant and the EMT model predicts a significantly different result from the single-wire model where the effect of neighboring wires is neglected. For the single-wire model, the capture cross-sections of adjacent wires overlap with each other which yield a large and overestimated total capture cross-section area and so the efficiency of the filter is also overestimated. In contrast, the capture cross-section from the EMT model is bounded by the fluid envelope, since the magnetic force is zero outside the fluid envelope, and the overlapping does not occur.

Figure 5.4 shows the capture cross-section area, obtained by integrating the area bounded by the capture cross-section boundary, based on the EMT model for F = 0.01, 0.07, 0.10 and K_c = 0.8 for varying normalized filter length (L_a). In dilute limit, F = 0.01, the capture cross-section increases monotonically with L_a. This confirms the result of Gerber [19] where the magnetic field was calculated using the single-wire approximation. At the higher packing fraction F = 0.07 and 0.10, the saturation of the capture cross-section area is observed in agreement with the experimentally observed saturation of filter efficiency [54].

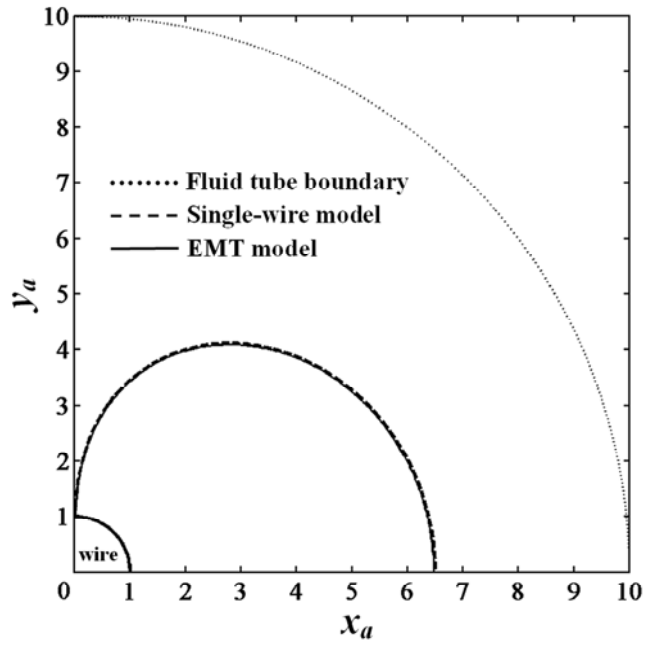

(a)

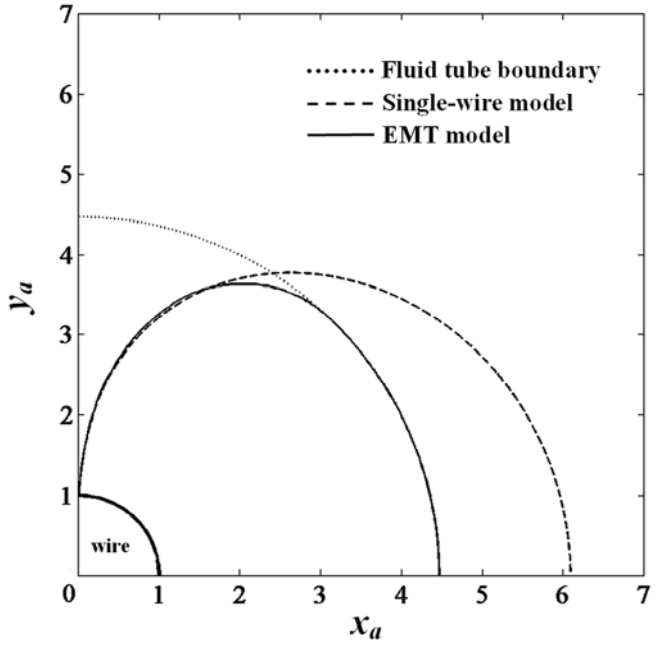

(b)

Figure 5.3: Comparison between the capture cross-section areas obtained from the single-wire and the EMT models for a packing fraction (F) of (a) 0.01 and (b) 0.05 with a fixed L_a = 400 and K_c = 0.8.

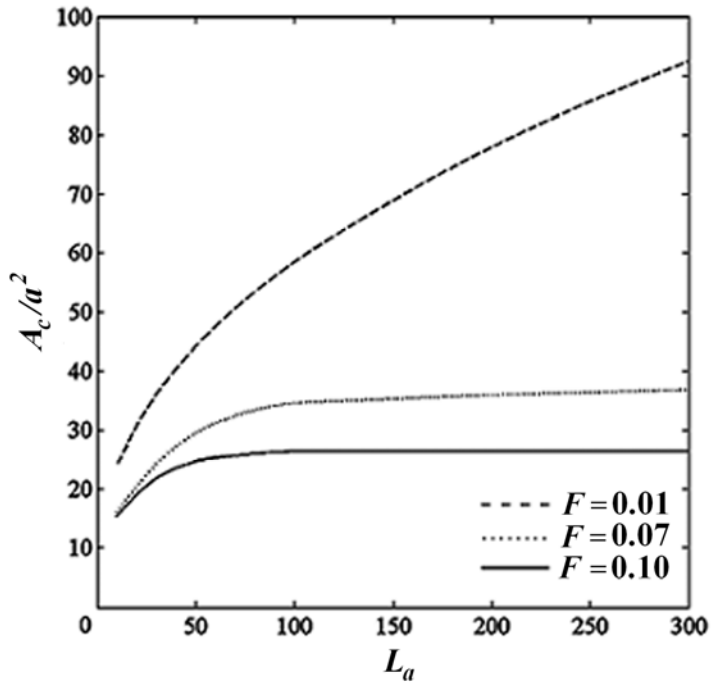

Figure 5.4: Comparison between capture cross-sections areas of the EMT model for F = 0.01, 0.07 and 0.10 with K_c fixed at 0.8.

5.1.3 The Effect of Packing Fraction on Magnetic Field in Representative Cell.

The packing fraction F affects the magnetic field, as seen in the factor $A = 1/(1 - FK_c)$ in Eq. (3.1) of Chapter III. So it is important to investigate the effect of F on the capture cross-section area. Figure 5.5 shows the variation of factor A^2, which appears in Eqs. (3.6a) and (3.6b), with the packing fraction F and K_c as parameters. The value of K_c depends on the material of the wire (such as stainless steel or nickel). The relative permeability of the wire is in the order of 10^2 (600 for Nickel [55] and 409 for SS430 [55]) and so K_c ranges from 0.8 to 0.99. From Fig. 5.5, it is seen that the magnetic effect from the neighboring wires becomes significant, this means the factor A^2 is significantly more than 1, when the packing fraction exceeds 0.1 for both values of K_c.

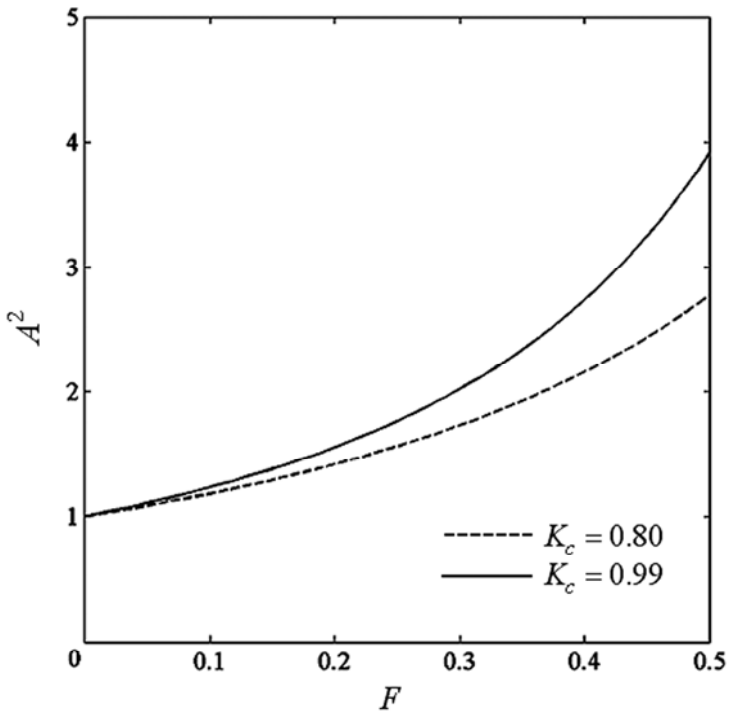

Figure 5.5: The variation of factor A^2 with the packing fraction F .

5.1.4 The Criterion of Validity of The Single-Wire Model

It is seen in Figs. (5.3a), (5.3b) and 5.4 that the single-wire model approximation for the magnetic field can be used to predict the capture cross-section only in the limited range of parameters (F and L_a). We, therefore, report in Fig. 5.6 a guidable criterion of the validity of the single-wire model for K_c = 0.8 and 0.99 in the range of packing fraction F from 0.01 to 0.50. Let L_a^* be the bound value of L_a within which the single-wire approximation is still applicable. L_a^* is defined as the value of L_a for which the corresponding capture cross-section area begins to reach the boundary of the fluid tube for a given value of packing fraction F . The single-wire model is valid when the coordinates of the packing fraction F and L_a (corresponding to a set of operating parameters, such as the applied magnetic field H_0, fluid entrance velocity V_0, wires packing fraction F, the filter length l) locate under the curve of L_a^* versus F,

as shown in Fig. 5.6. It is seen that, the values of L_a^* for different values of K_c deviated from each other when the packing fraction is larger than 0.1. Consequently, the magnetic effect from neighbouring wires on the magnetic field of the representative wire is significant when the packing fraction is more than 0.1. This behavior is consistent with the behavior of factor A^2 as shown in Fig. 5.5, In Fig. 5.6, higher K_c values give a lower L_a^* for a given value of packing fraction. This behavior is reasonable since the wire made from a material with a higher relative permeability produces a higher magnetic effect.

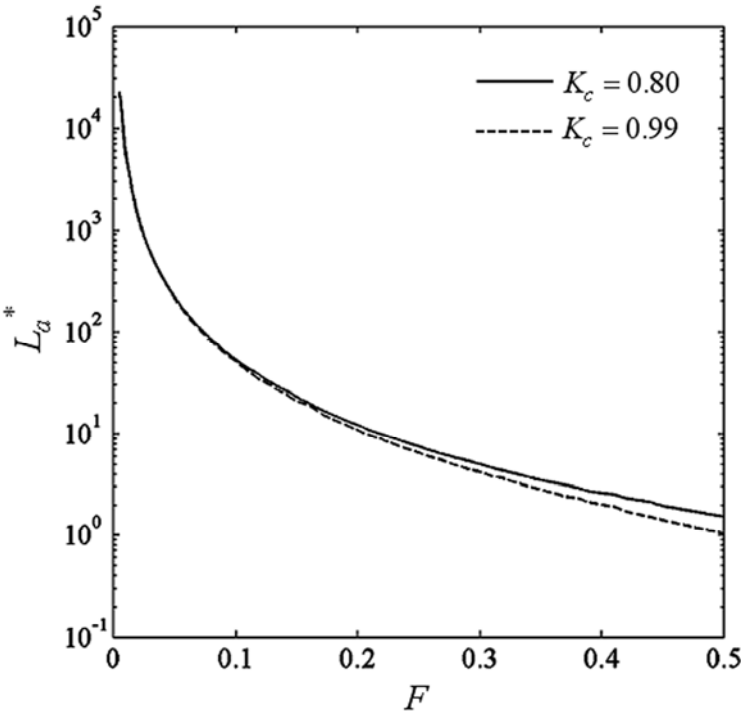

Figure 5.6: A guidable criterion of validity of the single-wire model for K_c = 0.80 and 0.99.

5.1.5 The Application of EMT Model for Prediction of Capture Efficiency of Proposed Macro-Scale Axial Magnetic Filter Used for Capture Red and White Blood Cells from Whole Blood.

The EMT model for the axial magnetic filter was next applied to predict

the efficiency of the capture of red blood cells (RBCs) and white blood cells (WBCs) from whole blood using a proposed macro-scale axial magnetic filter. The proposed macro-scale axial magnetic filter is modeled as a glass tube of 2.0 cm internal diameter, which is similar to that used in the experiment of Ref. [56]. The filter consistes of an assemblage of randomly distributed and parallel stainless steel wires (hence K_c = 0.99) of the average radius a = 12.5×10^{-6} m [56]. The filter length is l = 10 cm hence $l_a = l/a$ = 8000. The wire volume packing fraction is F = 0.10. The values of relative magnetic susceptibilities of RBCs and WBCs respect to plasma from Ref. [57], $\chi_{RBC} - \chi_{plasma}$ = +3.88×10^{-6}, $\chi_{WBC} - \chi_{plasma}$ = −1.3×10^{-6}, respectively, are used. The magnitudes of entrance velocities (V_0) of blood are 0.1 and 1.0 mm/s.

Figure 5.7 shows the predicted capture efficiency of RBCs for the magnetic flux density B_0 up to 0.2 T. It is seen that the efficiencies are saturate at about 85 %, for both values of V_0 (0.1×10^{-3} and 1×10^{-3} m/s). The saturation of capture efficiency is caused by the saturation of capture cross-section areas, can be seen in Fig. 5.3(b) and Fig. 5.4, since the capture cross-section areas are only within the region of attractive force and they are bounded by the fluid tube boundary. Consequently, the capture cross-section area could not grow further when it fully occupied the region of attractive force. By comparing our results with that of the experiments demonstrated in Refs. [24], the 85% predicted efficiency of RBCs capture by the proposed macro-scale axial magnetic filter is a little less than 91.1% [24] and 89.7 % [23] RBCs separation efficiency of micro-scale axial magnetic filter for V_0 = 0.1×10^{-3} m/s and B_0 = 0.2 T. If V_0 = 0.1 mm/s then the rate of blood volume flow through the proposed filter is about 113 mL/hr. The flow rate of blood could be increased to about 1130 mL/hr if V_0 was increased to 1.0 mm/s.

Figure 5.8 shows the efficiency of WBCs capture from whole blood for the same parameters as that in Fig. 5.7 but the range of B_0 is extended to 0.6 T to present saturation behavior of capture efficiency for both values of V_0. It is seen that the saturation efficiencies for both values of V_0 are 78.5 %. For V_0 = 0.1 mm/s, the

predicted 78 % capture efficiency at B_0 = 0.2 T (dashed line of F = 0.1) is comparable to that reported in the experiments of Refs [23] and [24].

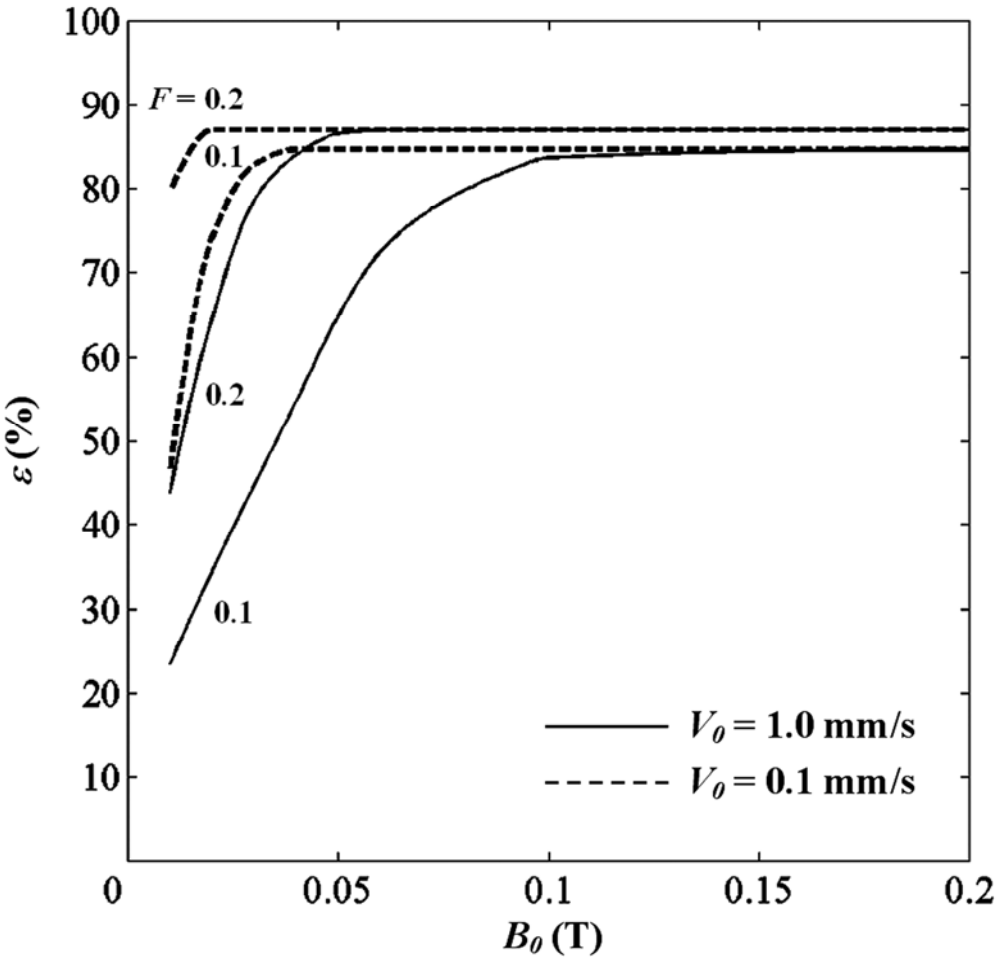

Fig. 5.7: The efficiency of RBCs capture from whole blood for F = 0.10 and 0.20, K_c = 0.99, V_0 = 0.1 and 1.0 mm/s.

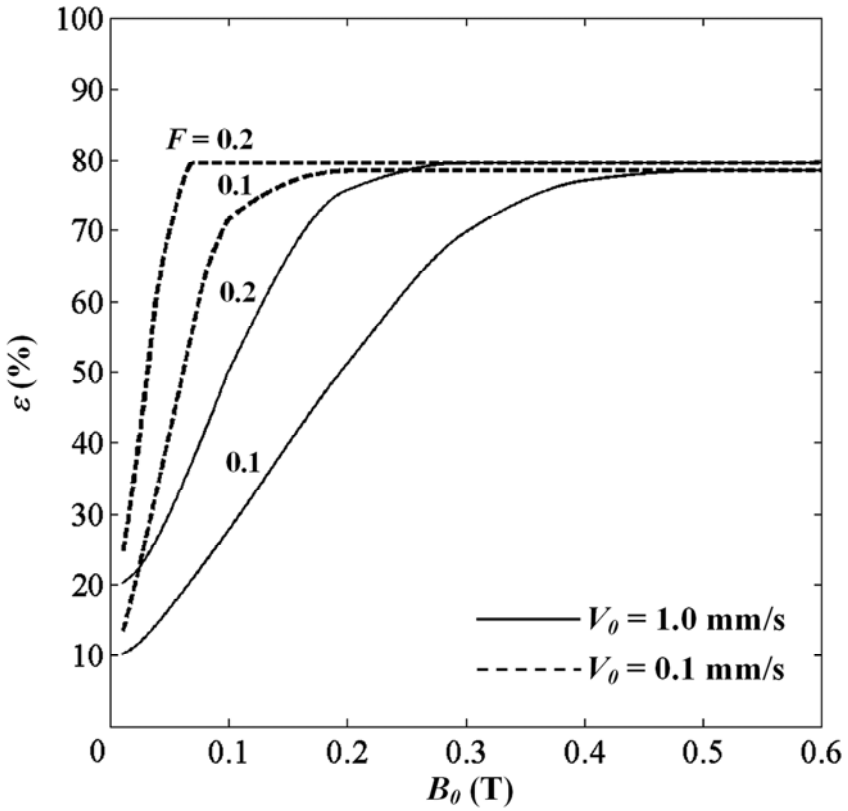

Figure 5.8: The efficiency of WBCs capture from whole blood for F = 0.10 and 0.20, K_c = 0.99, V_0 = 0.1 and 1.0 mm/s.

5.2 The Capture of Ferromagnetic Nano-Particles by Ferromangetic Wires in Blood Vessel

We investigate the capture of ferromagnetic nano-particles by a representative wire confined within certain region in blood vessel. The objectives are to explain the behavior of nano-particle capture and to examine the feasibility and the efficacy of implant assisted-magnetic drug targeting using micro-ferromagnetic wires for targeting ferromagnetic nano-drug carriers to certain region in blood vessel.

In the research, we investigate the effects of the strength of an external uniform magnetic flux density (B_0) across the considered region, the size of nano-drug carrier (b_p), and the magnitude of average blood velocity (V_{avg}) on capture behavior

and targeting efficacy. From parameters shown in Table 1 of Chapter IV, the values of $\rho_{fm,p}$ = 5.05 ×10^3 kg/m^3, $\rho_{pol,p}$ = 9.5×10^2 kg/m^3 and $\chi_{fm,p}$ = 0.4 are used for calculating the average density of a nano-drug carrier by using the relation [34]

$$\rho_p = \frac{1}{\left(\frac{\chi_{fm,p}}{\rho_{fm,p}}\right)+\left(\frac{1-\chi_{fm,p}}{\rho_{pol,p}}\right)}, \tag{5.1}$$

and we obtain ρ_p = 1.406×10^3 kg/m^3.

For all cases of simulation, the transverse mode of nano-particle capture is considered. The wire is magnetized by the uniform magnetic flux density normal to its axis and the direction of the incoming blood flow is perpendicular to the direction of uniform magnetic flux density. The initial concentration of nano-drug carriers is assigned as zero everywhere in the considered region. The value of nano-drug carrier volume concentraton in blood flow that enters the considered region is assigned as C_{in} = 4.4×10^{-5} [29]. By using the average density of a nano-drug carrier ρ_p = 1.406×10^3 kg/m^3, the volume concentration C_{in} = 4.4×10^{-5} is equivalent to the ratio of nano-drug carrier weight per blood volume of 6.2 mg/ml which is in the same order of magnitude as those in clinical experiment in human (10 mg/ml) [33] and in-*vitro* experiment (5 mg/ml) [38].

To estimate the saturation concentration of the simulation, we use the guiding data from experiment [29]. The work of Takayasu et al. [29] performed the experiment of the capture of nano-magnetite particles dispersed in both static and flowing water by a ferromagnetic wire in high gradient magnetic field. For the case of static water, the initial volume concentration was varied from 9.0×10^{-6} to 1.8×10^{-4} and saturation concentration for all cases is about the same as 6.5×10^{-3}. For the case of flowing water, the initial volume concentration was 1.8×10^{-4} and the flow velocities were 0.36 and 1.8 mm/s. It was observed that the saturation concentration increased with increasing flow velocity and was larger than that of the static water case (6.5×10^{-3}).

Because the average blood velocities in this research (1.1 and 2.2 cm/s) are larger than the values used in the work of Takayasu et al. [29] then we use the saturation concentration for static fluid case 6.5×10^{-3} as lower bound of saturation concentration in our simulations.

5.2.1 The Behavior of Diffusive Capture of Nano-Drug Carriers

To investigate the behavior of diffusive capture of nano-drug carrier particles by micro-wire, we simulate the continuity equation for the concentration of nano-drug carriers in the blood stream. The considered nano-drug carriers have radius of 10×10^{-9} m. Each nano-drug carrier consists of magnetite and polymer with attached drug molecules. The weight fraction of magnetite in drug carrier is $\chi_{fm,p}=0.4$. The magnetite has density of $\rho_{fm,p}=5.05\times10^{3}$ kg/m^3 and saturation magnetization $M_{fm,p,s}=4.55\times10^{5}$ A/m. The polymer and attached drug molecules are assumed to have the density of $\rho_{pol}=9.5\times10^{2}$ kg/m^3. The wire used for the capture of nano-drug carrier particles is considered made of stainless steel 409 of which radius $a=1.0\times10^{-6}$ m and saturation magnetization $M_{W,s}=1.397\times10^{6}$ A/m. The nano-drug carriers are carried into the considered region by blood stream of average velocity $V_{avg}=2.2\times10^{-2}$ m/s which is the value of average blood velocity in venules [53]. The density of blood is $\rho_b=1.04\times10^{3}$ kg/m^3 and blood viscosity is $\eta_b=2.0\times10^{-3}$ kg/m^3. We consider the capture behavior of nano-drug carrier particles when the strengths of uniform magnetic flux density across the considered region are B_0 = 0.1, 0.5, and 0.8 T. Figures 5.9, 5.10 and 5.11 illustrate the steady state distribution of relative concentration (C/C_{in}) in region near to the representative wire surface for the case of B_0 = 0.1, 0.5 and 0.8 T, respectively. In these figures, the horizontal and vertical distances are normalized by the wire radius. The magnetic flux density $\vec{B}_0$ is in positive x_a direction while the incoming blood flow is in negative y_a direction. The figures show the contours of relative concentration, C/C_{in} , to specify the region where nano-particles accumulate or

deplete. The relative concentration is larger and lower than one in accumulation and depletion regions, respectively.

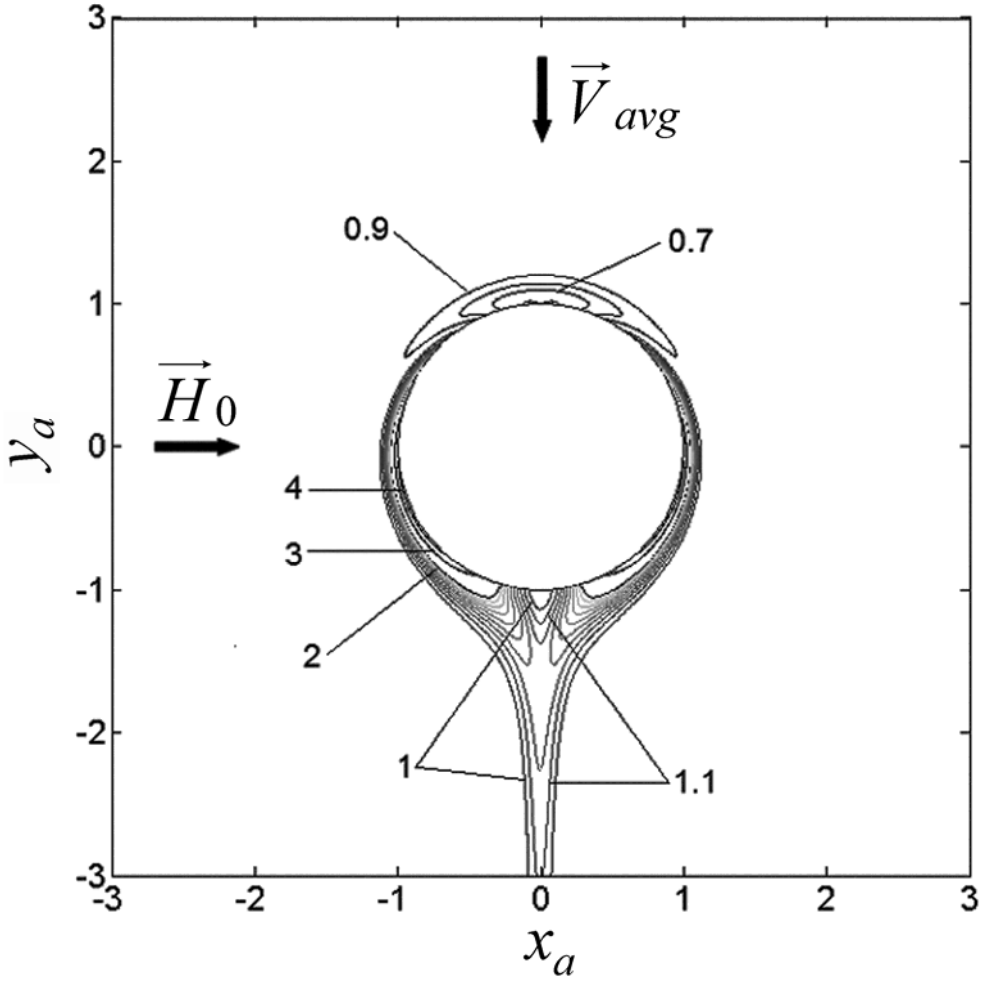

Figure 5.9: The relative concentration contours of nano-drug carriers in the region near to representative wire surface for b_p = 10×10^{-9} m, V_{avg} = 2.2×10^{-2} m/s, B_0 = 0.1 T, t = 8.79 ms (steady state).

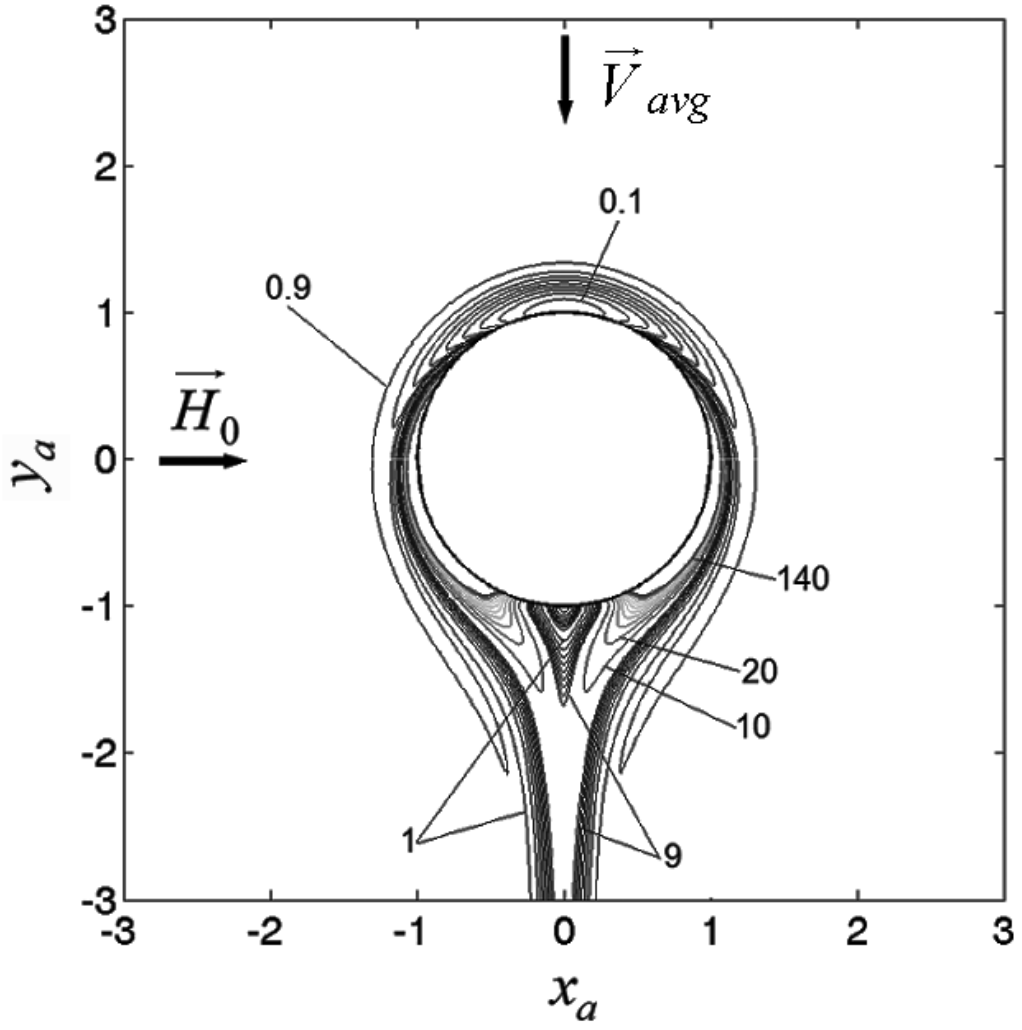

Figure 5.10: The relative concentration contours of nano-drug carriers in the region near to representative wire surface for b_p = 10×10^{-9} m, V_{avg} = 2.2×10^{-2} m/s, B_0 = 0.5 T, t = 8.79 ms (steady state).

.

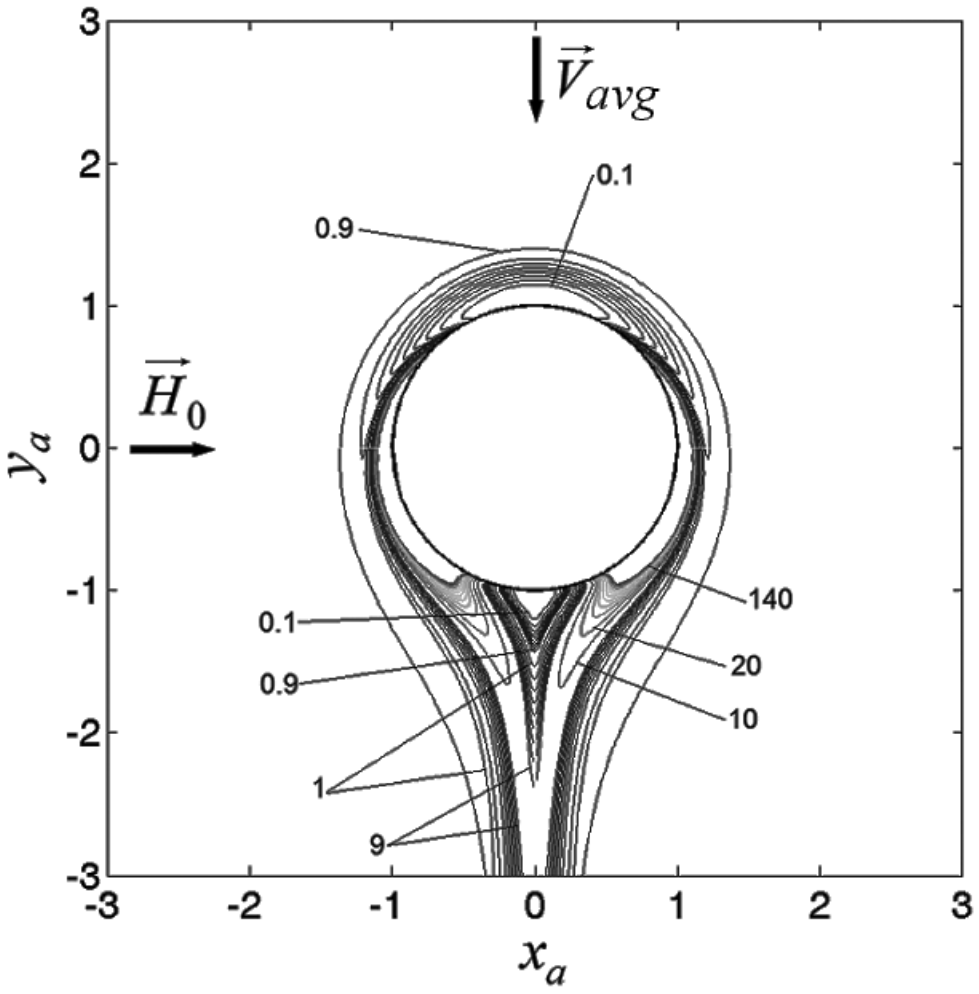

Figure 5.11: The relative concentration contours of nano-drug carriers in the region near to representative wire surface for b_p = 10×10^{-9} m, V_{avg} = 2.2×10^{-2} m/s, B_0 = 0.8 T, t = 8.79 ms (steady state).

It is seen in Fig. 5.9 that for B_0 = 0.1 T, the steady state maximal relative concentration is only about 4 times of C_{in}, no saturation concentration occurs and the accumulation region is very small. In Figs 5.10 and 5.11 where B_0 = 0.5 and 0.8 T, respectively, the maximal relative concentration on the wire surface reaches the saturation value which is about 140 times of C_{in}. Figure 5.12 illustrates the direction of magnetic force acting on nano-drug carrier particles in various regions around the representative wire [58]. In

Figs. 5.10 and 5.11, the saturation regions appear symmetrically on the left and right sides of the wire surface where the magnetic force acting on nano-drug carriers in those regions is attractive. The region on the top side of the wire is the depletion region because it is the region of repulsive magnetic force. For the bottom side of the wire, it is observed that there exist both depletion and accumulation regions near the bottom side of the wire but the depletion region is very smaller than the accumulation region.

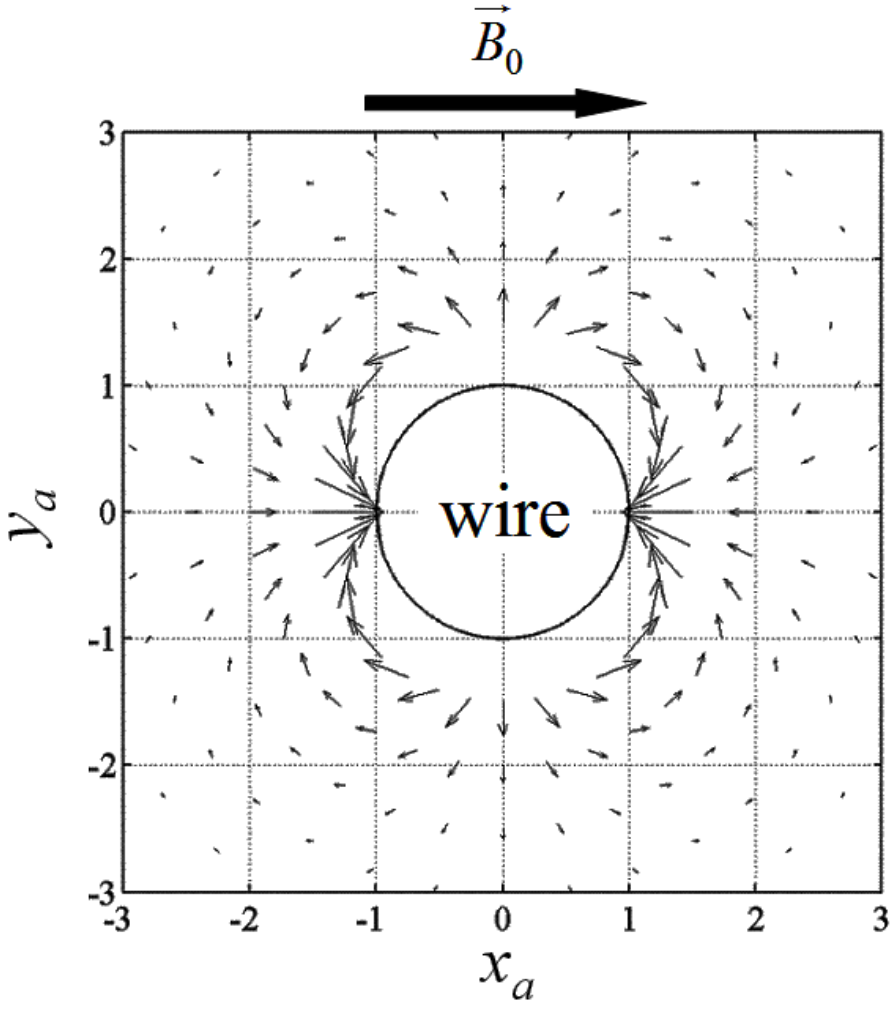

Figure 5.12: The direction of magnetic force acting on nano-drug carriers in various regions around the representative wire [58].

Fig. 5.12 is used for describing diffusive capture behaviors on nano-drug carriers as seen in Figs. 5.9 to 5.11 as follows. When nano-drug carriers, carried by

blood flow, reach the top side of the wire they experienced the repulsive magnetic force and are sweep, by both repulsive magnetic force and convection by blood flow, into the left and right sides of the wire. Consequently, the concentration of nano-drug carriers in region near the top of the wire decreases and the relative concentration in that region is lower than one. Nano-drug carriers which are sweep into regions on the left and right sides of the wires experienced the attractive magnetic force that try to bring the carriers towards wire surface. Consider the regions very close to the wire surface, blood velocities in these regions are close to zero and the magnetic force acting on the carriers is very strong. Consequently, certain amounts of nano-drug carriers are accumulate on the wire surface and the concentration on the wire surface increase very fast above the value of C_{in}. For the nano-drug carriers at farther region from wire center, the strength of the magnetic force decrease but the effects of convection by blood flow and diffusion from region of higher concentration increase. So concentration of nano-carriers in this region increases slower but the carriers still accumulate in this region. Consider the bottom side of the wire, transportation of nano-drug carriers into this region is mainly caused by the diffusion from regions of higher concentration in left and right sides of the wire and the convection by blood flow. The nano-drug carriers entering the region at bottom of the wire experienced the repulsive magnetic force. Certain amounts of the carriers are repelled directly away from the wire surface in the direction $\theta = 3\pi/2$ radian. There are some amounts of the carriers repelled and are transported into adjacent directions on the left and right sides of direction $\theta = 3\pi/2$ radian. This behavior causes the concentration of the carries on the bottom surface of the wire decrease and small depletion region occurs adjacent to bottom surface of the wire. In the regions more far from the bottom surface of the wire, the amount of carriers repelled from wire surface combine with the amount of carriers diffuse from neighbouring regions of higher concentration so the concentration in these far regions increase and accumulation regions occur. As time evolves, the nano-drug carriers are continuously supplied into the considered region. The concentration in the regions of attractive magnetic force on the left and right sides of wire surface increase

continuously until it reach the saturation concentration at which the flux of nano-drug carriers attracted into the region balance with the flux of the carries diffuse and carried, by blood convection, out of the region and the static buildup occurs.

To investigate time evolution of capture behavior, we observe Figs 5.13, 5.14 and 5.15 which show radial concentration distribution in the direction of θ = 0 radian at times t = 1.54, 1.76, and 8.79 ms (steady state), respectively, compared between the cases of B_0 = 0.1, 0.5 and 0.8. The direction θ = 0 radian is on the right side of wire surface (see Fig. 4.2 for the angle θ) and the magnetic force is attractive in this direction. In Fig. 5.13 where B_0 = 0.1, it is seen that the concentration near to wire surface is lower than C_{in} = 4.4×10^{-5}. This can be described that at t = 1.54 ms the stream of nano-particle just firstly reach to the side surfaces of the wire (in the directions θ = 0 and π radian) but particle transport due to blood convection in region near to wire surface ($1 \le r_a \le 1.4$) is very small since blood velocity decrease monotonically to zero in this region and the magnetic effect for attracting particles towards wire surface is rather small because of the small value of B_0. The dominant mechanism that transport particle into region near to wire surface is diffusion since the levels of concentration are highly different. The situations for B_0 = 0.5 and 0.8 T are different. Increasing the value of B_0 from 0.1 T to 0.5 and 0.8 T causes the stronger attractive magnetic force. Consequently, it is observed that the concentration levels in region near to the wire for B_0 = 0.5 and 0.8 T are higher than the case of B_0 = 0.1 T. For B_0 = 0.8 T, the attractive magnetic force is high enough to increase the concentration on wire surface (r_a =1) to further value of about 1.5×10^{-3} which is higher than C_{in} = 4.4×10^{-5}.

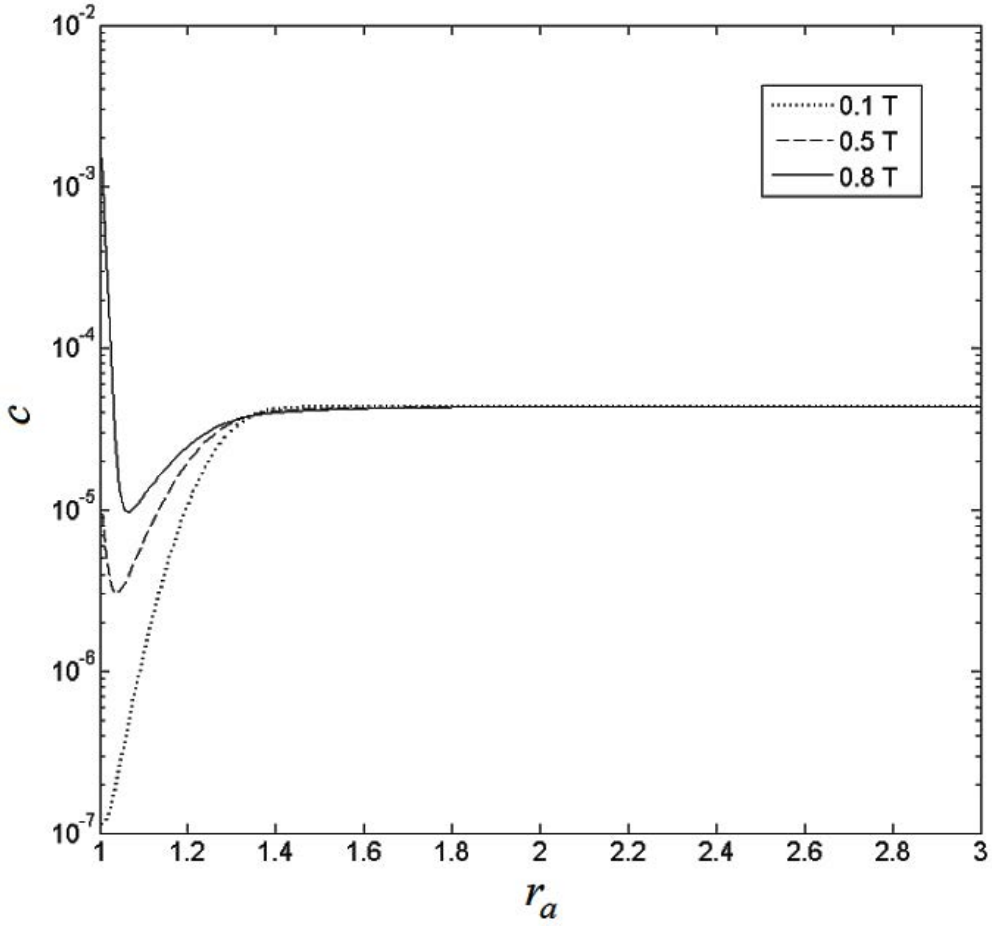

Figure 5.13: The radial concentration distribution of nano-drug carriers in direction θ = 0 radian at t = 1.54 ms for b_p = 10×10^{-9} m, V_{avg} = 2.2 cm/s, B_0 = 0.1, 0.5 and 0.8 T.

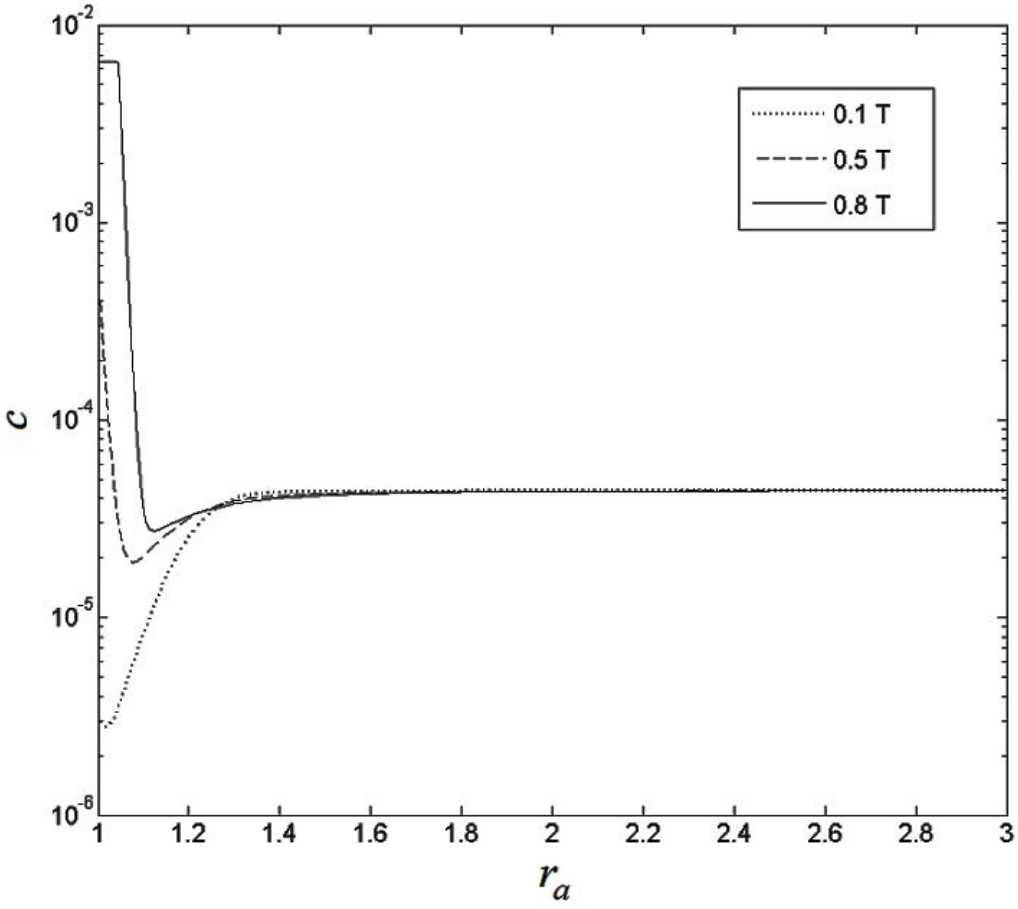

Figure 5.14: The radial concentration distribution of nano-drug carriers in direction θ = 0 radian at t = 1.76 ms for b_p = 10×10^{-9} m, V_{avg} = 2.2 cm/s, B_0 = 0.1, 0.5 and 0.8 T.

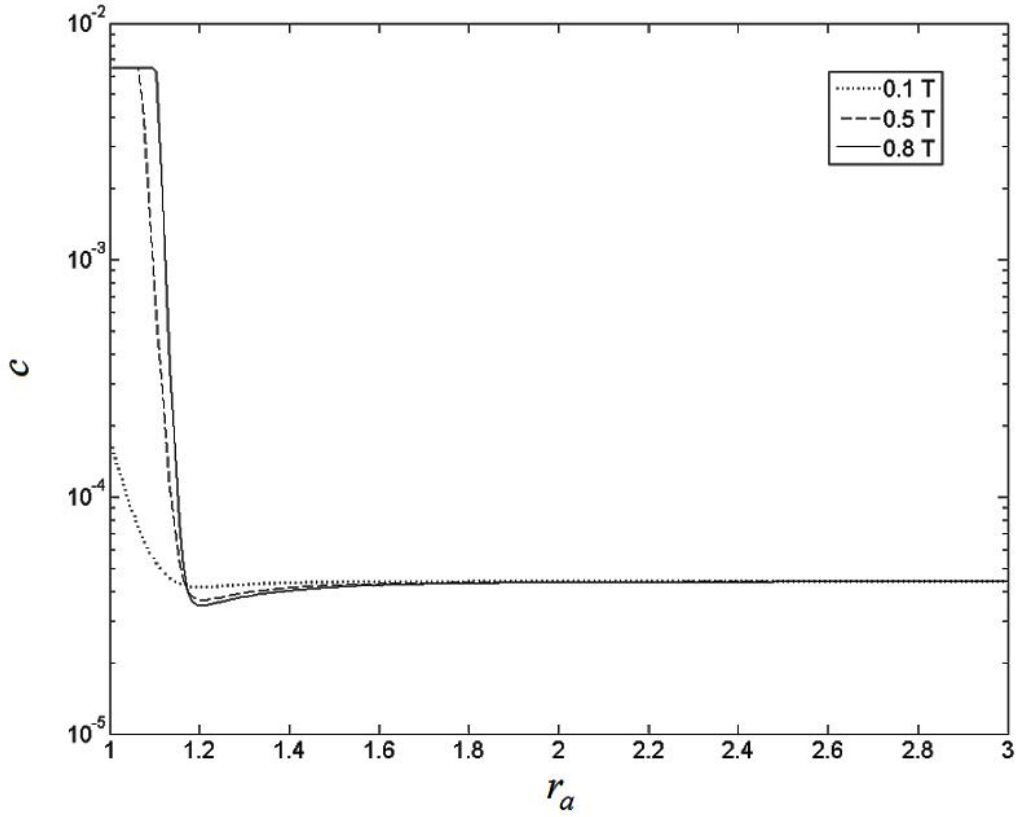

Figure 5.15: The radial concentration distribution of nano-drug carriers in direction θ = 0 radian at t = 8.79 ms for b_p = 10×10^{-9} m, V_{avg} = 2.2 cm/s, B_0 = 0.1, 0.5 and 0.8 T.

In Fig. 5.14, at t = 1.76 ms it is seen that the concentration levels in region near to wire surface increase from the initial value equal to zero for all value of B_0. This is because nano-drug carrier particles are carried continuously toward the wire by blood stream and all mechanisms (diffusion, convections due to blood stream and magnetic drift velocity) work along together. For B_0 = 0.1 and 0.5 T, the concentration levels on wire surface are increased from the values at t = 1.54 ms in Fig. 5.13 about 10 and 50 times, respectively. For B_0 = 0.8 T, the concentration level on wire surface reaches to the saturation level which is about 140 times of C_{in} due to the increasing magnetic force with increasing B_0 and the high magnetic field gradient in this region (θ = 0 radian).

In Fig. 5.14, at t = 8.79 ms at which the steady state is reached, The values of B_0 = 0.5 and 0.8 T can cause saturation concentration on the wire surface

with C_{sat} = 6.5×10^{-3} which is about 140 times of C_{in}. For the value of B_0 = 0.1 T, the concentration on the wire surface in direction θ = 0 radian is only about 4 times of C_{in}.

Figures 5.16, 5.17 and 5.18 show radial concentration distribution in the direction of $\theta = \pi/2$ radian (top surface of the wire) at times t = 1.54, 1.76, and 8.79 ms (steady state) compared between the cases of B_0 = 0.1, 0.5 and 0.8.

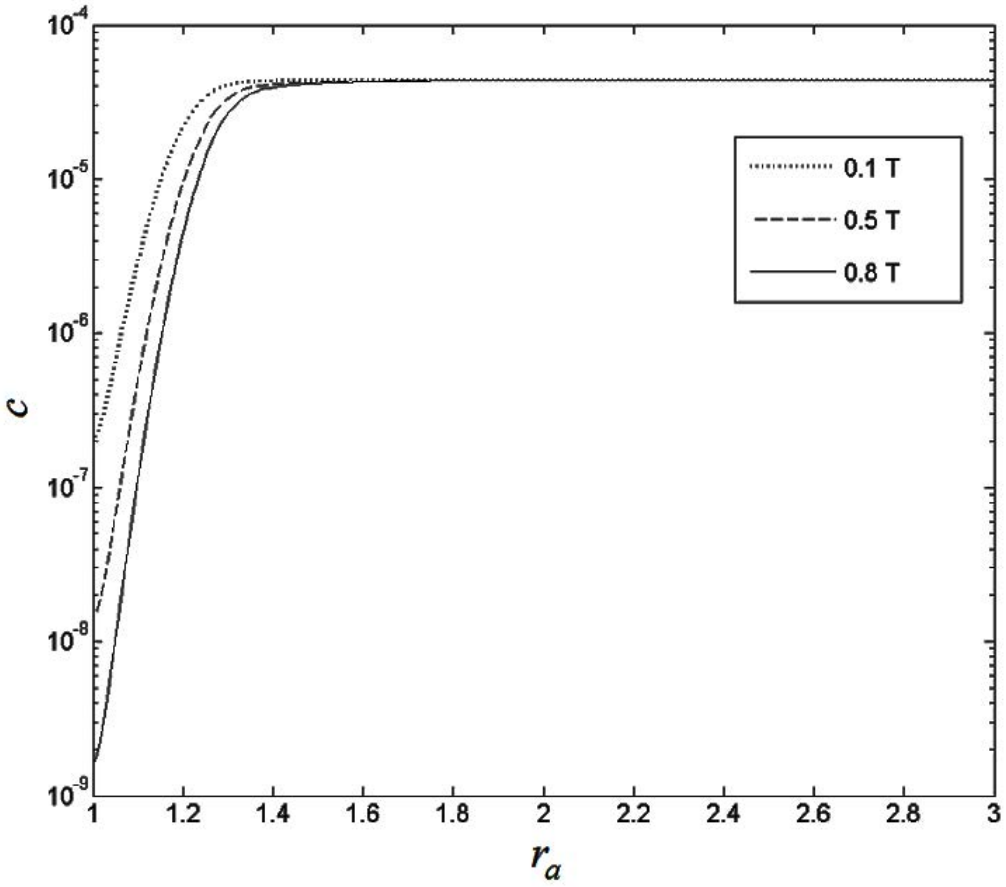

Figure 5.16: The radial concentration distribution of nano-drug carriers in direction $\theta = \pi/2$ radian at t = 1.54 ms for b_p = 10×10^{-9} m, V_{avg} = 2.2 cm/s, B_0 = 0.1, 0.5 and 0.8 T.

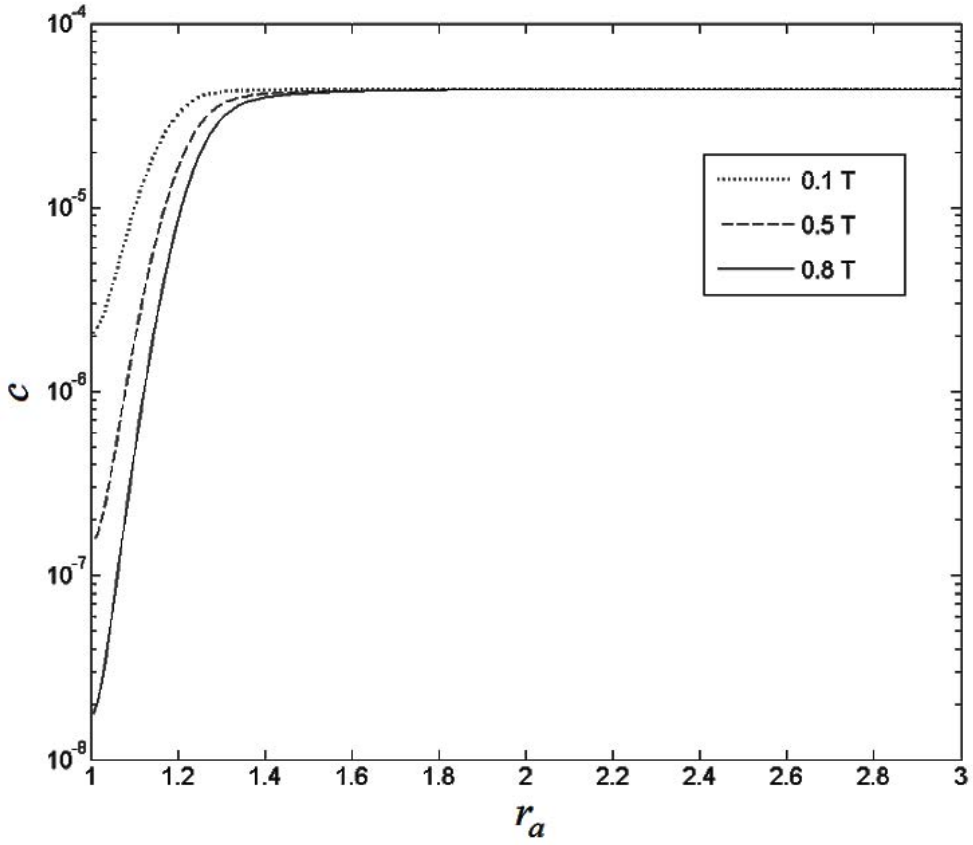

Figure 5.17: The radial concentration distribution of nano-drug carriers in direction $\theta = \pi/2$ radian at t = 1.76 ms for b_p = 10×10^{-9} m, V_{avg} = 2.2 cm/s, B_0 = 0.1, 0.5 and 0.8 T.

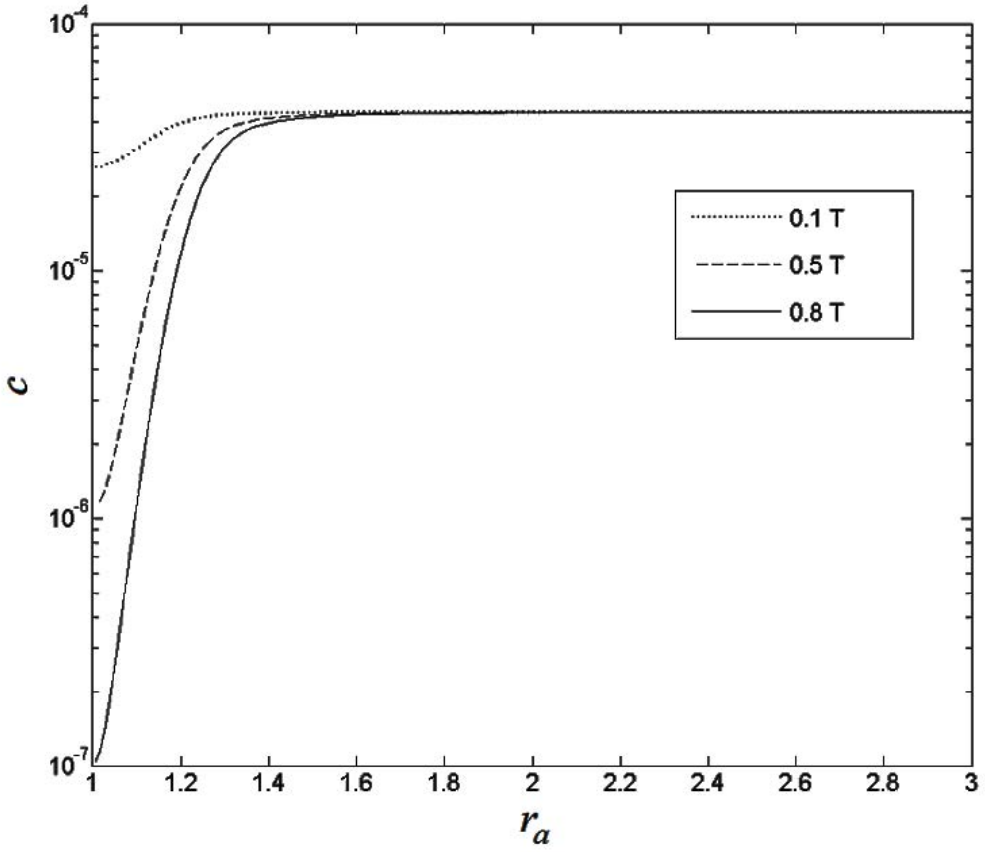

Figure 5.18: The radial concentration distribution of nano-drug carriers in direction $\theta = \pi/2$ radian at t = 8.79 ms for b_p = 10×10^{-9} m, V_{avg} = 2.2 cm/s, B_0 = 0.1, 0.5 and 0.8 T.

In Fig. 5.16, it is seen that the concentration level on the wire surface decreases when B_0 is increased. This can be described that at t = 1.54 ms the stream of nano-particles has already reach the top surface of the wire. However, the incoming particles experienced repulsive magnetic force and the larger B_0 provides the stronger repulsive magnetic force. Consequently, the value of B_0 = 0.8 T causes nano-particle near to wire surface to be transported into other region larger than the cases of smaller B_0.

In Figs. 5.17 and 5.18, as time increased to t = 1.76 ms and 8.79 ms (steady state), it is observed that the concentration levels on the wire surface and in

region near to wire surface are increased for all case. This is because nano-particles are continuously carried towards the top surface of the wire by blood stream. Although the incoming particles experienced repulsive magnetic force, the amount of nano-particles carried towards the wire by blood convection and diffusion is larger than that repelled away from wire surface.

Figures 5.19, 5.20 and 5.21 show radial concentration distribution in the direction of $\theta = 3\pi/2$ radian (bottom side of wire surface) at times t = 1.54, 1.76, and 8.79 ms (steady state) compared between the cases of B_0 = 0.1, 0.5 and 0.8.

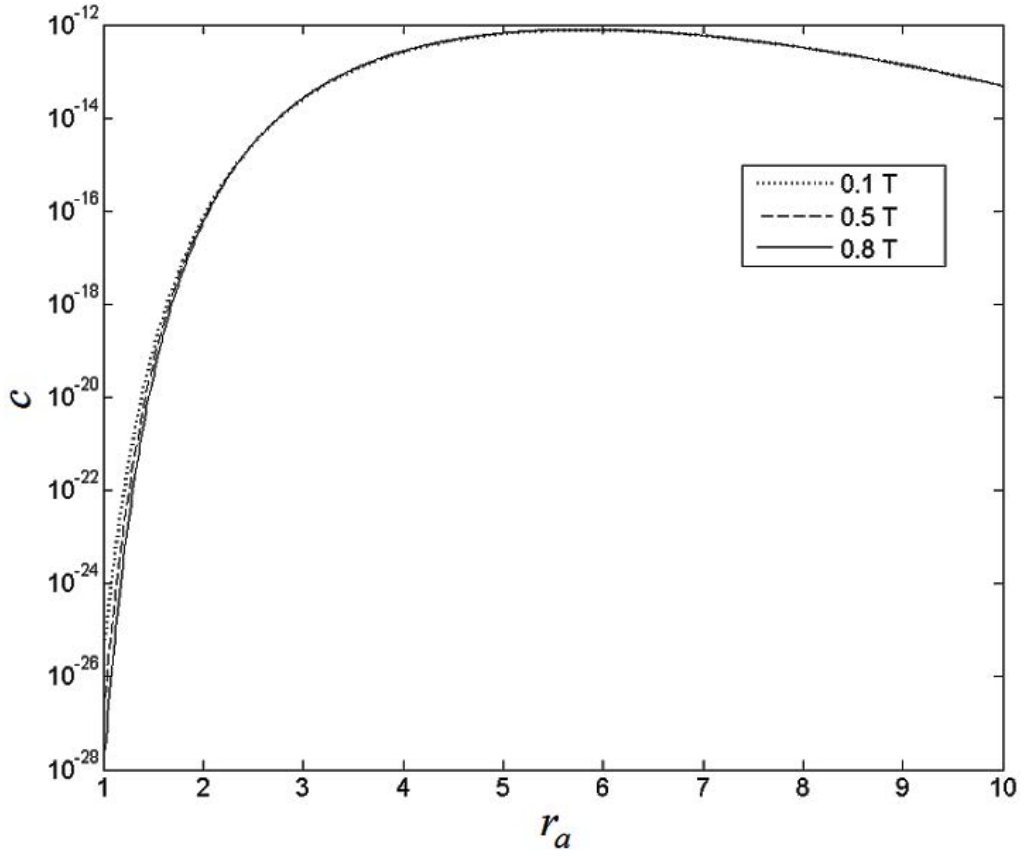

Figure 5.19: The radial concentration distribution of nano-drug carriers in direction $\theta = 3\pi/2$ radian at t = 1.54 ms, b_p = 10×10^{-9} m, V_{avg} = 2.2 cm/s, B_0 = 0.1, 0.5 and 0.8 T.

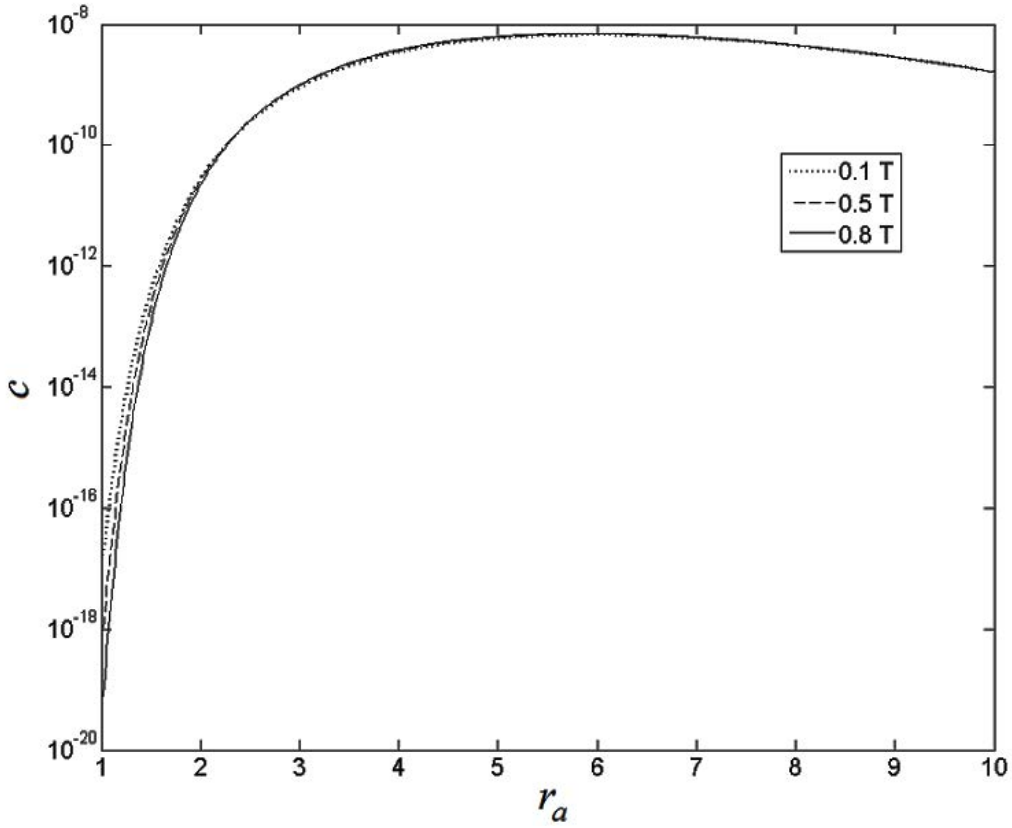

Figure 5.20: The radial concentration distribution of nano-drug carriers in direction $\theta = 3\pi/2$ radian at t = 1.76 ms, b_p = 10×10^{-9} m, V_{avg} = 2.2 cm/s, B_0 = 0.1, 0.5 and 0.8 T.

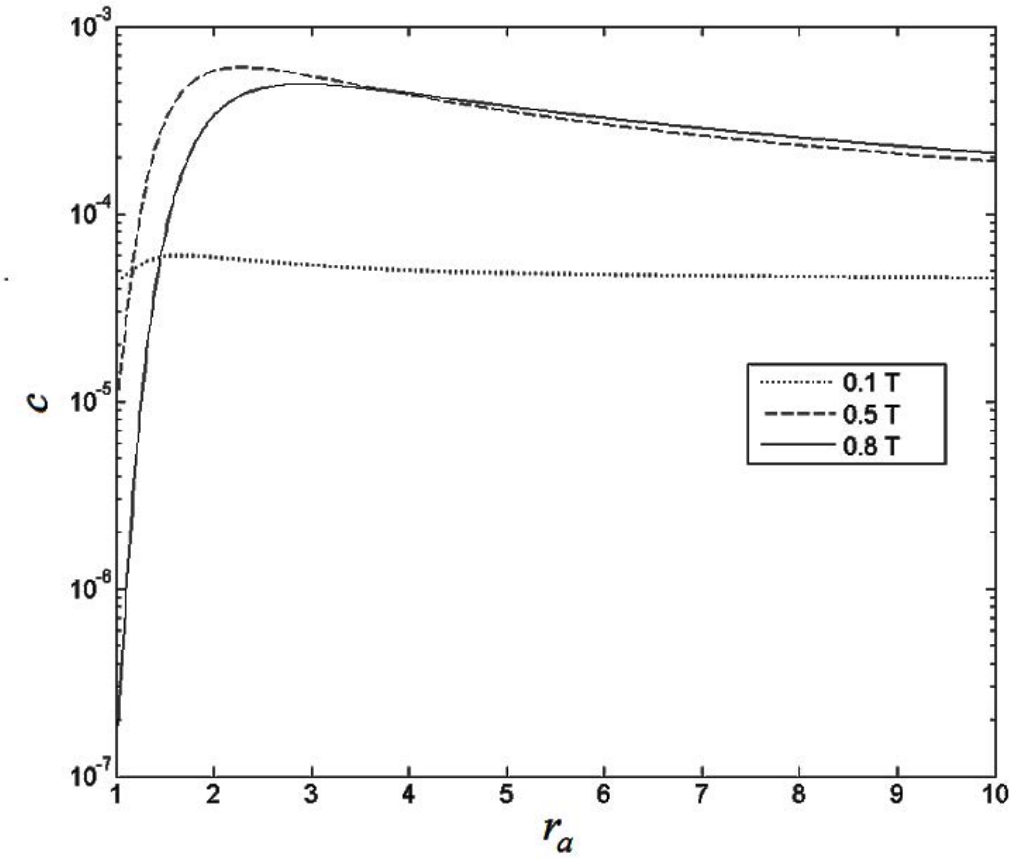

Figure 5.21: The radial concentration distribution of nano-drug carriers in direction $\theta = 3\pi/2$ radian at t = 8.79 ms, b_p = 10×10^{-9} m, V_{avg} = 2.2 cm/s, B_0 = 0.1, 0.5 and 0.8 T.

In Fig. 5.19, it is observed that the concentration at outer downstream boundary of considered region (r_a = 10) is very lower than the value of C_{in} = 4.4×10^{-5}. This is because at t = 1.54 ms, blood stream just firstly fill the considered region so very small amount of nano-particles reaches the downstream boundary. In region near to the wire surface ($1 \leq r_a \leq 2$), it is noted that the concentration is very lower than that in the region near to the downstream boundary. This is because the blood velocity in vicinity of the wire decreases to zero so particles that travel in region far from the wire reach the downstream boundary before particles that travel in region close to the wire reach the bottom surface of the wire. The differences between concentration on the wire

surface is caused by the repulsive magnetic force. The lower value of B_0 yields the higher value of concentration because of the weaker repulsive magnetic force that tries to push the particles away from the wire.

In Fig. 5.20, as time progress from t = 1.54 ms to t = 1.79 ms, the similar behaviors of radial concentration distribution are observed. However, the concentration levels at downstream boundary are increased because particles are continuously entering considered region. Concentration in region near wire surface also increases because of the amount of incoming particles caused by blood convection and diffusion from the region of higher concentration is higher than the amount of particles repelled away from wire surface.

In Fig. 5.21 at t = 8.97 ms (the steady state), it is seen for all cases that the concentration level on wire surface is smaller than the value C_{in} = 4.4×10^{-5}. For B_0 = 0.1, the concentration level in region a little farther from the wire surface is slightly more than C_{in} = 4.4×10^{-5} and the concentration level decrease to the value C_{in} in farther region up to the outer downstream boundary. For the case of B_0 = 0.5 and 0.8 T, the concentration level on the wire surface is very smaller than C_{in} then in the adjacent region the concentration level is higher than the value C_{in} and then decrease monotonically to a certain value larger than C_{in}. This behavior can be described that the repulsive magnetic force pushes particles away from the wire and, in the same time, other amounts of particles are transported, by diffusion and blood convection, from the left and right surface of the wire to the bottom surface then these two amounts of transported particle combine together and cause the increasing of concentration level beyond the value C_{in}. Nano-drug carries in the region of relative concentration higher than 1 are then transported to farther region on the downstream side.

5.2.2 Interception Capture of Nano-Drug Carriers

Beside the diffusive capture which is investigated in section 5.2.1, there is also the capture of nano-particles by interception where only effects of convections by

blood flow and magnetic drift velocity are considered. Figure 5.22 shows the trajectories of nano-drug carriers of 10 nanometer radius in region around the representative wire. The magnitude of blood average velocity is 2.2 cm/s and the magnitude of uniform magnetic flux density across the considered region is 0.8 T. All other parameters are the same as indicated in section 5.2.1.

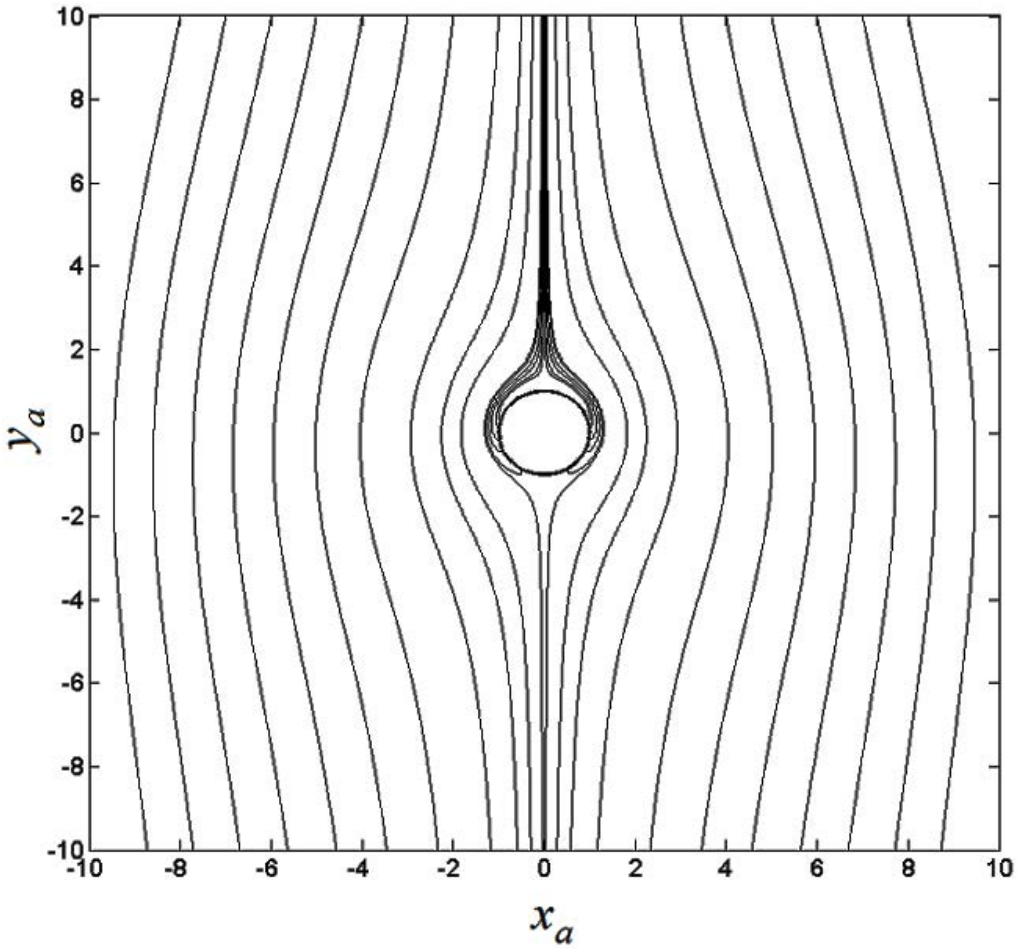

Figure 5.22: The trajectories of nano-drug carriers of radius b_p = 10×10^{-9} m for the case of V_{avg} = 2.2 cm/s and B_0 = 0.8 T.

In Fig. 5.22, it is seen that the regions that particle trajectories terminate on the wire surface are consistent with the saturation regions shown in Fig. 5.11. However, the interception does not occur at the accumulation regions near to the bottom surface of the wire and the trajectories show that particles which do not intercept with wire surface will escape the considered region. This result shows the significant effects of nano-drug carriers diffusion and also convection by magnetic drift velocity that provide significant contribution to the existence of accumulation region near to wire surface on downstream side.

5.2.3 The Efficacy of Capturing Nano-Drug Carriers

We investigate the feasibility and the efficacy of implanted assisted-magnetic drug targeting (IA-MDT) using ferromagnetic micro-wires for capturing ferromagnetic nano-particles in blood vessel, Moreover, we examine the capability of using IA-MDT for increasing the concentration of nano-drug carrier within the considered region.

For interception capture, we determine the normalized capture length, denoted by R_{ca}, which is the capture length (defined in section 4.6 of Chapter IV) normalized by wire radius The efficacy of interception capture is indicated by the relative capture length, denoted by λ_c, which is the ratio of total capture length and the diameter of simulation domain.

$$\lambda_c = \frac{\text{total capture length}}{\text{characteristic length of the simulation domain}}. \qquad (5.4)$$

In Eq. (5.4), the characteristic length is the diameter of simulation domain. It is observed that the problem is symmetry relative to y_a axis so the capture length should be symmetry relative to y_a axis too. Let R_{ca} be the normalized capture length measured from y_a axis in positive x_a direction then we can expressed λ_c as

$$\lambda_c = \frac{2R_{ca}}{D_a}, \qquad (5.5)$$

where D_a is the diameter of simulation domain normalized by wire radius.

To determine the efficacy of nano-drug carriers based on diffusive capture, we consider saturation region where nano-drug carriers accumulate densely and the static buildup exits because the incoming and outgoing particle fluxes are balanced. We calculate the ration between the volume of nano-drug carriers captured within saturation region and total volume of nano-drug carriers in the simulation domain denoted by P_{sat} [31],

$$P_{sat} = \frac{\text{volume of nano-drug carriers in saturation region}}{\text{total volume of nano-drug carriers in simulation domain}}. \qquad (5.6)$$

Moreover, we also calculate the average concentration of nano-drug carriers in simulation domain to investigate the capability of using the technique of IA-MDT to increase the average concentration of nano-drug carriers within the target site.

5.2.4 Capture Efficacy and Average Concentration of Nano-Drug Carriers in Simulation Domain for Varying B_0

We consider the capture of nano-drug carriers of 10 nanometer radius in blood stream of 2.2 cm/s average velocity while the value of B_0 is varied from 0.1 to 0.8 T. All other parameters are the same as indicated in section 5.2.1. Table 2 shows the data of P_{sat}, R_{ca}, λ_c and relative average concentration of nano-drug carriers in simulation domain (C_{avg} / C_{in}) for various value of B_0.

From Table 2, it is seen that P_{sat} and λ_c increase monotonically with increasing B_0. It is observed that P_{sat} equal to zero when B_0 = 0.1 and 0.2 T. For capture by interception, the values of B_0 = 0.1 and 0.2 T cause very small amount of nano-drug carriers to be retained on wire surface and λ_c is not zero which is different from the result of diffusive capture. For diffusive capture, the same values of B_0 are not

strength enough to cause static buildup (or saturation region) on wire surface since the convection by magnetic drift velocity does not overwhelm particle diffusion when nano-drug carriers try to attach on the wire surface. For B_0 larger or equal to 0.3 T, P_{sat} is larger than λ_c for all cases. This behavior can be described as follows. For nano-drug carriers that moving near to wire surface within the range of capture length, it is captured on the wire surface. For nano-drug carriers that moving in regions beyond the range of capture length where the convection by magnetic drift velocity does not overwhelm the convection by blood flow, they are not retained statically on the wire surface but form accumulation regions near to the bottom side of wire surface. At the bottom side of wire surface, magnetic force acting on nano-drug carriers is repulsive.

Table 2: The data of P_{sat}, R_{ca}, λ_c, and C_{avg}/C_{in} for the case of b_p = 10×10^{-9} m, V_{avg} = 2.2 cm/s, B_0 = 0.1 to 0.8 T.

B_0 (T)	P_{sat}	R_{ca}	λ_c	C_{avg}/C_{in}
0.1	0.00	0.008	8.0×10^{-4}	1.003
0.2	0.00	0.014	1.4×10^{-3}	1.05
0.3	3.9×10^{-2}	0.019	1.9×10^{-3}	1.17
0.4	7.0×10^{-2}	0.025	2.5×10^{-3}	1.21
0.5	9.3×10^{-2}	0.029	2.9×10^{-3}	1.25
0.6	1.1×10^{-1}	0.034	3.4×10^{-3}	1.27
0.7	1.3×10^{-1}	0.038	3.8×10^{-3}	1.30
0.8	1.4×10^{-1}	0.043	4.3×10^{-3}	1.31

In the direction $\theta = 3\pi/2$ radian, the magnetic force repels nano-drug carriers directly away from wire surface. In adjacent directions on the left and right sides of $\theta = 3\pi/2$ direction, magnetic force sweeps nano-drug carriers toward left and right sides. Consequently, nano-drug carriers in accumulation regions near the bottom side of the wire are sweep back into the region of capture length so they have certain chance to

be re-captured within the region of static buildup. Beside the action of magnetic force, diffusion also cause nano-drug carriers in accumulation region near to wire bottom surface to be transported back into the region of attractive magnetic force and increase the amount of the carriers that are captured within the region of static buildup.

Figure 5.23 shows the variation of average concentration, relative to C_{in}, of nano drug carriers at t = 8.79 ms (steady state) versus B_0. It is seen that the values of B_0 lower than 0.3 T do not cause significant increasing of average concentration above C_{in}. The average concentrations are only about 0.0 % and 5.0 % higher than C_{in} for B_0 = 0.1 and 0.2 T, respectively. The average carrier concentrations are significantly higher than C_{in} when the values of B_0 higher or equal to 0.3 T. The average concentrations of nano-drug carriers are higher than C_{in} from 16% up to 31% for B_0 from 0.3 T up to 0.8 T.

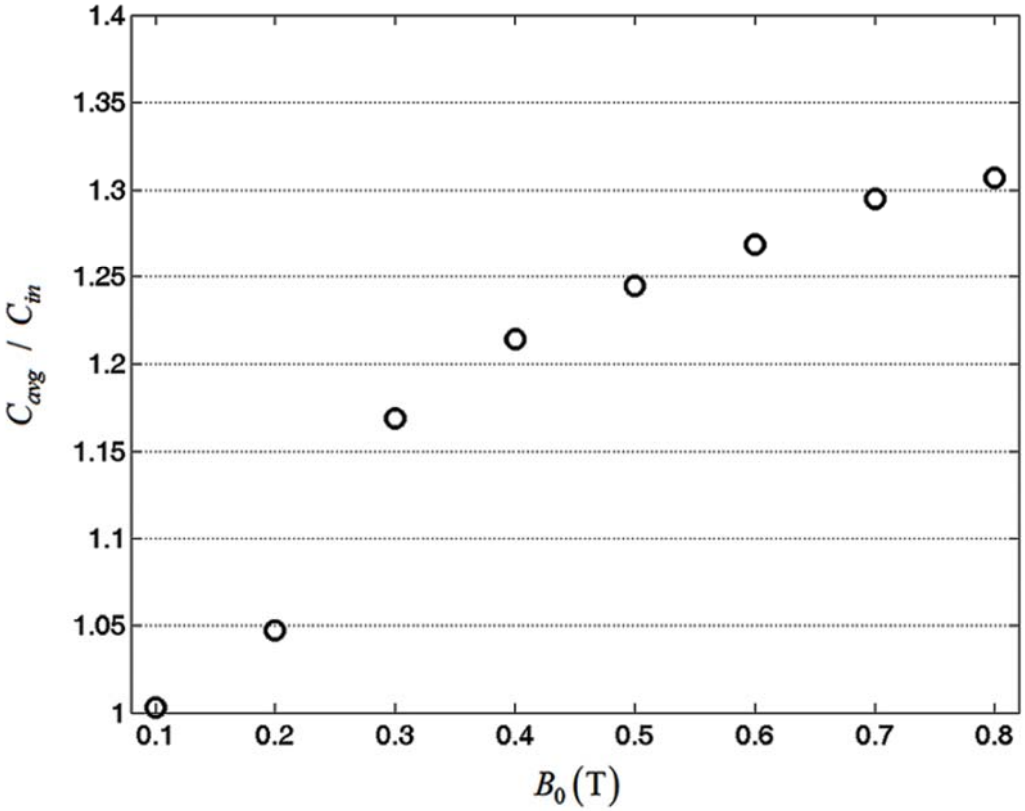

Figure 5.23: The variation of C_{avg}/C_{in} versus B_0 for the case of b_p = 10×10^{-9} m, V_{avg} = 2.2 cm/s, t = 8.79 ms (steady state).

From Table 2 and Fig. 5.23, it is seen that although the values of P_{sat} and λ_c are looked like very small, it is feasible to significantly increase the average concentration of nano-drug carriers around the magnetic drug target higher than the value of injected concentration C_{in}. These predicted results response to the major objectives of magnetic drug target: to confine the injected nano-drug carries within restricted regions and increase the concentration of nano-drug carriers within the region so iit is possible to reduce the injected doses of nano-drug carriers. Consequently, the concentration of escaping nano-drug carries can be reduced until it can not cause potential toxicities on other organs.

5.2.5 Capture Efficacy and Average Concentration of Nano-Drug Carriers in Simulation Domain for Varying V_{avg}

We consider the effect of blood average velocity on capture efficacy of nano-drug carriers and the value of average concentration of nano-drug carriers in simulation domain. The radius of nano-drug carriers is assigned as 10 nanometer, the values of B_0 are in the range from 0.1 to 0.8 T and the magnitudes of average blood velocity are 1.1 and 2.2 cm/s. All other parameters are the same as indicated in section 5.2.1. Table 3 shows the data of P_{sat}, R_{ca}, λ_c and C_{avg}/C_{in} for various B_0 when V_{avg} = 1.1 cm/s.

Figure 5.24 shows the comparison of P_{sat} between V_{avg} = 1.1 and 2.2 cm/s. It is seen that, for the same value of B_0, P_{sat} increases when the average velocity of blood in considered region is reduced. However, the value of B_0 = 0.1 T is still not enough to create static buildup or saturation concentration on wire surface. It is noted that the value of B_0 = 0.2 T can create static buildup on wire surface for V_{avg} = 1.1 cm/s while the situation does not exist for V_{avg} = 2.2 cm/s.

Table 3: The data of P_{sat}, R_{ca}, λ_c, and C_{avg}/C_{in} for the case of b_p = 10×10^{-9} m, V_{avg} = 1.1 cm/s, B_0 = 0.1 to 0.8 T.

B_0 (T)	P_{sat}	R_{ca}	λ_c	C_{avg}/C_{in}
0.1	0.00	0.014	1.4×10^{-3}	1.004
0.2	1.7×10^{-2}	0.025	2.5×10^{-3}	1.14
0.3	6.3×10^{-2}	0.034	3.4×10^{-3}	1.23
0.4	9.6×10^{-2}	0.043	4.3×10^{-3}	1.27
0.5	1.2×10^{-1}	0.051	5.1×10^{-3}	1.30
0.6	1.4×10^{-1}	0.059	5.9×10^{-3}	1.32
0.7	1.6×10^{-1}	0.066	6.6×10^{-3}	1.35
0.8	1.7×10^{-1}	0.073	7.3×10^{-3}	1.37

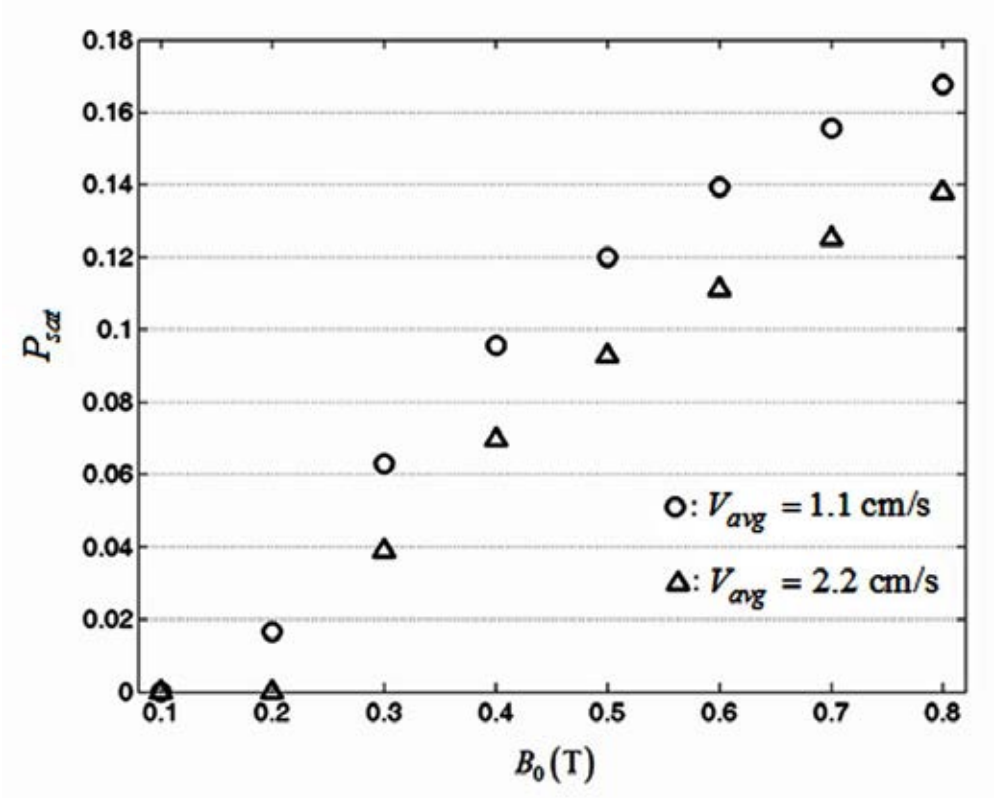

Figure 5.24: The comparison of P_{sat} between V_{avg} = 1.1 and 2.2 cm/s for the case of b_p = 10×10^{-9} m, B_0 = 0.1 to 0.8 T.

The results in Table 3 and Fig. 5.24 can be described that the effects of diffusion and convection due to magnetic drift velocity is more significant when they are compared with the effect of convection due to blood flow for lower average blood velocity. Consequently, R_{ca} and λ_c increase as seen by the comparison between data in Tables 2 and 3 and the influence of diffusion and convection due to magnetic drift velocity in regions near to the bottom side of wire surface becomes more significant compared with that of convection by blood flow. As a result, the nano-drug carriers in accumulation region near wire bottom side are better re-transported into regions within capture length.

Figure 5.25 shows the comparison between average concentration of nano-drug carriers for V_{avg} = 1.1 and 2.2 cm/s at t = 8.79 ms (steady state).

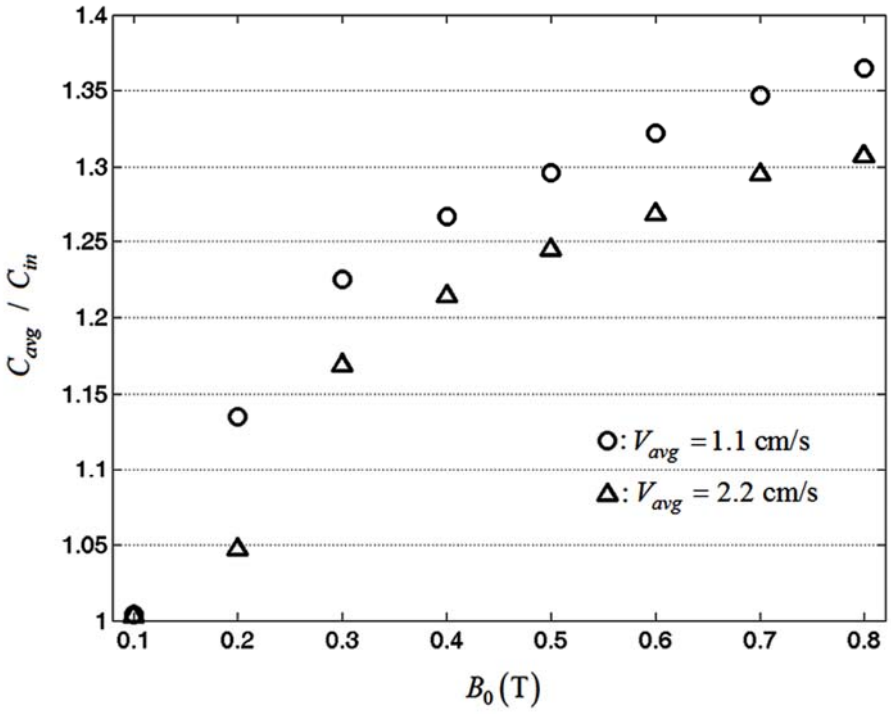

Figure 5.25: The comparison of C_{avg}/C_{in} between V_{avg} = 1.1 and 2.2 cm/s for b_p = 10×10^{-9} m, B_0 = 0.1 to 0.8 T, t = 8.79 ms (steady state).

In Fig. 5.25, it is seen that when the average blood velocity is decreased to 1.1 cm/s, the value of B_0 = 0.2 T can cause significant increasing of average concentration above

C_{in} (the average concentration is about 14 % higher than C_{in}). However, the value of B_0 = 0.1 T still not enough to create significant increasing of average particle concentration in simulation domain. For V_0 = 1.1 cm/s, the concentrations are increased higher than C_{in} from 14% up to 37% for values of B_0 from 0.2 T up to 0.8 T.

5.2.6 Capture Efficacy and Average Concentration of Nano-Drug Carriers in Simulation Domain for varying b_p

It Is seen in Table 2 and 3, Figs. 5.24 and 5.25 that the value of B_0 = 0.1 T is not high enough to create static buildup or saturation concentration on the wire surface and it does not significantly increase the average concentration of nano-drug carriers within the simulation domain. In this section, we study the effect of increasing the size of nano-drug carriers to compensate the low value of B_0 and investigate whether it is possible to capture and target nano-drug carriers within the target region of very small B_0. Table 4 shows the data of P_{sat}, R_{ca}, λ_c and C_{avg}/C_{in} for B_0 = 0.1 T, V_{avg} = 1.1 cm/s, t = 3 ms, b_p = 10, 30, 50, 70 and 100 nanometers. All other parameters are the same as indicated in section 5.2.1.

Table 4: The data of P_{sat}, R_{ca}, λ_c, and C_{avg}/C_{in} for B_0 = 0.1 T, V_{avg} = 1.1 cm/s, t = 3 ms, b_p = 10, 30, 50, 70 and 100 nanometers.

b_p (nm)	P_{sat}	R_{ca}	λ_c	C_{avg}/C_{in}
10	0.00	0.014	1.4×10^{-3}	0.95
30	4.2×10^{-2}	0.07	7.0×10^{-3}	0.99
50	2.1×10^{-1}	0.16	1.6×10^{-2}	1.19
70	2.8×10^{-1}	0.20	2.0×10^{-2}	1.30
100	4.4×10^{-1}	0.30	3.0×10^{-2}	1.67

Figure 5.26 shows the variation of P_{sat} versus b_p.

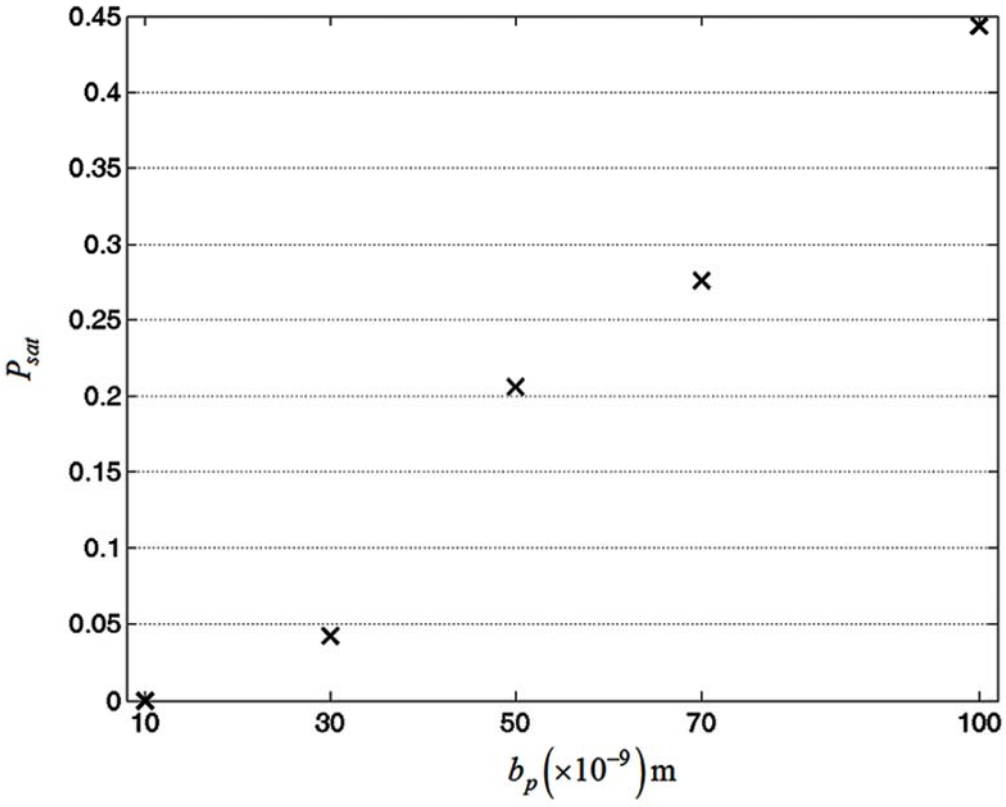

Figure 5.26: The variation of P_{sat} with b_p for B_0 = 0.1 T, V_{avg} = 1.1×10^{-2} m/s, t = 3 ms.

In Fig. 5.26, it is seen that the size of nano-drug carrier should not less than 50 nanometer to obtain significant capture of nano-drug carriers when the strength of an external uniform magnetic flux density across the simulation domain (B_0) is low. The larger nano-drug carrier provides higher capture efficacy since the magnetic force, and also the convection by magnetic drift velocity, depends on the cube of nano-drug carrier radius.

Figure 5.27 shows the values of relative concentration C_{avg}/C_{in} for various size of nano-drug carriers. In Fig. 5.27, nano-drug carriers of 50 nanometer radius cause the average concentration higher than the value C_{in} of about 19 %. If radius of the carrier is increased to 70 and 100 nanometers, the average concentration

in considered region can be increased to values higher than C_{in} about 30% and 67%, respectively.

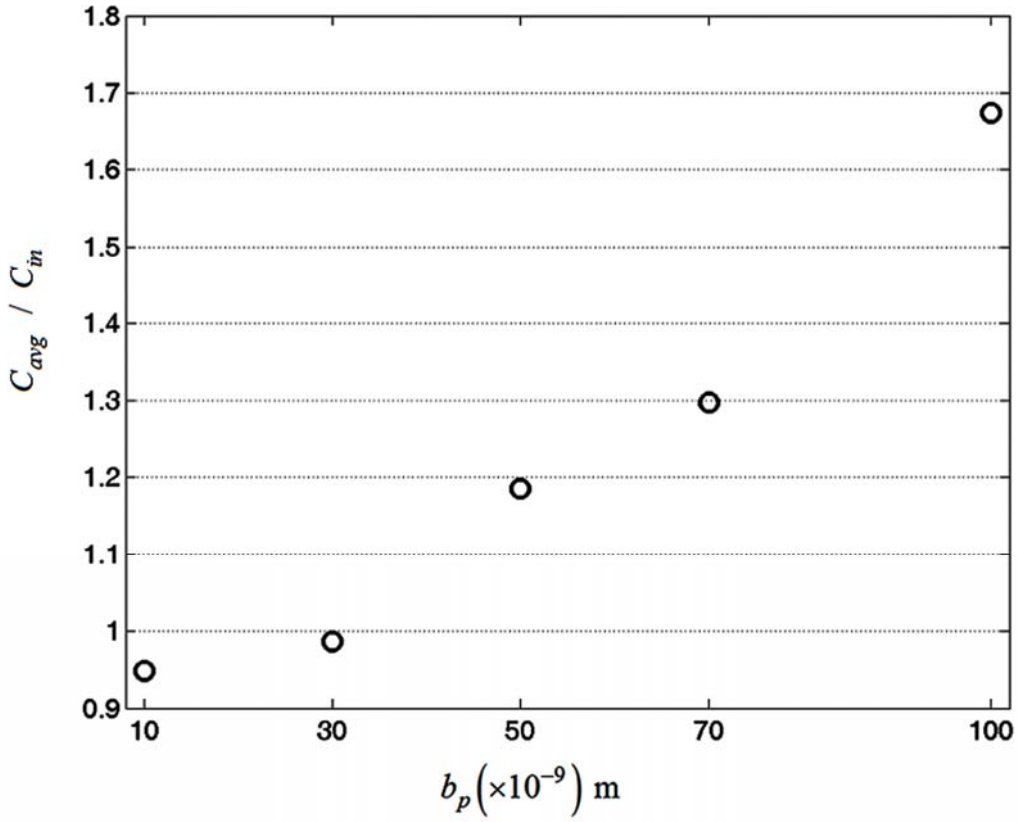

Figure 5.27: The relative average concentration (C_{avg} / C_{in}) in considered region for B_0 = 0.1 T, V_{avg} = 1.1×10^{-2} m/s, b_p = 10, 30, 50, 70, 100 nm, t = 3 ms.

From results in Figs. 5.26 and 5.27, it is predicted that the capture of nano-drug carriers in the region of weak magnetic flux density is feasible by increasing the size of nano-drug carriers.

CHAPTER VI

CONCLUSIONS

In this research, the captures of micro- and nano-particles in high gradient magnetic field are studied. For micro-particles, we study the capture of weakly magnetic micro-particles by an assemblage of parallel wires randomly distributed in axial magnetic filters. The single-wire model of particle capture in high gradient magnetic separation is generalized to a range of higher packing fraction. The magnetic field around the representative wire previously calculated by Natenapit [15] using the EMT model and the axial flow field of the viscous fluid, derived by Happel [19], relative to a bundle of parallel cylinders are used for magnetic and fluid laminar flow fields around any wires in the filter. Particle trajectories were traced numerically to determine the capture cross-section. Capture cross-sections are reported and compared with those obtained by using the magnetic field calculated from the single-wire approximation [16]. The limit and basic criterion of validity of the single-wire model is firstly represented and analyzed in this article. We also apply the EMT model to predict the efficiency of capturing red blood cells (RBCs) and white blood cells (WBCs) from whole blood in an axial magnetic filter. The feasibility of macro-scale blood cells separation that provides high gradient magnetic field and high efficiency is investigated.

For the capture of nano-particles, we firstly study implant assisted-magnetic drug targeting using ferromagnetic micro-wires, localized instantaneously within a blood vessel, for capturing ferromagnetic nano-drug carriers in blood stream. The micro-wires are very long compared with their radii and they are very smaller than the considered blood vessel volume. Therefore, diffusive capture behaviors are investigated in two dimension on a plane that is sliced through a representative wire's cross section. Diffusion of nano-drug carriers is taken into account and particle dynamic is described statistically by the continuity equation. The magnetic and flow fields around the representative wire is approximated by the single-wire approximation for

dilute micro-wire in the system. The condition of blood flow is considered as a laminar flow of single-phase viscous fluid pass a long cylinder. The value of velocity field around the representative wire is obtained from numerical solution of
Navier-Stokes' equation. Diffusive capture of nano-drug carriers is simulated by solving the continuity equation numerically for the given initial and boundary value of the carrier concentration. Then we determine the distribution of particle concentration within the simulation domain for varying time until the steady state. The feasibility of targeting nano-drug carriers to a representative wire target site in blood vessel is investigated. The capability of increasing average concentration of nano-drug carriers within the bounded region around to the wire is investigated.

From our study of micro-particle capture, the results obtained from the EMT model reduce to that obtained from the single-wire model in the limit of a very dilute packing fraction of the wires (F = 0.01) and a relatively low applied magnetic field strength. The results determined by using the magnetic field calculated based on the EMT model reasonably explain and qualitatively support the experimental result in the literature [50]. Since the proposed macro-scale axial magnetic filter provided relatively high capture efficiency. Consequently, it is feasible and useful to develop the proposed axial filter for therapeutic applications such as plasma separation from whole blood.

For the results of nano-particle capture, it is shown that diffusion process provides significant contribution to the capture of nano-drug carriers. Although the average velocity of blood flow in the vessel is in the order of centimeter per second, drug carriers that are very small as 10 nanometers can be significantly captured by the micro-wires implanted within blood vessel when the strength of uniform magnetic flux density (B_0) across the target site in the vessel is high enough (0.3 T to 0.8 T). The capture process progresses very rapidly and the steady state can be reach within the time scale of 10 ms. The average concentration of nano-drug carriers in simulation domain can be increased significantly higher than the value of injected concentration of nano-drug carriers. The efficacy of nano-drug carriers capture and the increasing of average carriers concentration can be increased when the average blood velocity

decrease or when the capture process is performed within smaller blood vessel. In the case that the strength of uniform magnetic flux density across the target site in blood vessel is very low, nano-drug carries are also significantly captured by increasing their sizes. From our results, when the strength of uniform magnetic flux density across the target site is not more than 0.1 T, the radius of nano-drug carriers should not smaller than 50 nanometers to achieve significant capture. Our investigations of implant assisted-magnetic drug targeting of nano-drug carriers in blood vessel can provide useful information about the understanding of capture mechanism and dynamics of nano-drug carriers concentration and also the feasibility and capability of increasing average concentration of the carries within the area around the magnetic wire target. This information are hoped to provide any contributions for development of modern therapies of cancers and tumors for the health of people in worldwide.

REFERENCES

[1] Kelland, R. D. High Gradient Magnetic Separation Applied to Mineral Beneficiation. IEEE Transactions on Magnetics 9 (September 1973): 307-310.

[2] Shigehiro, N., and Shin-ichi, T. Superconducting High Gradient Magnetic Separation for Purification of Wastewater From Paper Factory. IEEE Transactions on Applied Superconductibity 16 (June 2006): 1142-1145.

[3] Thomas, T. E., Abraham, S. J.R., Otter, A. J., Blackmore, E. W., and Lansdorp, P. M. High Gradient Magnetic Separation of Cells on the Basis of Expression Levels of Cell Surface Antigens. Journal of Immunological Methods 154 (October 1992): 245-252.

[4] Hiroshi, U., Koh, A., Kazuhiro, K., Mitsuho, F., Shuichiro, F., and Atsushi, I. Design and Test of Filter of High Gradient Magnetic Separation System for Trapping Immunoglobulin in Serum. IEEE Transactions on Applied Superconductivity 19 (June 2009): 2157-2161.

[5] Melville, D., Paul, F., and Roath, S. High Gradient Magnetic Separation of Red Cells from Whole Blood. IEEE Transactions on Magnetics 6 (November 1975): 1701-1704.

[6] Ritter, J. A., Ebner, A. D., Daniel, K. D., and Stewart, K. L. Application of High Gradient Magnetic Separation Principles to Magnetic Drug Targeting. Journal of Magnetism and Magnetic Materials 280 (September 2004): 184-201.

[7] Chuzawa, M., Mishima, F., Akiyama, Y., and Nishijima, S. Drug Accumulation by Means of Noninvasive Magnetic Drug Delivery System. Physica C: Superconductivity 471 (November 2011): 1538-1542.

[8] Chertok, B., David, A. E., and Yang, V. C. Brain Tumor Targeting of Magnetic Nanoparticles for Potential Drug Delivery: Effect of Administration Route and Magnetic Field Topography. Journal of Controlled Release 153 (November 2011): 393-399.

[9] Avilés, M. O., Ebner, A. D., and Ritter, J. A. Ferromagnetic Seeding for the Magnetic Targeting of Drugs and Radiation in Capillary Beds. Journal of Magnetism and Magnetic Materials 310 (March 2007): 131-144.

[10] Kempe, H. and Kempe, M. The Use of Magnetite Nanoparticles for Implant-Assisted Magnetic Drug Targeting in Thrombolytic Therapy. Biomaterials 31 (December 2010): 9499-9510.

[11] Avilés, M. O., Ebner, A. D., and Ritter, J. A. Implant Assisted-Magnetic Drug Targeting: Comparison of *In Vitro* Experiments with Theory. Journal of Magnetism and Magnetic Materials 320 (November 2008): 2704-2713.

[12] Bleaney, B. I. and Bleaney, B. Electricity and Magnetism. Vol. 1, 3 rd ed. London: Oxford University Press, 1993.

[13] Fletcher, D. Fine Particle High Gradient Magnetic Entrapment. IEEE Transactions on Magnetics 27 (July 1991): 3655-3677.

[14] Gerber, R. and Birss, R. R. High gradient magnetic separation. Chichester: John Wiley&Sons, 1983.

[15] Suchat Kuntabutr. Theory of Particle Capture in High Gradient Magnetic Field. Master's Thesis, Department of Physics, Faculty of Science, Chulalongkorn University, 1992.

[16] Watson, J. H. P. Magnetic Filtration. Journal of Applied Physics 44 (September 1973): 4209-4213.

[17] Natenapit, M., and Sanglek, W. Capture Radius of Magnetic Particles in Random Cylindrical Matrices in High Gradient Magnetic Separation. Journal of Applied Physics 85 (January 1999): 660-664.

[18] Natenapit, M. Magnetic Field for an Assemblage of Cylinders. Journal of Scientific Research Chulalongkorn University 13 (1988): 23-27.

[19] Gerber, R. Theory of Particle Capture in Axial Filter for High Gradient Magnetic Separation. Journal of Physics D: Applied Physics 11 (1978): 2119-2129.

[20] Birss, R., Gerber, R., Parker, M., and Sheerer, T. J. Laminar Flow Model of Particle Capture of Axial Magnetic Filters. IEEE Transactions on Magnetics 14 (November 1978): 1165-1169.

[21] Greiner, H., and Hoffmann, H. Efficiencies of Axially Ordered HGMS-Filters Calculated from a Multiwire Model. Journal of Magnetism and Magnetic Materials 38 (September 1983): 194-204.

[22] Happel, J. Viscous Flow Relative to Arrays of Cylinders. AIChE Journal 5 (June 1959): 174-177.

[23] Han, K. H., and Frazier, B. Diamagnetic Capture Mode Magnetophoretic Microseparator for Blood Cells. Journal of Microelectromechanical Systems 14 (December 2005): 1422-1431.

[24] Han, K. H., and Frazier, B. Paramagnetic Capture Mode Magnetophoretic Microseparator for High Efficiency Blood Cell Separations. Lab on a Chip 6 (February 2006): 265-273.

[25] World Health Organization. The Clinical Use of Blood in General Medicine Obstetrics Paediatrics Surgery & Anaesthesis Trauma & Burns [on line]. (n. d.) Available from: http://www.who.int/bloodsafety/clinical_use/en/Manual_EN.pdf [2012, May, 15]

[26] VanDelinder, V., and Groisman, A. Separation of Plasma from Whole Human Blood in a Continuous Cross-Flow in a Modeled Microfluidic Device. Analytical Chemistry 78 (June 2006): 3765-3771.

[27] Park, J., Cho, K., Chung, C., Han, D. C., and Chang, J. K. Continuous Plasma Separation From Whole Blood Using Microchannel Geometry. Proceeding of the third Annual International IEEE EMBS Special Topic Conference on Microtechnologies in Medicine and Biology, pp. 8-9, Kahuku, Oahu, Hawaii, USA, 2005.

[28] Gerber, R., Takayasu, M., and Friedlaender, F. J. Generalization of HGMS Theory: The Capture of Ultra-Fine Particles. IEEE Transactions on Magnetics 19 (September 1983): 2115-2117.

[29] Takayasu, M., Gerber, R., and Friedlaender, F. J. Magnetic Separation of Submicron Particles. IEEE Transactions on Magnetics 19 (September 1983): 2112-2114.

[30] Davies, L. P., and Gerber, R. 2-D Simulation of Ultra-Fine Particle Capture by a Single-Wire Magnetic Collector. IEEE Transactions on Magnetics 26 (September 1990): 1867-1869.

[31] Hournkumnuard, K., and Natenapit, M. Diffusive Capture of Magnetic Particles by an Assemblage of Random Cylindrical Collectors. Separation Science and Technology 43 (2008): 3448-3460.

[32] Arruebo, M., Fernández-Pacheco, R., Ricardo Ibarra, M., and Santamaria, J. Magnetic Nanoparticles for Drug Delivery. Nanotoday 2 (June 2007): 22-32.

[33] Lübbe, A. S., Bergemann, C., Riess, H., et al. Clinical Experiences with Magnetic Drug Targeting: A Phase I Study with 4′-Epidoxorubicin in 14 Patients with Advanced Solid Tumors. Cancer Research 56 (October 1996): 4686-4693.

[34] Chen, H., Ebner, A. D., Rosengart, A. J., Kaminski, M. D., and Ritter, J. A. Analysis of Magnetic Drug Carrier Particle Capture by a Magnetizable Intravascular Stent: 1. Parametric Study with Single Wire Correlation. Journal of Magnetism and Magnetic Materials 284 (December 2004): 181-194.

[35] Chen, H., Ebner, A. D., Kaminski, M. D., Rosengart, A. J., and Ritter, J. A. Analysis of Magnetic Drug Carrier Particle Capture by a Magnetizable Intravascular Stent-2: Parametric Study with Multi-Wire Two-Dimensional Model. Journal of Magnetism and Magnetic Materials 293 (May 2005): 616-632.

[36] Mardinoglu, A., Cregg, P. J., Murphy, K., Curtin, M., and Prina-Mello, A. Theoretical Modeling of Physiologically Stretched Vessel in Magnetisable Stent Assisted Magnetic Drug Targeting Application. Journal of Magnetism and Magnetic Materials 323 (February 2011): 324-329.

[37] Iacob, G., Rotariu, O., Strachan, N. J. C, and Häfeli, U. O. Magnetizable Needles and Wires – Modeling an Efficient Way to Target Magnetic Microspheres in *VIVO*. Biorheology 41 (2004): 599-612.

[38] Avilés, M. O., Ebner, A. D., and Ritter, J. A. In *Vitro* Study of Magnetic Particle Seeding for Implant-Assisted-Magnetic Drug Targeting: Seed and Magnetic Drug Carrier Particle Capture. Journal of Magnetism and Magnetic Materials 321 (May 2009): 1586-1590.

[39] Cregg, P. J., Murphy, K., and Mardinoglu, A. Calculation of Nanoparticle Capture Efficiency in Magnetic Drug Targeting. Journal of Magnetism and Magnetic Materials 320 (December 2008): 3272-3275.

[40] Cherry, E. M., Maxim, P. G., and Eaton, J. K. Particle Size, Magnetic Field, and Blood Velocity Effects on Particle Retention in Magnetic Drug Targeting. Medical Physics 37 (January 2010): 175-182.

[41] Furlani, E. J., and Furlani, E. P. A Model for Predicting Magnetic Targeting of Multifunctional Particles in the Microvasculature. Journal of Magnetism and Magnetic Materials 312 (May 2007): 187-193.

[42] Grief, A.D., and Richardson, G. Mathematical Modeling of Magnetically Targeted Drug Delivery. Journal of Magnetism and Magnetic Materials 293 (May 2005): 455-463.

[43] Hashin, Z. Assessment of the Self Consistent Scheme Approximation: Conductivity of Particulate Composites. Journal of Composite Materials 2 (1968): 284-300.

[44] Li, Y., and Park, C. W. Effective Medium Approximation and Deposition of Colloidal Particles in Fibrous and Granular Media. Advances in Colloid and Interface Science 87 (September 2000): 1-74.

[45] Boardman, A. D. Physics Programs: Magnetism. Belfast : John Wiley&Sons, 1980.

[46] Nacev, A., Beni, C., Bruno, O., and Shapiro, B. The Behaviors of Ferromagnetic Nano-Particles in and Around Blood Vessels under Applied Magnetic Fields. Journal of Magnetism and Magnetic Materials 323 (March 2011): 651- 668.

[47] Barbic, M. Magnetic Wires in MEMS and Bio-Medical Applications. Journal of Magnetism and Magnetic Materials 249 (August 2002): 357-367.

[48] Jackson, J. D. Classical electrodynamics. 2 nd ed. New York: John Wiley&Sons, 1975.

[49] Mao, Z. S., and Wang, Y. Numerical Simulation of Mass Transfer of a Spherical Particle Assemblage with the Cell Model. Powder Technology 134 (August 2003): 145-155.

[50] Pankhurt, Q. A., Connolly, J., Jones, S. K., and Dobson, J. Applications of Magnetic Nanoparticles in Biomedicine. Journal of Physics D: Applied Physics 36 (2003): R167-R181.

[51] Alexiou, C., Schmid, R. J., Jurgons, R. et al. Targeting Cancer Cells: Magnetic Nanoparticles as Drug Carriers. Biophysics Letter (January 2006): 446-450.

[52] Vitek, J. J. Carotid Stenting and Embolic Protection Devices. Neurointerventionist 4 (2004): 89-101.

[53] วัฒนา ผลากรกุล. จลนศาสตร์ของการไหลเวียนเลือด. กรุงเทพมหานคร: คณะแพทยศาสตร์ศิริราชพยาบาล, 2524.

[54] Birss, R. R., Gerber, R., Parker, M. R., Sheerer, T. J. Theory and Performance of Axial Magnetic Filters in Laminar Flow Conditions. IEEE Transactions on Magnetics 14 (September 1978): 389-391.

[55] Kraus, J. D. Electromagnetics. 4 th ed. Singapore: McGraw-Hill, 1991.

[56] Melville, D., Paul, F., Roath, S. High gradient magnetic separation of red cells from whole blood. IEEE Transactions on Magnetics 11 (November 1975): 1701-1704.

[57] Takayasu, M., Kelland, D. R., Minervini, J. V. Continuous magnetic separation of blood components from whole blood. IEEE Transactions on Applied Superconductibity 10 (March 2000): 927-930.

[58] Hournkumnuard, K., and Chantrapornchai, C. Parallel Simulation of Concentration Dynamics of Nano-Particles in High Gradient Magnetic Separation. Simulation Modelling Practice and Theory 19 (February 2011): 847- 871.

[59] Kanok Hournkumnuard. Diffusive Capture of Magnetic Particles by an Assemblage of Random Cylindrical Collectors. Master's Thesis, Department of Physics, Faculty of Science, Chulalongkorn University, 2004.

[60] ปราโมทย์ เดชะอำไพ. ระเบียบวิธีเชิงตัวเลขในงานวิศวกรรม. กรุงเทพมหานคร: สำนักพิมพ์แห่งจุฬาลงกรณ์มหาวิทยาลัย 2553.

APPENDICES

APPENDIX A

Approximating the Continuity Equation for the Elements Adjacent to the Impervious Surface

In this research, the surface of the collector and the surface of the saturation regions are considered as an impervious surface. The continuity equation will be approximated for all element adjacent to an impervious surface. From the continuity equation

$$\frac{\partial c}{\partial t} + \vec{\nabla} \cdot \vec{J} = 0 . \qquad \text{(A.1)}$$

In coordinates (r,q) the term $\vec{\nabla} \cdot \vec{J}$ can be written as

$$\vec{\nabla} \cdot \vec{J} = \frac{\partial J_r}{\partial r} + \frac{J_r}{r} + \frac{1}{r}\frac{\partial J_q}{\partial q} . \qquad \text{(A.2)}$$

Consider an impervious which can be the surface of the collector or surface of the saturation region as shown in Figure A.1 [59]. In the figure, the middle position of the element adjacent to impervious surface is specified by the symbol I of which the radial coordinate r_I. The middle position of the next element in radial direction is denoted by $I+1$ of which radial coordinate r_{I+1}. The radial distance between these two position is Δr.

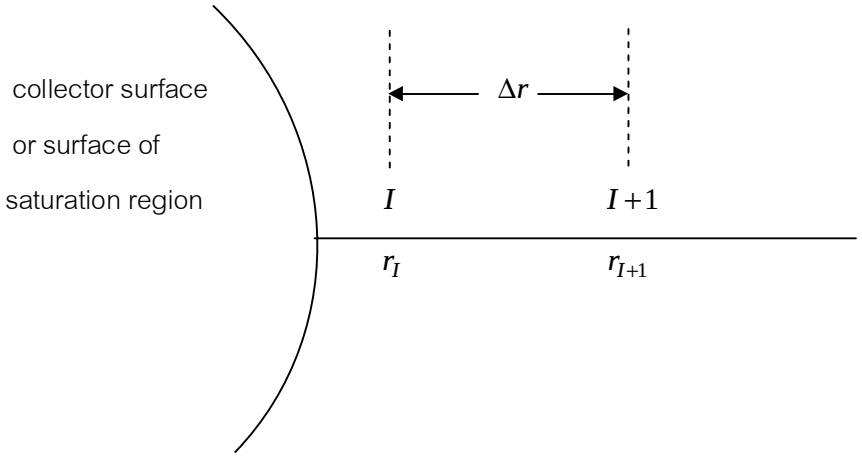

Figure A.1: Impervious surface at the surface of the collector or the surface of saturation regions.

From equation (A.2), if the element adjacent to the impervious surface is considered then the second term equal to zero. By approximating the first term on the right hand side of equation (A.2), we can write $\vec{\nabla}\cdot\vec{J}$ at the point I in approximated form as

$$\left(\vec{\nabla}\cdot\vec{J}\right)_Q \approx \frac{1}{r}\frac{\partial J_q}{\partial q} + \left[\frac{\left(J_r\right)_{I+1} - \left(J_r\right)_I}{\Delta r}\right]. \qquad \text{(A.3)}$$

Equation (A.3) obtained by approximating the term $\partial J_r / \partial r$ at point I by the first-order forward difference relation. From this equation we see that $\left(J_r\right)_I = 0$. By using expressions of J_r and J_q in coordinates (r,q) we obtain

$$\left(\vec{\nabla}\cdot\vec{J}\right)_I \approx \frac{1}{r_I}\frac{\partial}{\partial q}\left(-\frac{D}{r}\frac{\partial c}{\partial q} + v_q c\right)_I + \frac{1}{(\Delta r)}\left(-D\frac{\partial c}{\partial r} + v_r c\right)_{I+1}. \qquad \text{(A.4)}$$

By rearrange equation (A.4), we obtain

$$\left(\vec{\nabla}\cdot\vec{J}\right)_I \approx -\frac{D}{r_I^2}\left(\frac{\partial^2 c}{\partial q^2}\right)_I + \frac{1}{r_I}\left(\frac{\partial\left(v_q c\right)}{\partial q}\right)_I + \frac{1}{\left(\Delta r\right)}\left(v_r c - D\frac{\partial c}{\partial r}\right)_{I+1}. \qquad \text{(A.5)}$$

Now the continuity equation (A.1) can be approximated at the point I as

$$\left(\frac{\partial c}{\partial t}\right)_I \approx \frac{D}{r_I^2}\left(\frac{\partial^2 c}{\partial q^2}\right)_I - \frac{1}{r_I}\left(\frac{\partial\left(v_q c\right)}{\partial q}\right)_I + \frac{1}{\left(\Delta r\right)}\left(v_r c - D\frac{\partial c}{\partial r}\right)_{I+1}. \qquad \text{(A.6)}$$

When equation (A.6) is rewritten in terms of normalized radial distance $\left(r_a\right)$ and normalized time, we obtain the approximated continuity equation used in the computation of concentration in the element adjacent to the impervious surface as

$$\left(\frac{\partial c}{\partial t}\right)_I \approx \frac{1}{\left(r_a\right)_I^2}\left(\frac{\partial^2 c}{\partial q^2}\right)_I - \frac{1}{\left(r_a\right)_I}\left(\frac{\partial\left(G_q c\right)}{\partial q}\right)_I + \frac{1}{\left(\Delta r_a\right)}\left(G_r c - \frac{\partial c}{\partial r_a}\right)_{I+1}. \qquad \text{(A.7)}$$

APPENDIX B

Approximating Derivatives of Functions by Finite-Difference Relations

Consider a continuous function of real variable x denoted by $f(x)$, the derivative of this function with respect to x at a certain value of its argument, x_i, is defined as

$$\frac{dy}{dx} \equiv \lim_{\Delta x \to 0} \frac{f(x_i + \Delta x) - f(x_i)}{\Delta x} \quad . \tag{B.1}$$

Let us assume that f is a well-behaved function, then the derivative of f with respect to x can be determined in any order. Consequently, we can write Taylor's expansion of $f(x)$ at a point x_{k+1} which advance a point x_k with an amount Δx in the domain of f as

$$f(x_{k+1}) = f(x_k) + (\Delta x) f'(x_k) + \frac{(\Delta x)^2}{2!} f''(x_k) + \ldots \quad , \tag{B.2}$$

where $\Delta x = x_{k+1} - x_k$.

From equation (B.2), we can determine the first-order derivative of f with respect to x at the point x_k as

$$f'(x_k) = \frac{f(x_{k+1}) - f(x_k)}{\Delta x} - \frac{(\Delta x)}{2!} f''(x_k) + \ldots \quad . \tag{B.3}$$

The equation (B.3) can rewritten more compactly as

$$f'(x_k) = \frac{f(x_{k+1}) - f(x_k)}{\Delta x} + \mathrm{O}(\Delta x) \ , \tag{B.4}$$

where $\mathrm{O}(\Delta x)$ represent the terms of order (Δx) and higher. We can approximate the first-order derivative of f with respect to x at the point x_k as

$$f'(x_k) \approx \frac{f(x_{k+1}) - f(x_k)}{\Delta x}, \tag{B.5}$$

where the error of approximation is in the order (Δx).

The equation (B.5) is called the first-order forward difference approximation [60]. Now if we write Taylor 's expansion of $f(x)$ at a point x_{k-1} which lag a point x_k with an amount Δx in the domain of f as

$$f(x_{k-1}) = f(x_k) - (\Delta x) f'(x_k) + \frac{(\Delta x)^2}{2!} f''(x_k) - \ldots \ , \tag{B.6}$$

where $\Delta x = x_k - x_{k-1}$.

From equation (B.6), we can determine the first-order derivative of f with respect to x at the point x_k as

$$f'(x_k) = \frac{f(x_k) - f(x_{k-1})}{\Delta x} + \frac{(\Delta x)}{2!} f''(x_k) - \ldots \ . \tag{B.7}$$

The equation (B.7) can rewritten more compactly as

$$f'(x_k) = \frac{f(x_k) - f(x_{k-1})}{\Delta x} + \mathrm{O}\left[(\Delta x)\right] . \tag{B.8}$$

Then we obtain an alternative way to approximate the first-order derivative of f with respect to x at the point x_k as

$$f'(x_k) \approx \frac{f(x_k) - f(x_{k-1})}{\Delta x}, \tag{B.9}$$

where the error of approximation is also in the order (Δx). The equation (B.9) is called the first-order backward difference approximation [60].

If equation (B.6) is subtracted from equation (B.2) we obtain

$$f(x_{k+1}) - f(x_{k-1}) = 2(\Delta x) f'(x_k) + \frac{2}{3!}(\Delta x)^3 f'''(x_k) + \ldots \ . \tag{B.10}$$

From this equation we can determine the first-order derivative of f with respect to x at the point x_k as

$$f'(x_k) = \frac{f(x_{k+1}) - f(x_{k-1})}{2(\Delta x)} - \frac{(\Delta x)^2}{3!} f'''(x_k) + \ldots , \tag{B.11}$$

or

$$f'(x_k) = \frac{f(x_{k+1}) - f(x_{k-1})}{2(\Delta x)} + \mathrm{O}\left[(\Delta x)^2\right]. \tag{B.12}$$

From equation (B.12), we obtain an alternative way to approximate the first-order derivative of f with respect to x at the point x_k as

$$f'(x_k) \approx \frac{f(x_{k+1}) - f(x_{k-1})}{2(\Delta x)} \ , \tag{B.13}$$

where the error of approximation is also in the order $(\Delta x)^2$.

The equation (B.9) is called the first-order central difference approximation [60]. When equations (B.2) and (B.6) are added we obtain

$$f(x_{k+1}) + f(x_{k-1}) = 2f(x_k) + (\Delta x)^2 f''(x_k) + \frac{f^{(4)}(x_k)}{12}(\Delta x)^4 + \ldots \ . \tag{B.14}$$

This equation can be rewritten as

$$f''(x_k) = \frac{f(x_{k+1}) - 2f(x_k) + f(x_{k-1})}{(\Delta x)^2} + \mathrm{O}\left[(\Delta x)^2\right], \tag{B.15}$$

where $\mathrm{O}\left[(\Delta x)^2\right]$ represent the terms of order $(\Delta x)^2$ and higher. We can approximate the second-order derivative of f with respect to x at the point x_k as

$$f''(x_k) \approx \frac{f(x_{k+1}) - 2f(x_k) + f(x_{k-1})}{(\Delta x)^2}, \tag{B.16}$$

where the error of approximation is in the order $(\Delta x)^2$. The equation (B.16) is called the second-order central difference approximation [60]. These approximations are used in Chapter IV of this research.

Vitae

Name: Mr. Kanok Hournkumnuard

Birthdate and Birhtplace: April 3, 1978 at Petchaburi, Thailand

Father and Mother: Mr. Boonchoo and Mrs. Kuweeta Hournkumnuard

Educations

1999 B.Eng. (Control Engineering), Faculty of Engineering, King Mongkut's Institute of Technology Ladkrabang, Bangkok, Thailand.

2004 M.Sc. (Physics), Faculty of Science, Chulalongkorn University, Bangkok, Thailand.

Working

2000 until now, Lecturer, Department of Physics, Silpakorn University, Nakhorn-Pathom, Thailand.

Publication

2008 Hournkumnuard K. and Natenapit M. Diffusive Capture of Magnetic Particles by an Assemblage of Random Cylindrical Collectors. Separation Science and Technology 43 (2008): 3448-3460.

2012 Hournkumnuard K. and Natenapit M. The Capture of Micro-Particles by Random Cylindrical Wires in Axial magnetic Filters. Article has been submitted for publishing.

2012 Hournkumnuard K. and Natenapit M. Diffusive Catpure of Nano-Drug Carriers by High Gradient Magnetic Field Generated in Blood Vessel. Article is under preparation for submission.

Conference Presentations

2009 Horunkumnuard K. and Natenapit M. Computational Model of Particle Capture by Random Cylindrical Wires in Axial Magnetic Filters. The 5th Mathematics and Physical Sciences Graduate Congress, Chulalongkorn University (8 December 2009).

2011 Horunkumnuard K. and Natenapit M. HGMF of Blood Cells from Whole Blood using Macro-Scale Axial Magnetic Filters. The 7th Mathematics and Physical Sciences Graduate Congress, National University of Singapore (13 December 2011).